MOLECULAR DYNAMICS OF P21 AND FLUORESCENT SPHINGOMYELIN IN KERATINOCYTES EXPOSED TO UVB

A Thesis

Presented to

The Faculty of California Polytechnic State University

San Luis Obispo

In Partial Fulfillment

of the Requirements for the Degree

Master of Science in Biomedical Engineering

by

Tyler Malcolm Fraser

December 2018

COMMITTEE MEMBERSHIP

TITLE:	Molecular Dynamics of p21 and Fluorescent Sphingomyelin in Keratinocytes Exposed to UVB
AUTHOR:	Tyler Malcolm Fraser
DATE SUBMITTED:	December 2018
COMMITTEE CHAIR:	Lily Hsu Laiho, Ph.D. Professor of Biomedical Engineering
COMMITTEE MEMBER:	Kristen Cardinal, Ph.D. Professor of Biomedical Engineering
COMMITTEE MEMBER:	David Clague, Ph.D. Professor of Biomedical Engineering

ABSTRACT

Molecular Dynamics of p21 and Fluorescent Sphingomyelin in Keratinocytes Exposed to UVB

Tyler Malcolm Fraser

Non-melanoma skin cancer (NMSC) is the most common malignant tumor, representing more than a third of all malignant tumors combined and the incidence is increasing every year. Ultraviolet (UV) radiation from the sun is the most dominant factor contributing to tumor initiation and progression. The condition is most prevalent in populations with lighter skin and older age. Current pharmaceutical molecular research targets the inhibition of the Epidermal Growth Factor Receptor (EGFR), a receptor which is commonly overexpressed or dysregulated in skin malaganancies. This study evaluates the content and location of the damage marker p21 within keratinocytes that were incubated in sphingomyelin (SM) and later exposed to UV. Confocal microscopy and automated image processing provided the tools to assess large populations of keratinocytes in the effort to accuratly identify the photoprotective qualities of sphingomyelin. Classification of individual cells into subpopulations yeilded results suggesting SM may be involved in the inhibition of EGFR, and could potentially be a more naturally derived treatment.

ACKNOWLEDGMENTS

Cal Poly has given me a different perspective in all aspects of biologically-related engineering and I am so grateful that I was able to have this opportunity. I have met some of the most brilliant and respectable teachers and students with my time here. First, I would like to thank my advisor, Lily Laiho for taking a chance on me. I am still in awe that I was able to get into graduate studies so close to where I grew up. My lab mates, Stephanie and Rebecca, were some of the most helpful people with excellent patience. Thank you to my parents both in Morro Bay and Stockton for supporting me in my graduate studies so that my daughter Elliott will have the best life I can give her. Finally, to my wife Jessie, thank you for essentially being a single parent while I was locked away writing.

TABLE OF CONTENTS

Page

LIST OF TABLES

Table Page

LIST OF FIGURES

Figure Page

Chapter 1: Introduction

1.1 Overview

Skin cancer is the most common malignancy in the Caucasian population and the incidence is increasing every year [1]. Increased ultraviolet radiation (UVR) exposure and longer life spans mainly contribute to the increase in incidence [1]. Melanoma and Non-melanoma skin cancer (NMSC) make up the majority of skin cancers, with NMSC experiencing an incidence rate 18-20 times higher than that of melanoma [1][2]. Keratinocyte (KRT) carcinomas account for 99% of the tumors in NMSC since they are the most prevalent cell in skin tissue [1][3]. It was estimated, that for a child born in 1994 in Rhode Island; over its lifetime there was a 28-33% chance of developing basal cell carcinoma(BCC) and a 7-11% chance of developing squamous cell carcinoma (SCC), of which both are NMSC [1][2].

UVR is the most dominant environmental factor that effects formation of NMSC. UV radiation, specifically UVB can cause single and double strand DNA breaks, formation of cyclobutene pyrimidine dimers, DNA cross-links, and (6-4) photoproducts [4][5][6]. Genetic damage causes an upregulation of damage protein p21, which competes for DNA repair binding sites with PCNA, slowing down the repair process [7].

Sphingomyelin (SM) is a natural lipid where 70-80% of a cell's SM content is found in the plasma membrane, of which is mostly found in lipid rafts [8][9]. Altering SM lipid content in the plasma membrane results in drastically different phosphorylation events of lipid raft bound transmembrane signaling proteins, depending on the type of cell [10][11][12][13][14]. Bovine sphingomyelin incubated keratinocytes have been found to have reduced levels of p21 after UVB, when compared to controls that were not incubated with SM [15].

The aim of this study is to investigate the protective qualities sphingomyelin instills on human keratinocytes in culture against UVR. Using confocal microscopy, coupled with

immunofluorescence, allowed for the visualization of the molecular dynamics of fluorescent-tagged SM and p21 within keratinocytes following ultraviolet radiation. Location of intensity of these two molecules were evaluated in order to determine what SM was doing to these cells to reduce the number of cells exhibiting high levels of nuclear p21 content.

Chapter 2: Background

2.1 Skin Anatomy

The skin accounts for about 16% of the body's mass, making it the largest organ [16]. The organ consists of 3 layers; the epidermis, dermis and hypodermis, Figure 1. The deepest layer, the hypodermis is made up of blood vessels, hair follicles, sensory neurons, and adipose lobules [17]. Superficial to that layer is the dermis which also consists of blood vessels, hair follicles, sensory neurons, but also has sweat glands and is split into two layers: the reticular layer with dense connective tissue and collagen fiber bundles, and the papillary layer that contacts the epidermis with looser connective tissue [17][18]. Fibroblasts are the most prevalent cell type in this layer, creating the rigid ECM [19].

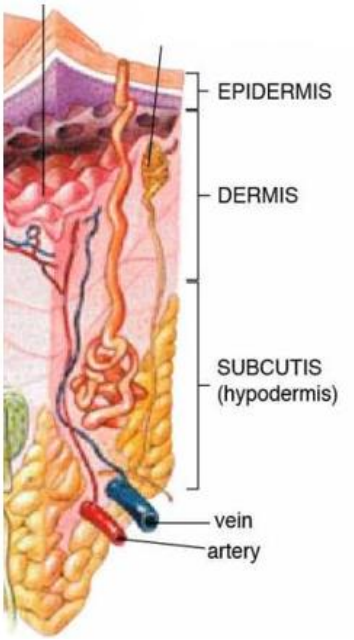

Figure 1. Anatomy of the skin [17].

2.1.1 Epidermis

The most superficial layer of the skin is the epidermis, which is made of keratinocytes, melanocytes, Langerhans' and Merkel cells. The epidermis is split into 4 layers: basal, spinous, granular and horny, seen in Figure 2 [17].

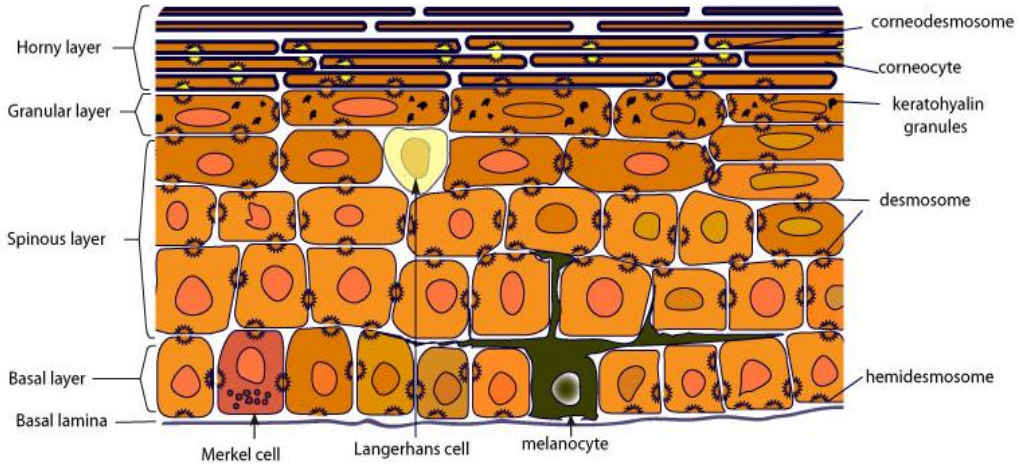

Figure 2. Layers of the Epidermis [20].

2.1.1.1 Basal Layer

The deepest layer, the basal layer, is comprised of one layer of cuboidal to columnar stem cells, but can have 2 or 3 layers at times [18]. The basal lamina separates the layer from the dermis, and hemidesmosomes attach this layer to the dermis, Figure 2 [17][18]. Stem cell-like keratinocytes with elliptical nuclei dominate this layer, but small populations of Merkel cells are present along with melanocytes at a ratio of 1:36 to keratinocytes [19].

2.1.1.2 Stratum spinosum (Spinous layer)

Basal layer keratinocytes divide to form more keratinocytes with limited divisions remaining. Those cells migrate superficially making up the spinous layer with 8-10 sheets of keratinocytes [18]. Also known as the prickle cell layer, this layer gets its name due to spiny intercellular attachments due to desmosomes, which cause the cells to look spiny under a microscope [17]. Morphologically, the cells are irregular and polyhedral, and along with the keratinocytes are some Langerhans cells, at a ratio of 1:53 [19]. When keratinocytes reach the upper spinous layer they start to release lamellar bodies containing various lipids [17][18][19].

2.1.1.3 Stratum Granulosum (Granular layer)

Superficial to the spinous layer are 3-5 sheets of non-dividing differentiating keratinocytes making up the stratum granulosum (SG) [19]. In this layer, the cells become diamond shaped and start producing keratohyalin granules [17]. These granules are found in the cytoplasm and promote dehydration of the cell, as well as causing the cells to gradually lose organelles [18]. Continuing in the SG, keratinocytes release lamellar bodies that contain glucosyl ceramides, cholesterol variants, and long chain fatty acids. The lamellar bodies are processed in

extracellular spaces, and contents are organized as the stratum corneum is being developed to help make the skin barrier [19][21][22][23][24].

2.1.1.4 Stratum Corneum (Horny layer)

The last layer before exposure to the environment is the stratum corneum. Keratinocytes in this layer have fully differentiated into corneocytes, which are non-viable, but biochemically active cells linked together by corneodesmosomes [19]. 15 to 30 sheets of these corneocytes make up this layer [19]. The lamellar bodies released in the SG have released their contents that surround the corneocytes, making the physical barrier [17]. This barrier is both protective and controls moisture[17]. Sheading of corneocytes occurs regularly and is known as desquamating [19]. The sheading, along with antimicrobial peptides and pH control are defensive mechanisms to rid of harmful microbial invasions. The sheading will take microbial loads with it [17][18][19][21][25].

2.2 Non-melanoma skin cancer

Melanoma and non-melanoma skin cancer are the most common malignant tumors making up more than a third of all tumors. Non-melanoma skin cancer (NMSC) occurs at a rate of 18-20 times higher than that of malignant melanoma [1][26]. Of NMSC cases, 99% are either basal cell carcinoma (BCC) or squamous cell carcinoma (SCC), of the keratinocytes. In the United states, 70-80% of NMSC are BCC, while 20-30% are SCC [1][3]. NMSC occurs mostly in; people over the age of 50, where they are geographically located in terms of UV irradiance, being male and having white skin [1][27]. The incidence in the older population is increasing while the older population is also increasing [1][2][3][18][27][28]. In the last 30 years SCC have been rising in incidence 3-10% every year, while BCC rates have increased 20-80% in the same time frame [1][29]. Fortunately, mortality and metastasis rates are very low with BCC seeing a 0.00281-

0.05% incidence rate and SCC with a 0.5-16% incidence rate [1][30]. However, due to the large number of cases, Medicare spends about $13 billion a year treating skin cancer in the United States [27]. Ultraviolet radiation (UV) is the most dominant environmental factor that is associated with risk of NMSC [27][28].

BCC tends to develop after many years in tissue beds that seemed to have been undamaged, where short intense exposures to UVB in the youth may be more important than lifetime doses. They can cause local destruction of tissue, but rarely metastasis. On the other hand, SCC can metastasize making it much more dangerous [18][2].

2.3 Ultraviolet Light

There is a continual increase in ultraviolet radiation (UV) due to release of pollutants like chlorofluorocarbons, chlorocarbons, and organobromides that cause the stratospheric ozone layer to deplete [4]. There are three types of UV radiation with varying exposure to humans. UVA (315-400nm), UVB (280-320nm) and UVC (200-280nm) are emitted by the sun, but only UVA and UVB reach humans since UVC cannot penetrate the atmosphere, Figure 3 [4][5][6]. Of the UV that does reach human skin, 1-10% is UVB while the remaining is UVA [6].

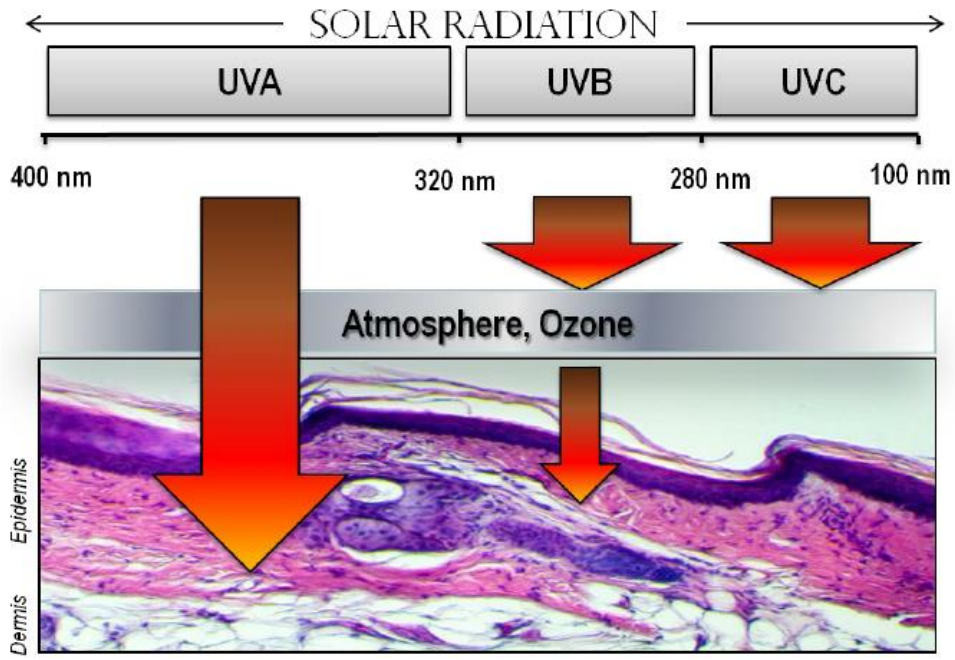

Figure 3. Ultraviolet Penetration [31].

2.3.1 Genetic Damage from UV

The effects of direct UV radiation damaging the DNA can result in single and double strand breaks, formation of cyclobutene pyrimidine dimers, DNA cross-links, and (6-4) photoproducts [4][5][6]. In the case that the DNA is not repaired after UV damage, a permanent mutation could be left in the cell's genome [4][5][6]. The cyclobutane dimers formed will replicate and lead to these mutations with CC →TT, or C →T mutations [6]. It has been discovered that these types of mutations occur to the tumor suppressor gene p53 in; SCC, actinic keratoses and damaged cells from chronic UV exposure, making p53 mutations an early indicator of skin carcinomas [5][6].

2.4 Sphingolipids

A sphingolipid is a natural lipid characterized as having a sphingosine backbone. The most common sphingolipid, sphingomyelin, is comprised of phosphoryl choline and ceramide. Ceramide is constructed of a sphingosine N-acylated to fatty acids [36]. Within a cell, 70-80% of

SM has been found to be on the outside of the plasma membrane or outer leaflet [9]. The majority of sphingomyelin in the membrane is associated with lipid rafts [8]. Sphingolipids are bioactive molecules playing a large role in signal transduction involved in the regulation of apoptosis, maturation, and proliferation of the cell [37].

Ceramide is one of the most important sphingolipids, being the precursor to other bioactive sphingolipids like sphingosine and sphingosine-1-phosphate, Figure 4, but also regulates PKC, raf-1, and cathepsin D and inhibits phospholipase D and Ras (indirectly via kinase suppressors) [38][39]. Many factors influence the increase of ceramide production, including ultraviolet radiation [39][40][41][42]. For example, UV activates acid SMase, upregulating SM hydrolysis, leading to formation of ceramide-enriched domains on the plasma membrane [39][42]. These domains amplify apoptotic signals by clustering specific receptors on the membrane [39][42]. The major source of ceramide comes from the de novo pathway, however the anabolic pathway of sphingomyelin hydrolysis creates a large amount of ceramide [39].

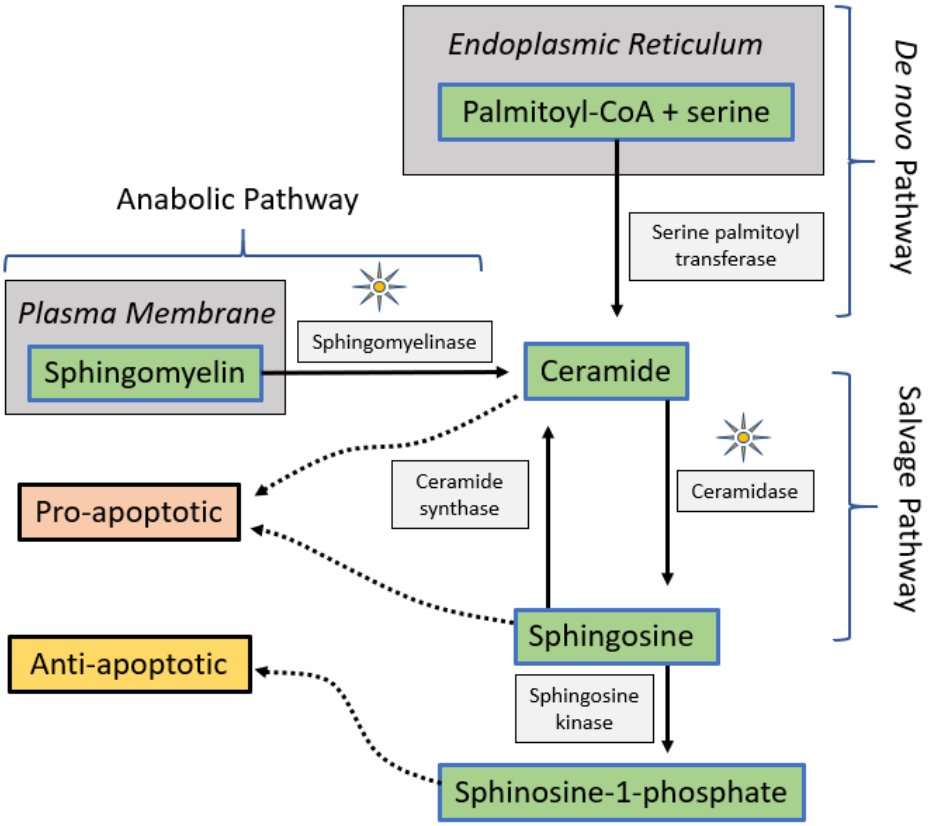

Figure 4. Sphingomyelin/Ceramide metabolism pathways. Sun represents influences from ultraviolet radiation.

De novo ceramide synthesis occurs in the endoplasmic reticulum on the cytosolic surface, but it may also be synthesized in other membranes associated with the endoplasmic reticulum and mitochondria, Figure 5 [38][43]. To make more complex metabolites like SM, CERT transports ceramide from the ER to the Golgi where SM is subsequently synthesized. The SM is then transported to the plasma membrane by vesicular transport [44][38]. SM within the plasma membrane can also be broken down into ceramide through the anabolic pathway by either neutral SMase in the inner leaflet, or acid SMase on the outer leaflet, Figure 4 & Figure 5 [38].

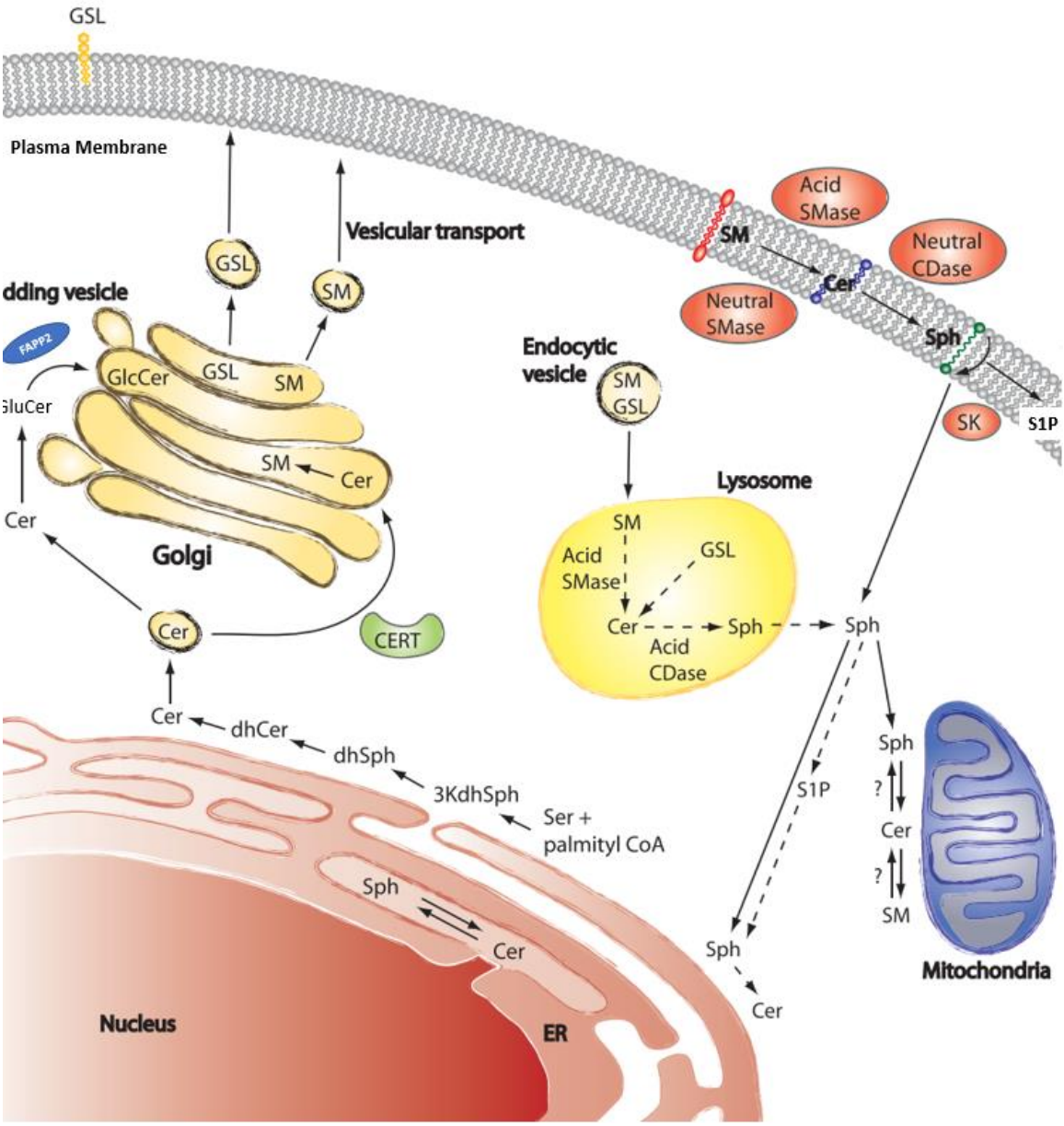

Figure 5. Sphingomyelin/Ceramide intercellular metabolism compatibilization. Cer: Ceramide, SM: Sphingomyelin, S1P: Sphinosine-1-phosphate, Sph: Sphingosine [38].

The salvage pathway, seen in Figure 4 and visualized intracellularly in Figure 5, can take SM from the plasma membrane and break it down in to ceramide by acid SMases within the lysosome. Ceramide is further broken down into sphingosine by acid CDase. Since sphingosine is

positively charged, it can leave the lysosome and travel throughout the cytosol. Once reaching the endoplasmic reticulum, the sphingosine can be recycled back in to ceramide [38][45].

2.4.1 Lipid Rafts and EGFR

Lipid rafts are microdomains of cholesterol, sphingolipids, and gangliosides found on the plasma membrane. These rafts are less fluid than bulk plasma membrane and act as cellular signaling platforms [10]. A large number of receptors are found within lipids rafts, like insulin growth factor receptor, H-Ras, and EGFR [46]. It has been shown in multiple studies that EGFR tend to localize with lipid rafts [10][47]. There are elevated levels of these lipid rafts in cancers like melanoma, prostate and breast [10][48][49].

Some studies show that localization of lipid rafts and EGFR could inhibit activation of EGFR in fibroblasts and HeLa cells [10][11][12]. However, other studies show that the localization upregulates EGFR ligand binding in kidney (Vero) and prostate cancer cells [10][13][14].

Calay et al. used keratinocytes (HaCat) to show that disruption of cholesterol-enriched lipid raft results in abrupt downregulation of Akt activity in normal, premalignant, and malignant cells. This disruption did not affect activation of EGFR or PI3K, but since it affected Akt activation, the team proposes that the lipid rafts act as ‘reaction nanochambers’, which allow for interactions between complexes due to close proximity [50]. It was found that EGFR and PI3K complexes move out into the more fluid membrane when the rafts were disrupted, allowing for ligand activation, but no downstream activation since the complexes were not in proximity [50].

Mound et al. demonstrated that SM-depletion, like cholesterol depletion, disrupted the lipid raft suggesting that SM is required in some amount to stabilize the raft [51]. They also found that EGFR is frequently localized in SM-rich lipid rafts, in accordance with other studies

[12][52][51]. When keratinocytes enter replicative senescence SM-rich domains dramatically decrease, while cholesterol remain unchanged [51]. When Mound et al. introduced exogenous SM to these cells, the SM concentrated back into the domains they were observing, showing that these cells retain SM-attractive domains in senescence [51].

2.4.2 Ceramide and Microdomains

Ceramide strongly associates with lipid rafts and lipid raft stabilization [53]. Cuijuan et al. as well as Megha et al. both created lipid raft membrane models and found that adding exogenous ceramide displaced cholesterol from the rafts [53][54]. In cultured immortalized Schwann cells, Cuijuan et al. used bacterial SMase to increase endogenous ceramide levels, which significantly displaced cholesterol in lipid rafts [54].

Acid Sphingomyelinase (ASM) can be activated within seconds by many stimuli, including UV [42][53][55]. Activated ASM molecules translocate to the outer membrane leaflet and rapidly hydrolyze a large portion of SM into ceramide [42][53][55]. The ceramide released reorganize and form large ceramide-enriched domains on the membrane [42][53][55]. These newly developed domains cluster together specific receptors to amplify signals required for apoptosis [42][55].

2.4.3 Commonalities between IGF-IR and EGFR

Insulin growth factor receptor (IGF-IR) is another type of transmembrane receptor that also activates the PI3k/AKT pathway. This receptor is also localized within lipid rafts [46][56]. Huo et al. used 3t3 cells and disrupted lipid rafts with the cholesterol binding agent, methyl-beta-cyclodextrin, finding a decrease in Akt activation, but not in the initial activation of the receptor itself, similar as Calay et al. study with HaCat cells [56]. This suggests receptors localized in lipid rafts lets the receptor be in close contact with the downstream signaling

molecules [56][46]. In another study with HepG2 cells (Hepatocytes) Li, et al. saw decreased Akt activation after adding exogenous sphingomyelin; however they saw an increase in activation when adding ($C_{16:0}$) Ceramide [57].

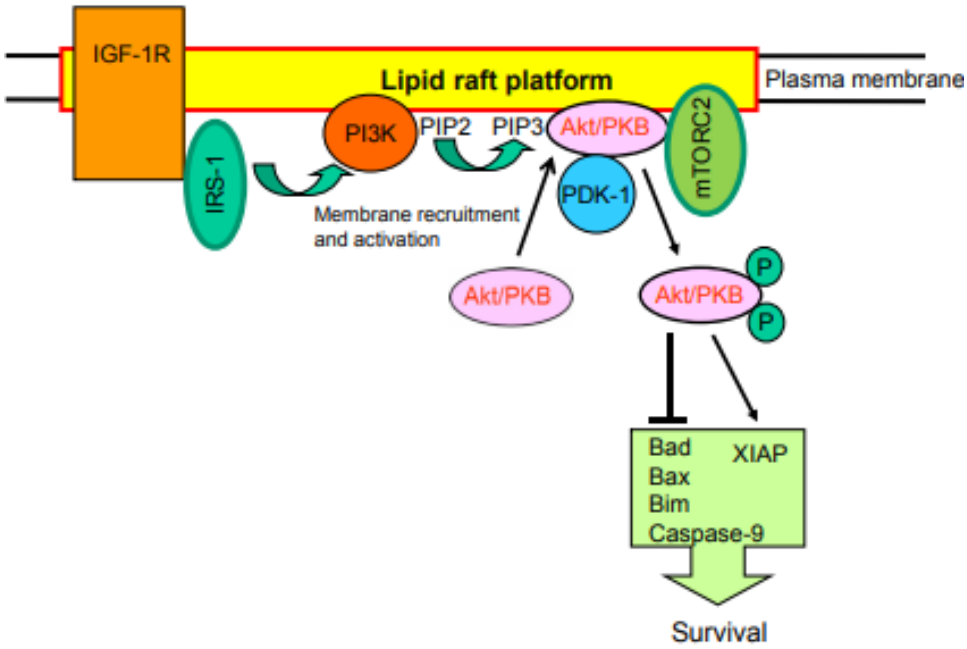

Figure 6. IGF Receptor/PI3K Pathway [46].

2.4.4 UV light induces PI3K-AKT pathway via EGFR

PI3k is an upstream regulator of several pathways that are deregulated in carcinogenesis [6][32][33]. Gonzales, et al. reported that 250 J/m^2 UVB induces PI3k activity in cultured human keratinocytes [6][34]. Taghrid, et al. used genetically initiated mouse models to observe effects of inhibiting the single transmembrane glycoprotein cell surface receptor, epidermal growth factor receptor (EGFR), in activating the PI3k-AKT pathway after UVB irradiation. Results showed that initiated-mice treated with the EGFR inhibitor, AG1478, blocked the development of half the tumors, while more so reducing tumor progression. The team suggests that EGFR may be a target for preventing UV induced skin cancer, Figure 7 [5][35].

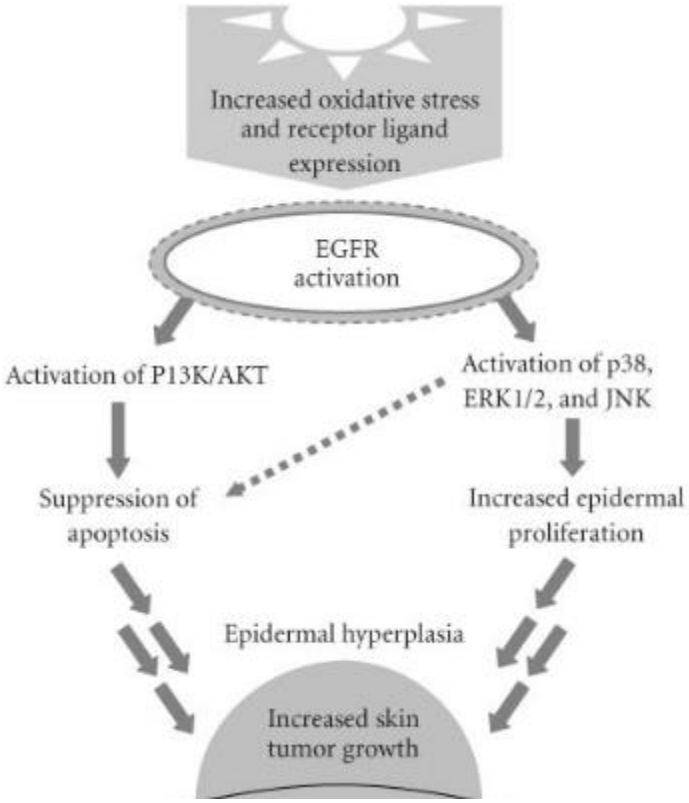

Figure 7. UV light Induces the PI3K-AKT pathway [35].

2.5 p21

The cell cycle is regulated by a group of enzymes called cyclin dependent kinases (CDK) [58]. p21 is a CDK inhibitor in the same family of CDK inhibitors as p27 and p53 where inhibition is achieved by interacting with the N-terminal homologous sequences [7]. It is best known to inhibit cell proliferation by acting as the primary inhibitor to CDK2, but can also indirectly inhibit CDK1 by interfering with phosphorylation [59][7]. p21 slows down the repair process of DNA

when it becomes damaged by competing with proliferating cell nuclear antigens (PCNA) binding sites, where PCNA repair DNA [7].

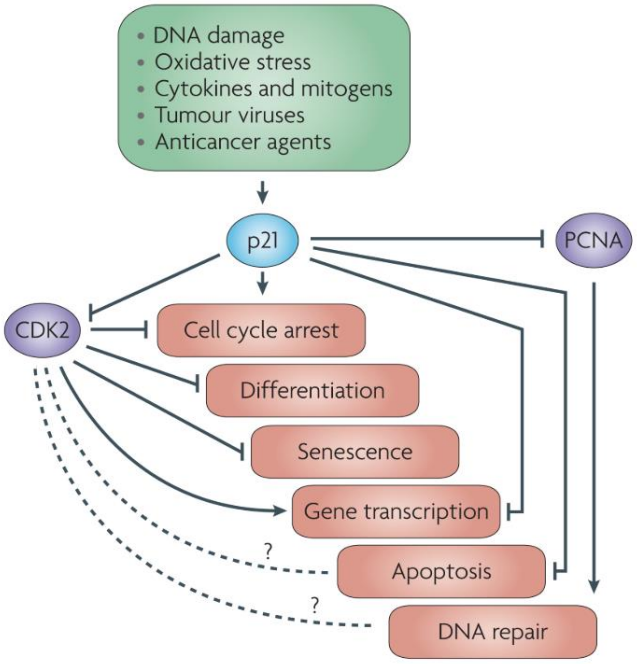

Figure 8. Paradoxical Functionality of p21 [7].

Other than growth inhibition, p21 has the paradoxical effect of also being anti-apoptotic, Figure 8. The reason being is that if the cell is presented with genotoxic stimuli it will most likely go through apoptosis, but p21 can protect the cell from apoptosis if present in the cytoplasm [7]. Cytoplasmic p21 inhibits apoptotic proteins like procaspase 3, caspase 8, and caspase 10 [7]. Xia et al., found that in breast cancer patients, 59% had high expression of p21 where of those patients: 26% of the p21 was in the nucleus while 33% was in the cytoplasm. They also found that cytoplasmically located p21 had the worst patient outcome compared to nuclear or negative p21 expression [60].

It has been identified that cytoplasmic localization of p21 is controlled by the phosphorylation of p21 by Akt [7][60][61]. When Akt is activated, it is detached from the inner surface of the plasma membrane and localizes in the nucleus within thirty minutes [61]. Akt is

known to promote cell survival and reduce apoptosis [61][62]. Zhou et al. demonstrated that blocking the Akt pathway inhibits cell growth and that blocking results in nuclear p21 localization [61]. Visualization of the process can be seen in Figure 9. The cellular response of p21 can also be regulated through the transcriptional repression of CDKN1A [7].

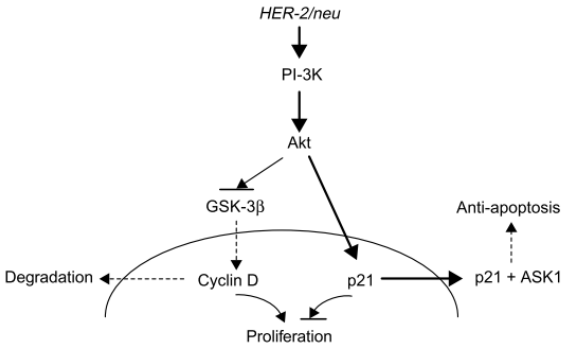

Figure 9. Akt pathway affects p21 localization [61].

2.6 Immunofluorescence Microscopy

2.6.1 Fluorochromes

Immunofluorescence (IF) is widely used both in clinical diagnostics and biologic research. IF allows the researcher to target specific molecules with special antibodies. These antibodies have fluorochromes attached to them that will absorb a certain range of wavelength of light, known as the excitation spectrum. Following absorption, the fluorochrome immediately emits a photon, but with a longer and lower energy wavelength. To observe the emitted light, a specific filter is used to block out the excitation wavelength and only let through the emission wavelength [63]–[65].

There are two types of techniques used in IF for antibody binding. The first being direct staining where the fluorochrome is directly attached to the primary antibody that binds to the target molecule. The second is indirect staining where the primary antibody attaches to the target molecule, while another antibody with a fluorochrome attached, the secondary, binds to the primary antibody. There are advantages and disadvantages between the two techniques:

direct is faster, requires less steps and has less background noise, but is generally much more expensive and has a much more limited range of fluorochromes to use; indirect has a longer process and needs more optimization, but has a range of secondary antibodies that can be used with many different excitation/emission spectrums. Multiple secondary antibodies can bind to one primary molecule allowing for signal amplification [63]–[65].

2.6.2 Confocal Microscopy

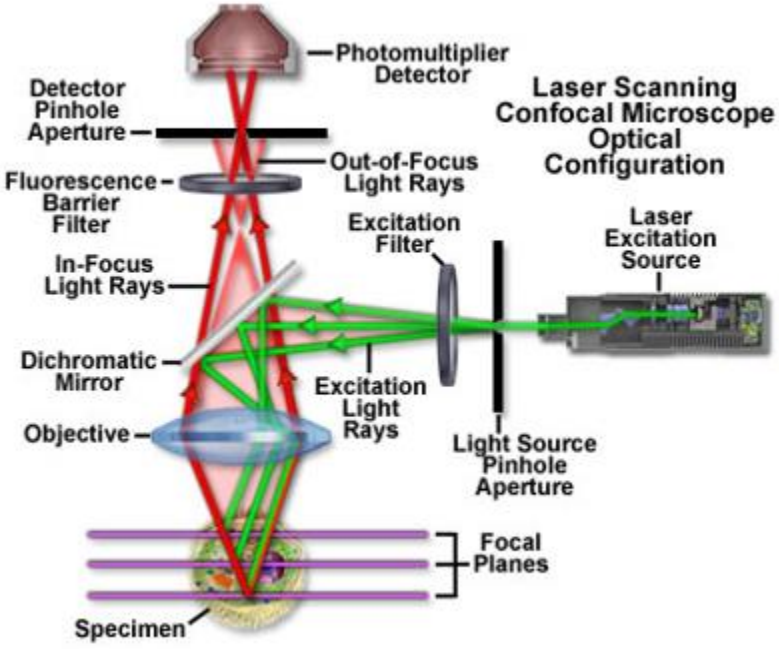

Figure 10. Example of how a Confocal Microscope Works [66].

What makes confocal microscopy different than a fluorescent microscope is that it can visually section a sample giving accurate locations of fluorochromes within a cell. Fluorescent microcopy sees every fluorochrome between the observer and the specimen. (Figure 10) The laser source emits a narrow wavelength-band of light that a specific fluorochrome can absorb. That light reflects off a dichromatic mirror where it is then focused onto the specimen where fluorochromes are present. Reflected light and light emitted by the fluorochromes pass back

through the dichromatic mirror and emission filter to remove the reflected light and retain the emitted light. Depending on the aperture hole size and position, the observer will only see a specific plane in the specimen. Other light either above or below the observed plane does not pass through the aperture [66].

2.7 Past Lab Experiments

Kevin Cambell analyzed keratinocytes p21 and p53 biomarkers within the nucleus. He found that these two biomarkers for damage were significantly less in UV+SM+ cases in comparison to UV+SM-. The way he quantified the biomarkers was binary; either positive or negative. Visual inspection was used to make this assessment with the aid of ImageJ to keep count. He also established the optimized p21 protocol that has been used in the lab and this thesis [15].

Rebecca Kandell built from what Kevin Campbell did, but ventured into using fluorescently tagged sphingomyelin (fSM) to understand localization of the lipid over time. After optimizing the fSM protocol, she wanted to know what the optimal incubation time of sphingomyelin should be, incubating cells at 10 min, 30 min, 1hr, 2hrs, 3hrs, 4hrs, 12hrs and 24hrs. It was found that trafficking of fSM was independent of the incubation time. When incubating for either 1hr or 24hrs and fixing at different times, the 1hr had a consistently higher cytoplasmic intensity. She suggested higher sample sizes for all of her experiments to accurately understand the effects of fSM and SM [67].

After establishing fSM protocol, Rebecca optimized staining procedure to see endogenous SM and ceramide. Unfortunately, there was no significance in fSM or ceramide with variable incubation times, except that endogenous SM was significantly higher in the 2-hour than the 10-minute incubation. She describes that sensitivity cannot be validated unless with a positive control of acid SMase, which should be a future step [67].

Her final experiments worked towards making 3D spheroids composed of keratinocytes and 3T3 fibroblasts. These spheroids were developed in order to create a microenvironment simulating tissue. 3T3s had to be used since KRTs would not make spheroids on their own and suggests using a more relevant fibroblast to act as the dermal layer. She also mentions that using higher concentrations of calcium could help with stratification. Both of these improvements have been in recent studies [67].

Chapter 3: Methods

3.1 Keratinocyte Culture

Primary Human Epidermal Keratinocytes from Neonatal Foreskin (HEKn PCS-200-010, ATCC Manassas, VA) were cultured in physiological conditions (37°C, 5% CO_2) with aseptic technique by the lab culturist. Media was prepared under manufacturer guidelines of combining a Keratinocytes Growth Kit (PCS-200-040, ATCC, Manassas, VA) with Dermal Cell Basal Media (PCS-200-030, ATCC, Manassas, VA) and sterile filtering the solution via a 0.22um filter. Keratinocytes were expanded in T-75 Corning Tissue Culture Flasks (BD353136, VWR, Visalia, CA) and passed into either 8-well Chambered Coverglasses or 1-well Chambered Coverglasses. No. 1 borosilicate coverglass was used in order to work with the inverted confocal microscope. Cell culturist replaced media every two days while morphology and confluence were assessed daily.

3.5 Poly(D-Lysine)

Poly(D-Lysine) or PDL (P6407, Sigma-Aldrich, St. Louis, MO) was received sterilized in a dark glass bottle with 5mg of powder. To create the stock solution, 25ml of sterile-filtered deionized (DI) water was added into the dark glass bottle using aseptic technique under a lamellar flow hood, resulting in a solution of 200 ug/ml. The stock solution was stored at 4°C.

The working solution was made by adding equal parts stock solution with sterile filtered DI water for a working concentration of 100 ug/ml. The working solution was pipetted into new 8-well or 1-well plates at 100ul per cm^2. Cell culture plates were incubated in the lamellar flow hood for 30min to an hour, aspirated, then set back in the hood to dry for 1 to 2 hours.

3.2 Bovine & Fluorescent Sphingomyelin

Bovine Milk Sphingomyelin (BSM) (860063P-25mg, Avanti Polar Lipids, Alabaster, AL) came in powdered form where it was added to the keratinocyte media solution, sonicated and vortexed to make a 0.1% BSM solution. A 0.22um filter was used to sterilize the solution.

Fluorescent SM (fSM) (810218P-1mg, Avanti Polar Lipids, Alabaster, AL) came in powered form where it was dissolved in ethanol for a 1mM stock solution. Stock solution was stored at -20°C and away from light. The stock solution was combined with 5uM Bovine Serum Albumin (BSA) and Keratinocyte media to make a 5uM fSM final solution, ready for cells.

When keratinocytes reach 70% confluency, either BSM or fSM was applied to the cells at 200ul per well for the 8-well plates or 2ml for the 1-well plates. Cells were incubated for 1 hour with the SM treatment before being exposed to ultraviolet (UV) light, unless otherwise specified.

3.3 UVB Irradiation

UVB was irradiated at 35 mJ/cm^2 with a UV lamp (95-0251-01, UVP, LLC, Upland, CA) after KRTs were incubated with SM. A UV sensor (S120UV, ThorLabs, Newton, NJ) measured irradiated wattage and displayed on the power meter (PM100, ThorLabs, Newton, NJ). The measurement was used in order to prescribe the correct amount of Joules to the cells using Equation 1 below.

$$Exposure\ (Seconds) = \frac{35\frac{mJ}{cm^2}}{Measured\ UV\ Irradiance(\frac{uW}{mW}) * (\frac{1mW}{1000\ uW})} \quad (1)$$

KRTs in cell culture plates from the incubator had their media or SM solution replaced. They then were placed under the UV lamp for the calculated time under a sterile hood. KRTs then were placed back in the incubator to rest for a day before the fixing and staining process.

3.4 Immunofluorescence Reagents

3.4.1 Dead Stain

Ethidium Homodimer-1 (L3224, Invitrogen, Carlsbad, CA), also known as the 'dead stain' or EthD, enters permeable cells and tags them as dead. If used, it must be added before fixation for proper staining.

Stock received as 2mM concentration and stored at -8°C. When plated cells were ready to be stained the culture media was gently removed by pipette and stock diluted with PBS to 2uM was added at 200ul per well for 8-well plates, or 2ml for the 1-well plate for 15 minutes. Prior to fixation the EthD solution is removed without washing in between.

3.4.2 Fixation

Before continuing immunofluorescent staining, cells were fixed in 3.7% paraformaldehyde (PFA) for 20 minutes after removing culture media and washing once with 1X Phosphate Buffered Solution (PBS). 200ul of PFA was pipetted into each well of the 8-well plate or 2ml on the 1-well plate. After fixing, each well was washed 3 times with PBS. Fixed cells were stored for a maximum of 2 weeks in 4°C.

3.4.2 p21

Indirect immunofluorescent staining was used to probe for p21. The use of this stain required permeabilization of the plasma membrane by TritonX-100 to let antibodies infiltrate, followed by blocking with goat serum to reduce non-specific binding of primary and secondary antibodies. All staining solutions were added to wells at 200ul in 8-well plates, or 2ml for a 1-well plate.

After fixation and washing stock TritonX-100 was diluted with PBS to 0.1% and added to each well and incubated for 20 minutes followed by three washes of PBS. Blocking solution was 10% Normal Goat Serum (500622, Life Technologies, USA) diluted with PBS to 1% and added to the cells where it incubated overnight at 4°C, for around 12 hours. Blocking solution was then removed and cells were washed three times with PBS. Primary anti-21 antibody (ab18209, Abcam, USA) cultured in rabbits were diluted 1:400 with PBS and added to cells where it incubated for 9 hours at 4°C. The solution was removed, and cells were washed three times with

PBS. The secondary, goat anti-rabbit Alexa Fluor 488 (A-11034, ThermoFisher, USA), was also diluted 1:400 with PBS, added to the cells and incubated for an hour at room temperature in darkness, followed by three washes with PBS.

3.4.3 Hoechst

Hoechst 34580 (H21486, ThermoFisher, USA), a fluorescent dye that stains DNA, was diluted with PBS to 0.03%, added to cells and incubated for 15 minutes in darkness. Cells were then washed three times with PBS. Permeabilization and blocking is not needed for Hoechst to bind appropriately.

3.6 Confocal Imaging

Stained keratinocytes imaged with an Olympus FluoView FV1000 confocal microscope (Olympus America, Centerville, PA) with accompanying FluoView acquisition program. For eight-well plates images were taken in the middle of each well since cells near the wall most likely had varying degrees of UVB exposure. One-well plates ended up taking four large area stitched images in the middle of the plate, as seen by Figure 11 and explained in section 3.6.1. Images were saved as '.oib' files where all acquisition parameters were saved with the image.

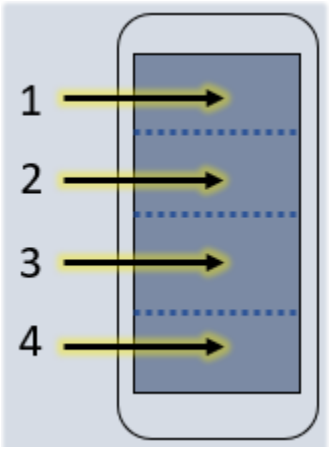

Figure 11. 1-well Plate Zones.

3.6.1 Large Area Stitch

This was the final image acquisition protocol formulated in order to obtain a larger number of samples in a shorter time while retaining image quality for accurate measurements. At first 10x images were used as the magnification setting, which ran into image quality issues. Due to the large image an unlevel stage made it very difficult to get the entire stitched image in focus. Results using this method can be found in section 4.5 p21 Expression of SM Treated KRT

1. Magnification was switched to 40x, which reduced sample size, but significantly improved quality and still obtained more samples than traditional methods.

Table 1. Laser Settings of Quantifiable Experiments

P21 Expression of SM Treated KRT 1				P21 Expression of SM Treated KRT 2				fSM Distribution Time Study			
Stain	Laser	Power	PMT (HV)	Stain	Laser	Power	PMT (HV)	Stain	Laser	Power	PMT (HV)
Hoechst	405	10%	520	Hoechst	405	13%	564	Hoechst	405	1%	564
p21	488	49%	699	p21	488	34%	756	fSM	488	6%	756
EthD-1	559	35%	475	EthD-1	559	61%	573				

The first step is to load acquisition parameters as needed. The laser settings for the experiments can be seen in Table 1. The easiest way to do this was to select pre-defined dyes where the DAPI filter setting was used for the Hoechst nuclear stain, the Alex Fluor 488 filter was used for the p21 or fSM stain, and the PI filter was used for the Ethidium Homodimer-1 dead stain, see in Figure 12. Critical parameters to use:

1. Kalman filter - samples the same pixel as many times as defined by the user and averages. This makes very high-quality images but takes a longer time. Set to at least to 2 in every application. This parameter should be
2. Sequential - eliminates bleed through by taking images one channel at a time, or by group.
3. Time per pixel - set to at least 4.0us/Pixel. Higher creates higher quality images at expense to time.
4. Resolution - set as desired, higher resolution creates higher quality images at expense to time. 800x800 or 1024x1024 yielded good quality images at reasonable speed.

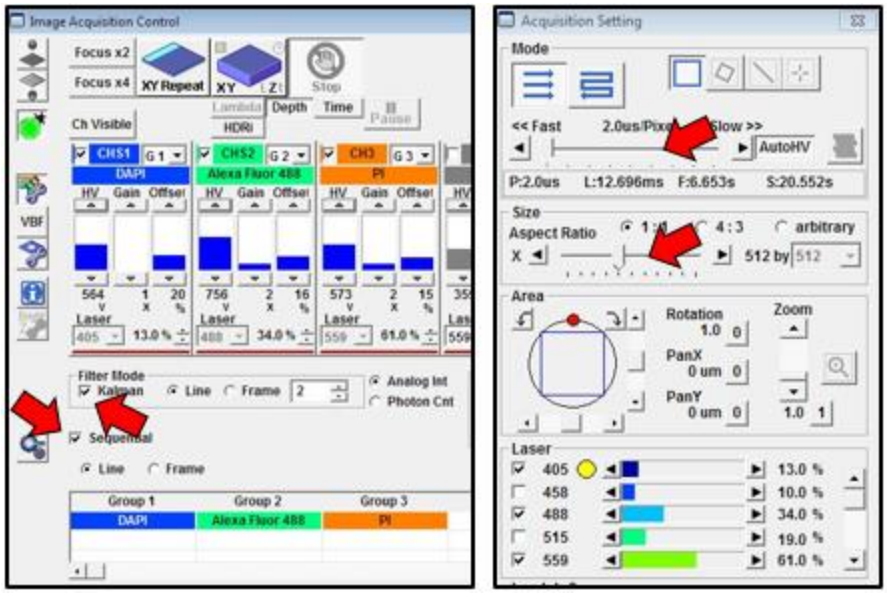

Figure 12. Common Acquisition Settings. Red arrows point to critical parameters.

After settings are established, open 'Multi Area Time Lapse Controller', which will automatically find 'home' of the stage. Now, bring cells into partial focus with epi-fluorescence or brightfield. Select 'XY Repeat' to view cells on the computer screen. Using the Hoechst channel, bring as many cells into focus as possible. Figure 13 shows out of focus (Left) and in-focus (Right) nuclei. In-focus nuclei will have dark zones in the middle and strong fluorescence on the border, pointed out by the blue arrow. Diameter of the cell is also a quick and easy way to make sure nuclei are in focus, where generally the biggest diameter is the center of the nuclei. The orange line is the same length in both images. It is vital to make sure this first image is in focus, otherwise the stitched image could be out of focus in a corner.

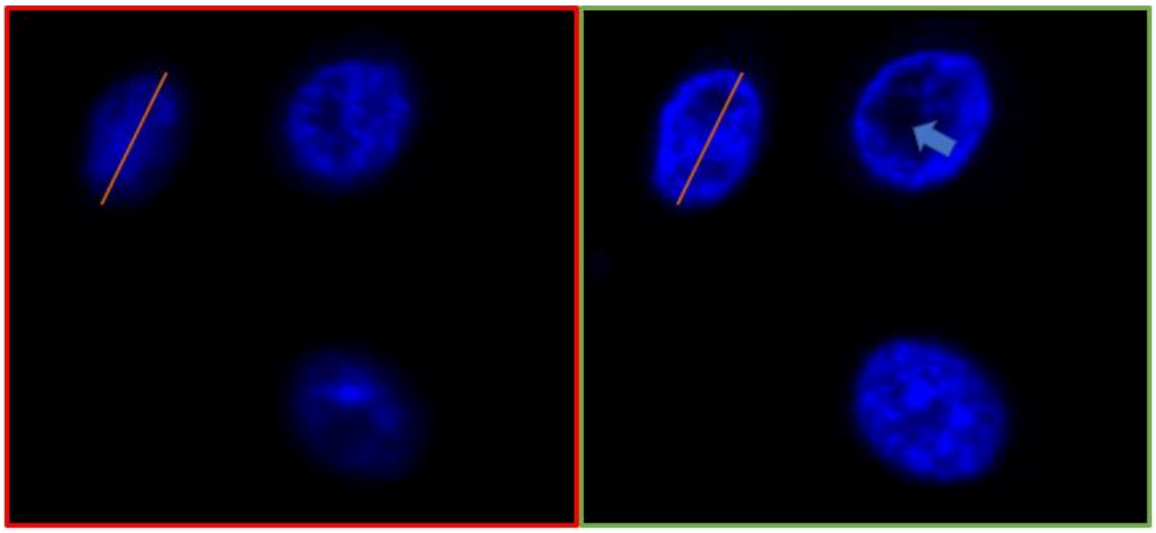

Figure 13. Middle Image Focus when using MATL. Left Image is out of focus, right is in focus. Orange line compares diameters between focal planes. Blue arrow points to dark center of an in focus nuclei.

3.6.1.1 Z-Stack

When the ideal focus is found, Z-stack must be defined, Figure 14. Z-Stack Setup. Select 'Set 0' to define the middle of the Z-stack. Select 'Slices' and set it to 3, for 3 images. Set 'Start' to 1.00 µm and 'End' to -1.00 µm. Make sure values stay as they are set when click elsewhere on the screen. Select 'Depth' in the Image Acquisition Control window.

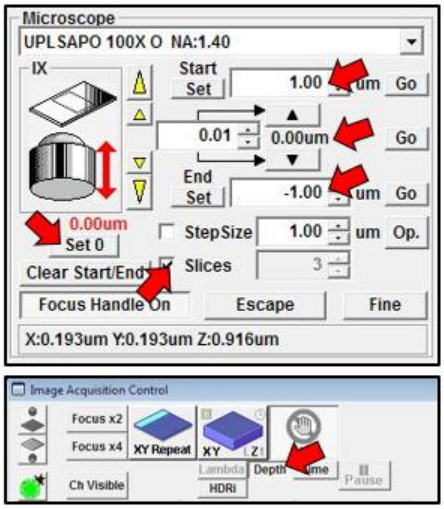

Figure 14. Z-Stack Setup.

What this will do is take an image where focus was established, then take two more images, one 1.00um above and one 1.00um below. The three images are to make sure that for each cell, at least one image is in focus.

3.6.1.2 Multi-Area Time lapse Image Stitch

The Multi Area Time Lapse (MATL) Controller should be still open, if not: open it, bring cells back into focus and redefine the Z-stack parameters from 3.6.1.1. The yellow circle in the

middle is where the field of view is at, Figure 15. Select ‘Define Matrix’ in the MATL Controller and set as a 3x3 matrix.

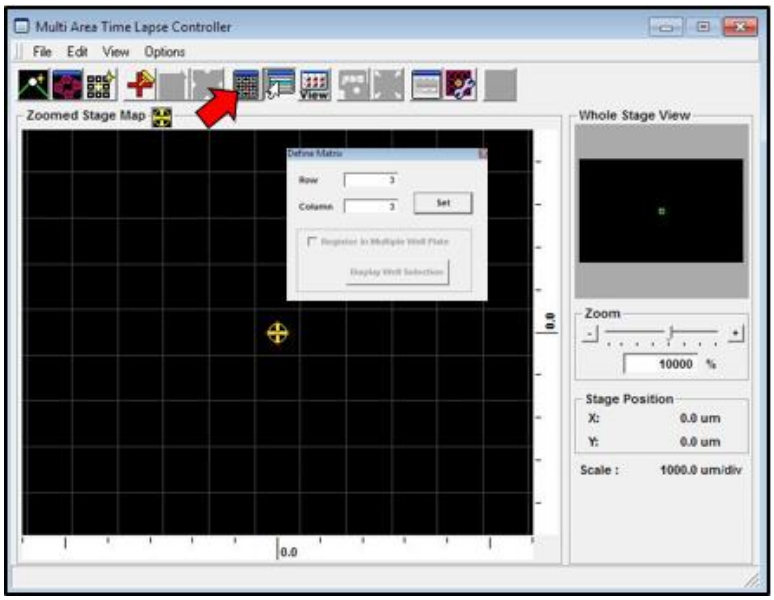

Figure 15. Multi Area Time Lapse Controller. Arrow pointing at ‘Define Matrix’

This will populate the Registered Point list, seen in Figure 16. If Z-stack settings are set correctly ‘Z’ should be 0, ‘Z Start’ should be 1.00 and ‘Z End’ should be -1.00 for all points. Select ‘Ready’ in the bottom left of the registered points list, this will verify the process. The start button next to ‘Ready’ will bold if errors were not encountered, selecting will initiate the process.

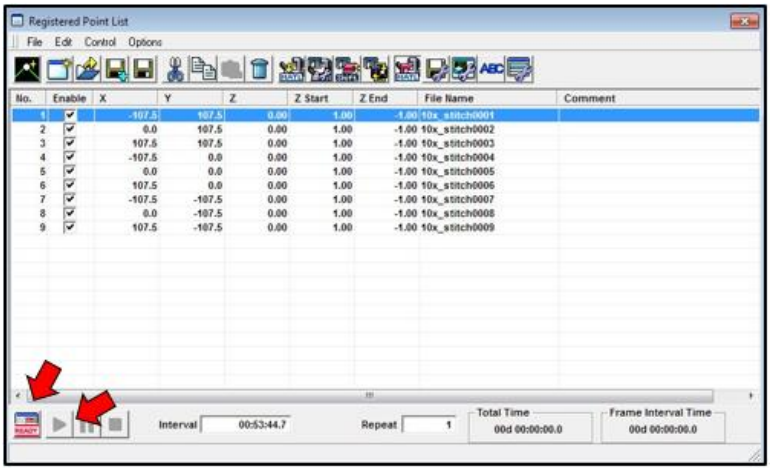

Figure 16. Registered Point List. Left arrow points to ‘Ready’ and right arrow points to start, which will bold after clicking ready

3.7 Image Processing Techniques

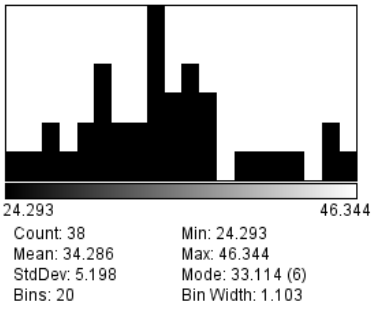

Figure 17. Sample Histogram of Mean Nuclear p21 Expression

ImageJ (NIH) was used to process images obtained from the confocal microscope. Image automation allows for accurate and quick measurements of fluorochrome expression within or around a cell. For example, to conclude how much p21 expression a population of cells is expressing. Previous methods of quantifying p21 expression dealt with manually counting each cell that had p21 expression in the nucleus and dividing by the total cells in the image. This method was very time-consuming and resulted in a binary count of either expressing or non-expressing cells. In reality there is a continuous gradient of how much expression each cell has, as seen in Figure 17.

3.7.1 Cell Viability

The “Cell Viability” macro is a basic image processing program that creates a region of interest (ROI) using the Hoechst channel around the nucleus. The ROIs are placed on the p21 channel to measure p21 expression only within the nucleus of each cell. The macro is summarized in Figure 18.

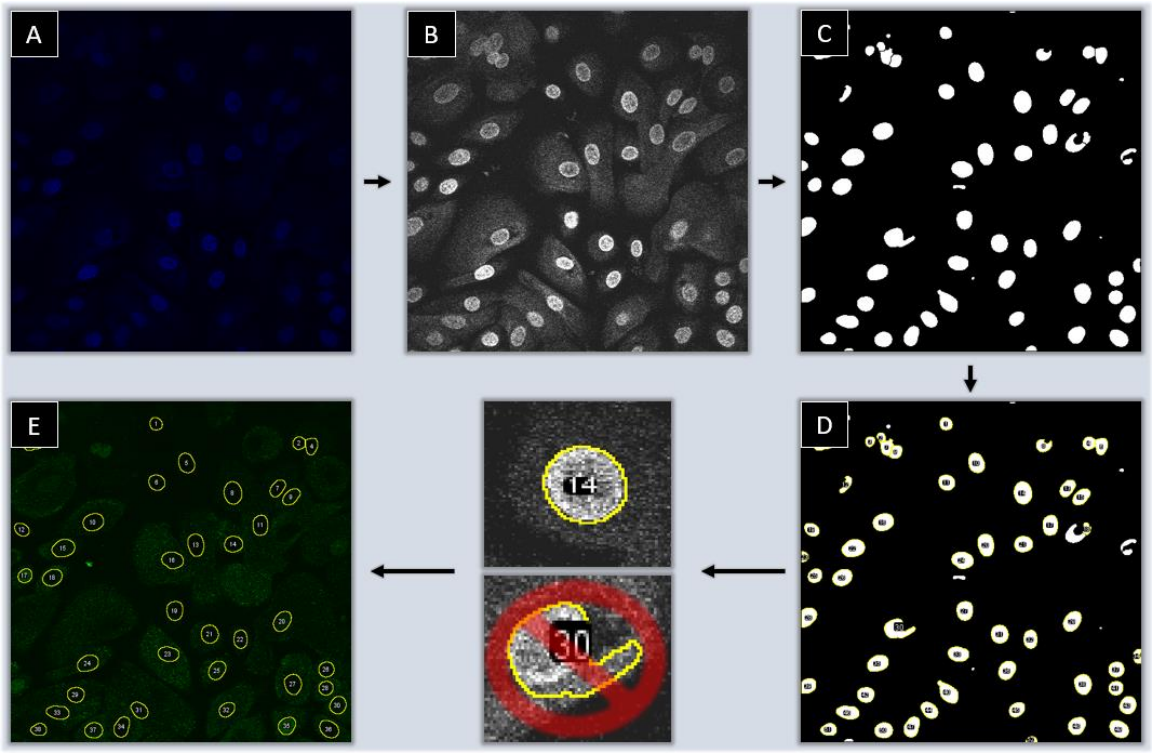

Figure 18. Cell Viability Flowchart. A) Raw tiff image obtained from the confocal microscope of the Hoechst channel. B) Converted to gray scale to see each nucleus clearer. C) Binary image after processing. D) Regions of interest found with the "Analyze Particles" function. Incorrect ROIs are manually deleted. E) ROIs placed on the p21 channel.

Processing

The macro initially runs the "Subtract Background" command to remove smooth continuous background noise while preserving the higher intensity pixels signifying the nucleus, seen to the right in Figure 19 A-B. This noise could be attributed to the confocal not taking level pictures do to a misaligned stage. Next, each pixel value is set to the lowest value of its surrounding pixels and then with the highest surrounding pixel values, with a connectivity of 8. The idea here is to reduce the value of pixels not near high value

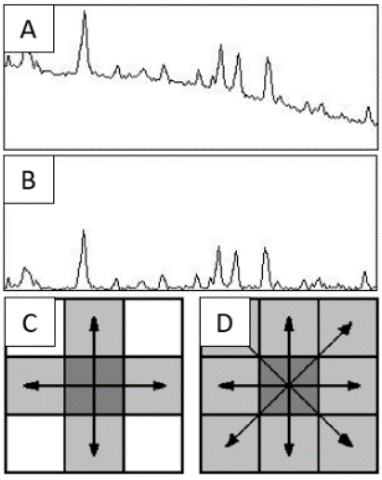

Figure 19. Example of Subtract Background and Pixel Connectivity.
A) Before and B) after using "Subtract Background". C) Pixel connectivity of 4. D) Pixel connectivity of 8.

pixels, while retaining the pixels that are near the high value pixels. This effectivly distances the higher nuclear values from the lower cytoplasmic and background pixel values. A Gaussian blur is used to smooth the image since the max and min filters cause blockiness. Contrast is then enhanced by saturating 0.25% of pixels to remove high expression outliers. A Binary threshold is applied to set each pixel to a value of either 0 or 1 depending on pixel value.

Figure 20. Cell Viability Processing Functions.

Binary Operations

The threshold applied does not consider surrounding pixels, so some nuclei may have holes, or have broken borders that were set to 0 on accident. To account for these errors "Dilate" followed by "Fill Holes" and "Erode" can complete the border, as seen in Figure 21. below.

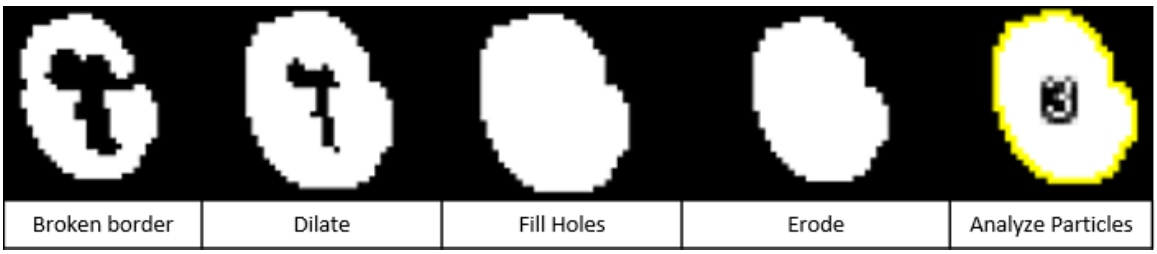

Figure 21. Cell Viability Binary Operations.

"Dilate" sets a pixel to a value of 1 if any pixels with a connectivity of 4 are 1. "Fill Holes" will set 0 values to 1 if connected 0 values are surrounded by 1. "Erode" does the opposite of "Dilate" to retain the original size of the cell. Note; "Dilate" is the same exact command as

"Maximum, radius=0.5" where they both only look at pixels with a connectivity of 4, whereas "Maximum, radius=1" would have a connectivity of 8.

Measurements

The final step of this macro uses the "Analyze Particles" command to find objects. This command identifies objects in binary space based on connected '1' values. If the identified objects are within the set parameters for size and circularity an ROI will be placed around them, identifying a nucleus.

3.7.2 Hoechst Image Tilt Correction

The 'Hoechst Image Tilt Correction' program was created when "Subtract background" was not performing well enough to account for an unlevel microscope stage. Instead of subtracting pixels, it attempts to retain all signal by multiplying a 3-dimensional parabolic gradient across all pixels depending on the pixel's location.

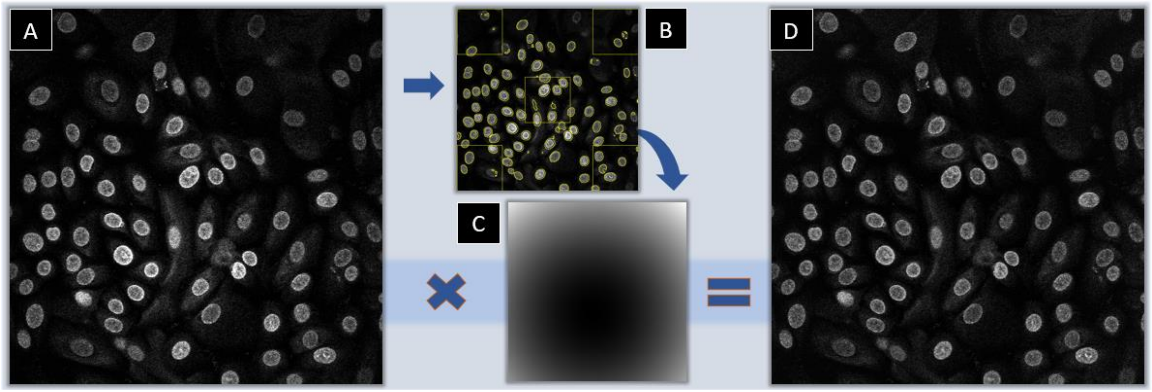

Figure 22. Flowchart of Hoechst Image Tilt Correction. Flowchart of the Hoechst Image Tilt Correction macro. A) Raw image. B) Measuring nuclei within specific zones. C) Generated parabolic gradient based on the measurements obtained. D) Raw image multiplied by the parabolic gradient.

The first part of the macro uses components of the 'Cell Viability' macro in order to find some nuclei in the image. Five squares are created that are a fourth of the height and width of the image in size. ROIs previously found by 'Cell Viability' are measured within each square to

get a mean pixel value and location of the centroid for each square, figure xx. B. In order to generate the parabolic gradient, two parabolas are averaged across the image, one in the x-direction, and the other in the y-direction. The two parabolas are created by solving a system of equations using three points, seen in Equation 2, where the x values denote the three centroid x positions of the top left, middle and top right squares, and the z values are their respective means.

$$\begin{bmatrix} \boldsymbol{x_1^2} & \boldsymbol{x_1} & \boldsymbol{1} \\ \boldsymbol{x_2^2} & \boldsymbol{x_2} & \boldsymbol{1} \\ \boldsymbol{x_3^2} & \boldsymbol{x_3} & \boldsymbol{1} \end{bmatrix} = \begin{bmatrix} \boldsymbol{z_1} \\ \boldsymbol{z_2} \\ \boldsymbol{z_3} \end{bmatrix} \tag{2}$$

Solving the matrix yields three equations to solve for 3 coefficients, A, B and C:

$$\boldsymbol{A_x} = \frac{x_3(z_2-z_1)+x_2(z_1-z_3)+x_1(z_3-z_2)}{(x_1-x_2)(x_1-x_3)(x_2-x_3)} \tag{3}$$

$$\boldsymbol{B_x} = \frac{x_1^2(z_2-y_3)+x_3^2(z_1-z_2)+x_2^2(z_3-z_1)}{(x_1-x_2)(x_1-x_3)(x_2-x_3)} \tag{4}$$

$$\boldsymbol{C_x} = \frac{x_2^2(x_3z_1-x_1z_3)+x_2(x_1^2z_3-x_3^2z_1)+x_1x_3(x_3-x_1)z_2}{(x_1-x_2)(x_1-x_3)(x_2-x_3)} \tag{5}$$

The coefficients are then used to complete the parabola formula of Equation 6.

$$z(x) = A_x\, x^2 + B_x x + C_x \tag{6}$$

The same set of equations are used to find the y-direction parabola. The two equations are then simply averaged together as Equation 7.

$$z(x,y) = \frac{A_x x^2 + A_y y^2 + B_x x + B_y y + C_x + C_y}{2} \tag{7}$$

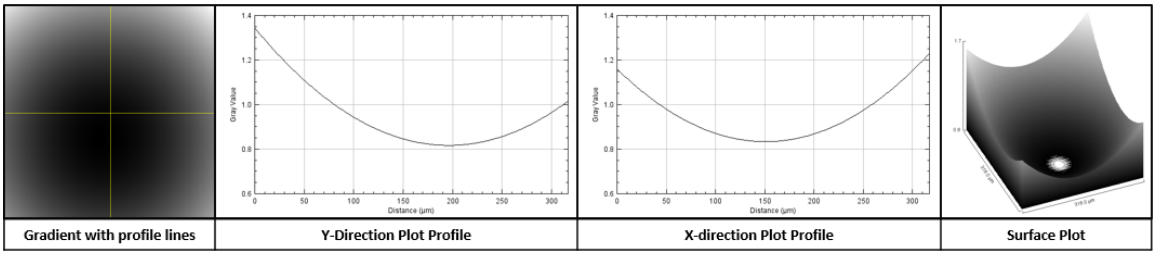

Figure 23. 3-Dimensional Parabolic Gradient. Visual representation of the parabolic gradient in terms of two plot profiles going through the middle in the x and y direction, and a 3-dimensional surface plot.

Equation 6 can be visualized in Figure 2, if the gradient were an image. The gradient would then be multiplied against the initial raw image to produce the corrected Hoechst channel. Darker values decrease pixel intensity, while lighter values increase pixel intensity.

3.7.3 Hoechst Local Area Contrast Normalization

The 'Hoechst Local Area Contrast Normalization' macro is similar to the 'Hoechst Image Tilt Correction' such that it is intended to brighten dimmer nuclei as a pre-processing technique. It is different though, that it does not use previous nuclei ROI to use as measurement zones and global values do not influence each other. Instead It only looks at local values and performs operations within. This macro only processes local segments of an image as a 6x6 matrix, making 36 zones. Each zone's processes will not affect other zones values whatsoever.

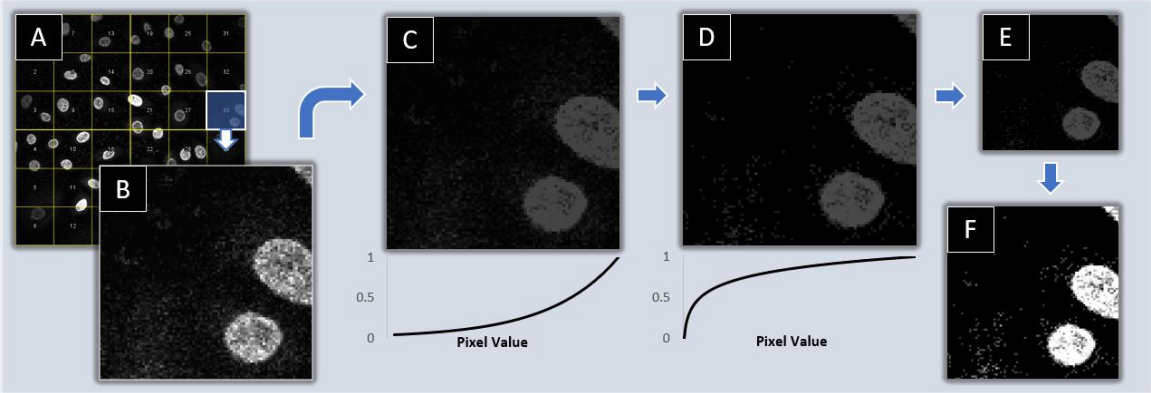

Figure 24. Flowchart of the Hoechst Local Area Contrast Normalization. A) Raw image in a 6x6 grid. B) One square from the grid. C) After pushing saturated pixels down. C.1) Scale to be applied to every pixel below the mean. Removes background noise. D) After scale has been applied. D.1) Logarithmic scale to be applied from 0 to max pixel intensity measured within the square. Isolates higher intensities from lower. E) After scale has been applied. F) linear scale to match 8-bit max of 255.

The program first measures a zone for the mean, max and standard deviation of that zone in order to 'push down' the max. This is done by creating a new maximum based on the mean and standard deviation, seen by Equation 8.

$$NewMax = (mean + 1.7 * Standard\ Deviation) \quad 8$$

This can be seen by a higher number of saturated pixels in Figure 24C. With the new maximum set the zone is measured again and an exponential equation, Equation 9, is used to descale all the pixels below the mean in order to remove noise and some cytoplasmic expression. Where 'v' is the observed pixel value, m is the mean, and p is scaled pixel value.

$$if(pixel\ value < mean), p = \frac{e^{v*\frac{\log(m)}{m}}}{m} \quad (9)$$

The result of that operation can be seen in Figure 24D. After remeasuring the zone again, a logarithmic contrast equation, Equation 10, is then applied to all values, up to the max of the zone. Where the v is the observed pixel value, p is the scaled pixel value, and Max is the max value within the zone.

$$p = v * \frac{\log(v)}{\log(Max)} \quad (10)$$

A linear scale is then applied to raise the max zone value to the 8-bit maximum of 255 with Equation 11.

$$p = v * \frac{255}{Max} \quad (11)$$

Figure 24F Shows the result of the process. The program then goes to the next zone and repeats the process for all 36 zones.

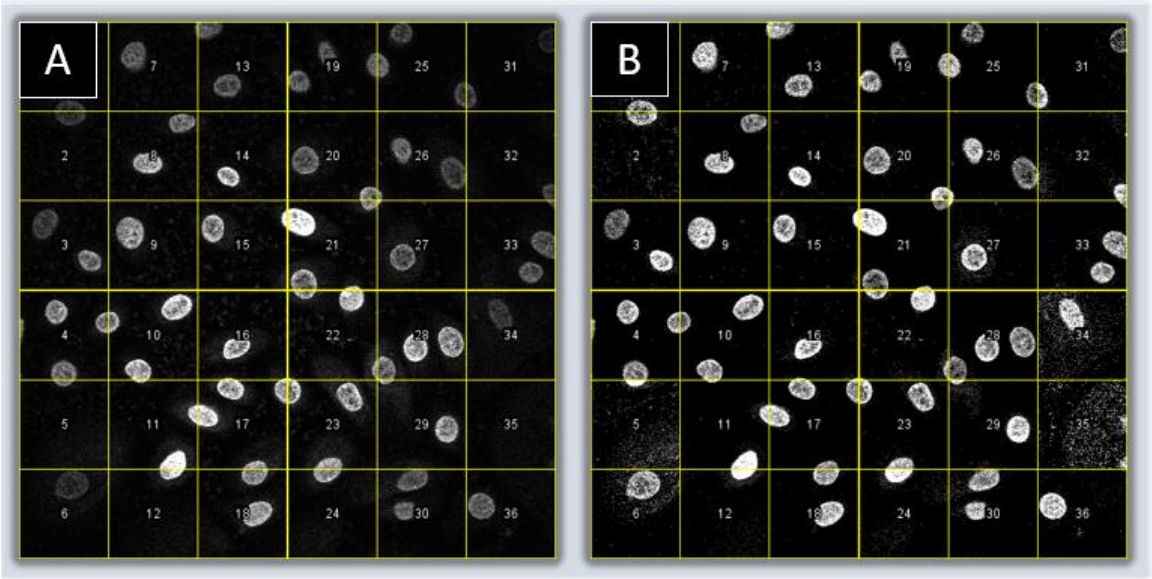

Figure 25. Result of Hoechst Local Area Contrast Normalization. A) Before and B) after the Hoechst Local Area Contrast Normalization macro.

3.7.4 Maxima Point to ROI

The Maxima Point to ROI was the first program to look at a large number of cells that were imaged with a magnification of 10x. It was intended to see how many dead cells there were in a population since the borders of the nuclei were not very accurate.

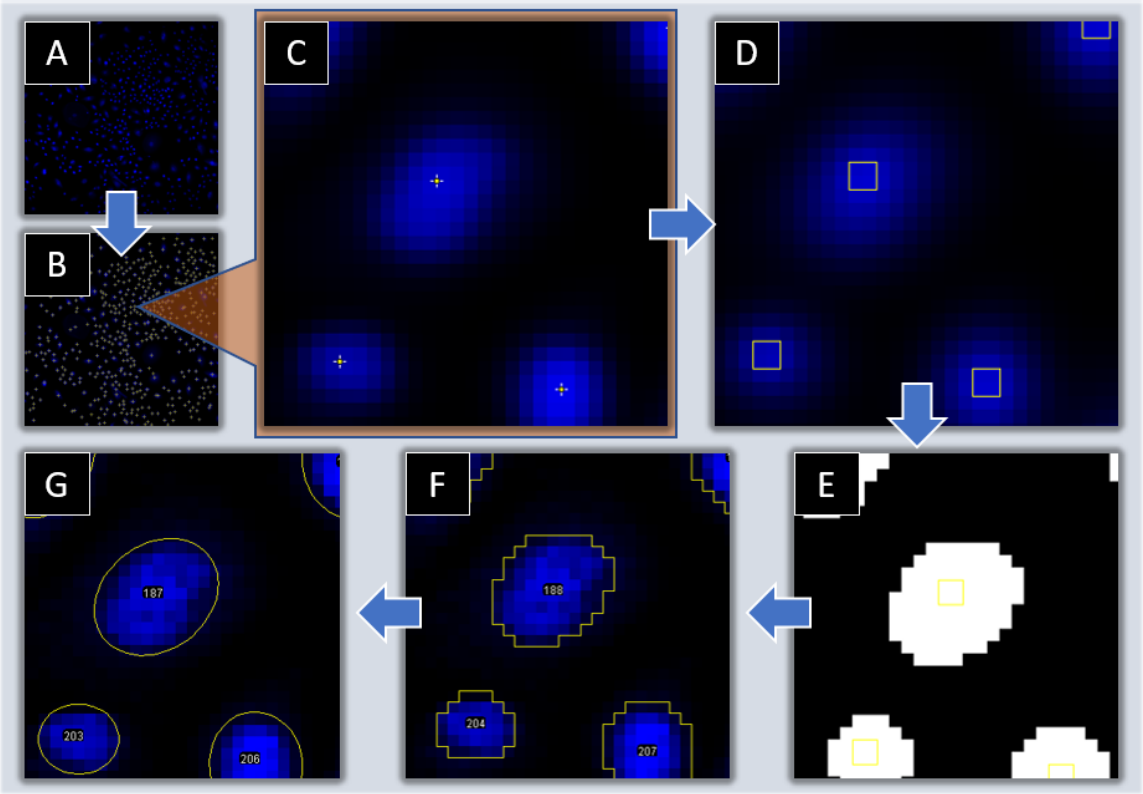

Figure 26. Maxima Point to ROI A) Raw 10x image. B) All nuclei marked with "Find Maxima" after a Gaussian blur. C) Exploded view observing one cell. D) After setting the marked pixels to max value and gaussian blur looped four times. E) Binary conversion after "Moments" threshold applied. "Watershed" is the only binary operation used. F) Result of "Analyze Particles". G) Converted ROI to an ellipse, moved center to centroid, and filtered.

The first part of the Maxima Point to ROI macro uses the "Find Maxima" function to mark every nucleus in the image. A Gaussian blur is applied beforehand to smooth for noise reduction so only one maxima is found for each nucleus. Then each point is converted into a 2x2 ROI where that ROI is set max then blurred four times. The idea here is to spread out the pixels set to the max value, so the threshold will pick it up. A "Moments" threshold is applied follow by "Analyze Particles" to find the nuclei borders. Since resolution is low for these images an ellipse

is fit to each ROI to smooth out the ROI borders. The ROIs are then moved so the center matches the centroid, or center of mass. The macro finishes up by filtering out ROIs with a mean less than an eighth of the scale, which would be about 32 out of an 8-bit scale, or 500 for a 16-bit.

3.7.5 Stack to Optimal Raw Image

This macro processes '.OIB' images from stacks and saves them as individual entities per channel. The loaded '.OIB' image file is first converted from a stack to individual images and then re-stacked into one stack per channel. Each stack is scaled by interpolation, by a multitude of 2, to increase resolution in every axis. The p21 stack is saved as a stack for measurement analysis in section 3.7.7. The Ethidium Homodimer-1 channel, or "Dead" channel, is saved as a single image of the max intensity projection, where the max intensity is chosen within the stack for each pixel. The Hoechst channel has each image in the stack go through a background subtraction process, seen in Figure 27.

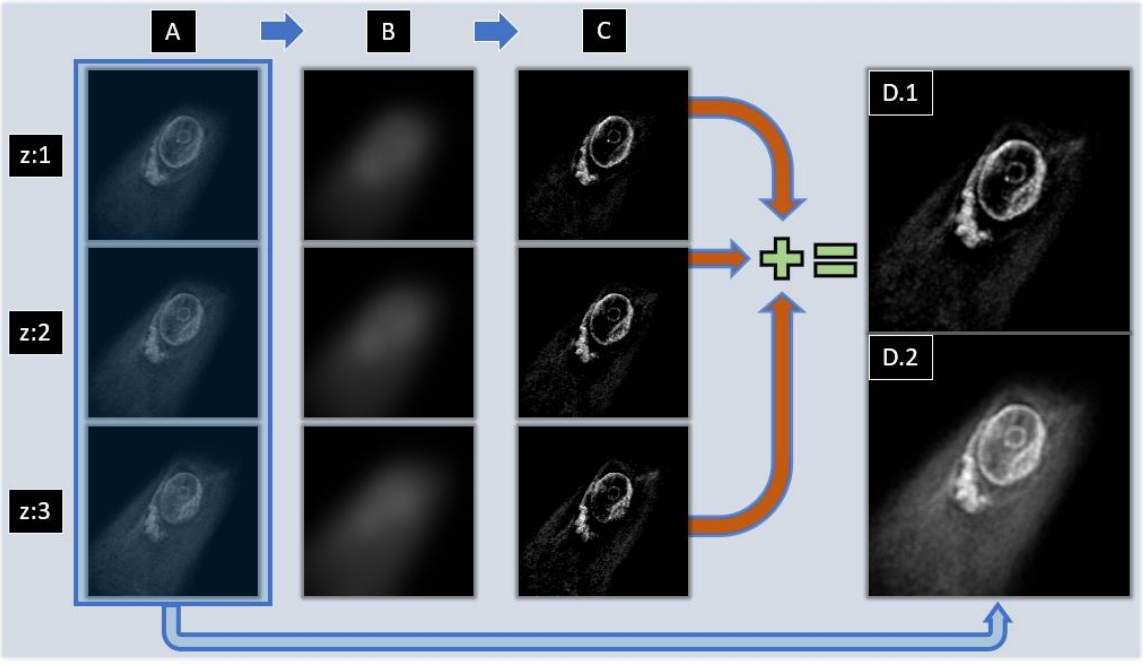

Figure 27. Hoechst background subtraction process comparison. A) Raw image stack. B) After severe Gaussian blur C) Gaussian blur subtracted from the original D.1) Resultant summed z-projection. D.2) Without background subtraction, z-projection sum of the raw stack. Interpolated images not shown.

After the subtraction the images are restacked, and a vertical filter is applied to all of the images. The filter chooses the highest value 3 images away for all 6 images to ensure the nucleus does not have a broken border. A broken border can be seen in Figure 27C for z:3. The stack images are then all summed together and saved.

3.7.6 Binary Threshold Drop

The Binary Threshold Drop is the last macro created to accurately find Hoechst borders in large images, specifically 3x3 40x stitched images. It was made to be robust with minimal tweaking for the code to work properly, where the only parameter needed to change is minimum area of a nucleus. It takes attributes from all the previously described programs where it corrects the image first, applies an image process algorithm, and goes through several logic filters.

Image Correction

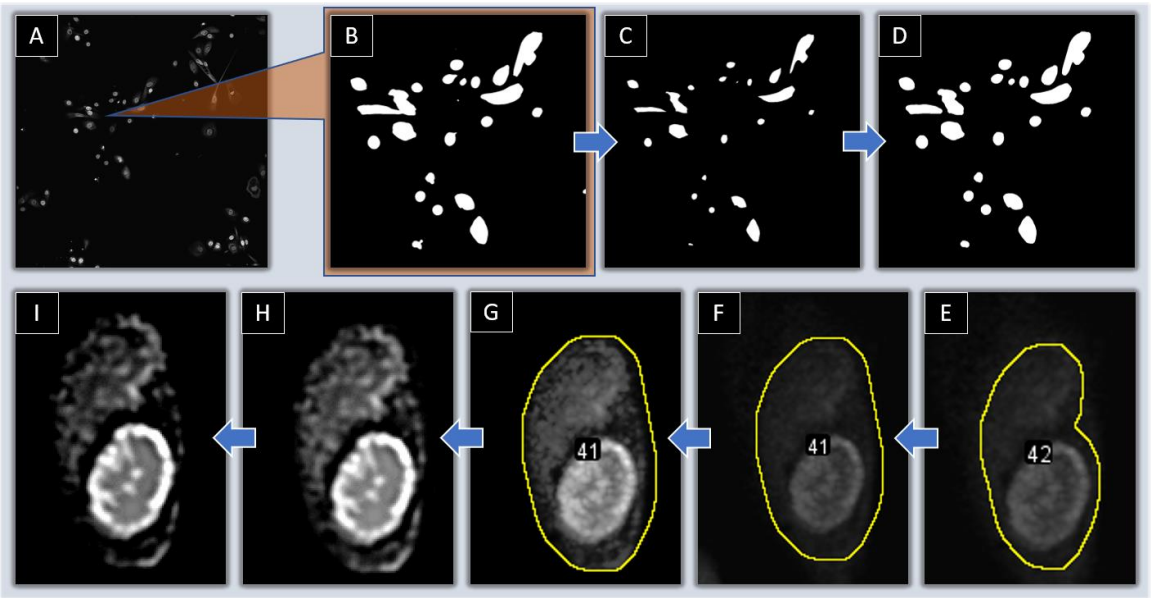

Figure 28. Binary Threshold Drop, Image Correction Flowchart. A) Raw 3x3 stitched matrix of 40x images. B) 1-255 8-bit threshold after subtracting by the median. C) Minimum filter looped until anything under the set "minimum area" has been erased. D) Maximum filter looped as much as the minimum filter to regain original size. E) After "Analyze Particles". F) Convex hull applied and enlarged 2um. G) Exponential scale applied to all pixels under the median. Median measured without including zeros. Scaled max to 8-bit max of 255. H) 'Fill Holes', 'Gaussian Blur' and 'Unsharp Mask' applie¿d in order. I) Pixels with value less than half the median are removed.

The first stage corrects the image by normalizing contrast between nuclei. The first goal is to get the largest ROI around each cell and minimizing capturing more than one cell per ROI. Achieving this makes normalization more effective as it was designed to process each ROI with only one whole cell in it, including potentially cytoplasm and background. It was found that

removing all pixels under the median, not including zero, removed enough background information to nearly always isolate all the cells. The image is turned into binary by making every value above one, equal one. To further isolate cells a “Minimum” filter is used to shrink the binary objects enough to remove all objects with an area less than the set “Minimum Area”, formula seen in Equation 12 and visualized in Figure 28 A “Maximum” filter is performed with the same method to restore original size.

$$AreaStop = \frac{sqrt\left(\frac{\frac{MinimumArea}{VoxelWidth}}{\pi}\right)}{3},$$

$$for(i = 0, i < AreaStop)\ \{\text{ Maximum, radius=3}\} \quad (12)$$

“Analyze Particles” captures all objects larger than the set “Minimum Area”, a sample cell is seen in Figure 28 E. Each ROI goes through a convex hull transformation and enlarged to ensure the ROI has all of the cell within, and also is not processing a non-cell like shape. For each ROI, an exponential scale is applied to all pixels under the median and is scaled to the 8-bit max of 255. The “Fill Holes” macro, developed by David Legland and Ignacio Arganda-Carreras, fills in the valleys of the nucleus [68]. However, does not fill enough to match the intensity of the edges, so a Gaussian blur is applied to distribute the brighter pixels, followed by “Unsharp Mask”. The “Unsharp Mask” command subtracts a blurred image from the original and rescales to match the original images contrast. The image is now ready for the ‘Threshold Drop’ algorithm.

Dropping the Threshold

The threshold described is characterized as the pixel-value range observed for processing. Starting at the maximum value of 255, over iterations the threshold lowers in increments uncovering nuclei. Within iterations ROIs are captured, which results in numerous ROIs per cell after the threshold drop has finished.

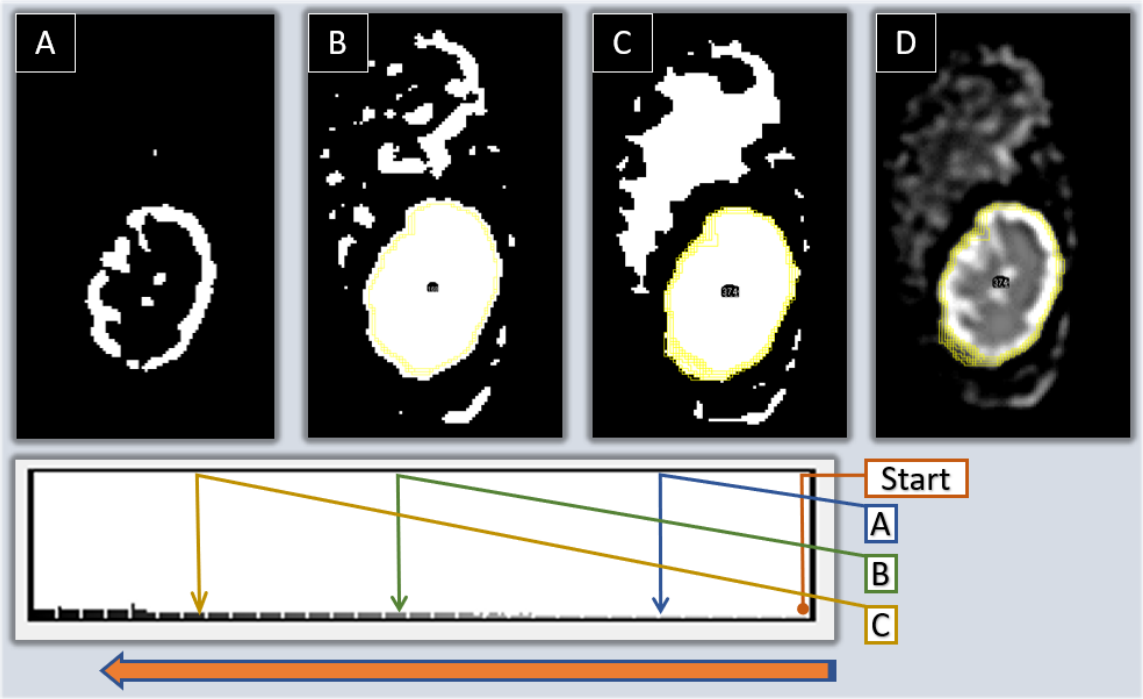

Figure 29. Threshold Drop Corrected Image. Starting at the max pixel value of 255, over iterations the threshold is lowered slowly uncovering pixels in terms of value. ROIS are obtained as the threshold drops A) Threshold from 190-255. B) Threshold from 75-255. C) Threshold from 20-255. D) Completed threshold drop with several ROIs around the same nucleus.

Prior to starting the threshold drop, the median pixel value is measured of the entire image, without counting 'zero' values. The threshold drop is repeated three times with different circularity parameters set each time for "Analyze Particles".

The first repetition has a circularity range of '0.80 to 1.00', where circularity is defined in Equation 12 as a function of area A and perimeter P. The increment of how fast the threshold dropped is defined by Equation 13. This means the threshold will drop from '255', the max value, to '3', the minimum defined value, but in five increments.

$$Circularity = \frac{4\pi A}{P^2} \tag{13}$$

$$Increment = \frac{(255-3)}{5} \tag{14}$$

The second repetition retains the same increment as the first. The circularity is reduced to a range from 0.60 to 0.80.

The third iteration has a further reduced circularity of ‘0.40’ to ‘0.60’ in order to register the remaining nuclei that had non-ideal shape. The increment has changed to Equation 15, so the drop does not go too far down and register the cytoplasm. Instead the lower-bound threshold of ‘3’ is changed to the median measured prior to the threshold drop algorithm. The maximum area “Analyze Particles” uses is also dropped from ‘600’ to ‘400’. If the threshold is dropped too low with this low of a circularity, there is a very large chance non-nuclei are captured.

$$Increment = \frac{(255 - med)}{5} \tag{15}$$

Figure 30. Binary operations performed between iterations.

Within each threshold increment the image is converted to binary where several operations are performed prior to “Analyze Particles”. First is a median filter to smooth, then “Fill Holes” to fill in any non-solid objects, followed by “Erode” to reduce object size and “Watershed” to split objects. The reduction in object size causes necking which can make watershed more effective. Objects are further reduced using a minimum filter to eliminate or distance cytoplasm. The median filter is used again since it has a greater effect on small objects, like the cytoplasm, than it does on the larger cell. The cell will smooth whereas the small objects will just be eliminated or greatly reduced. This is crucial as after the maximum filter a “Close” command is used to reattach the broken cell seen in Figure 30, but if the median filter isn’t used it could reconnect cytoplasmic objects. The final operation is another median filter to smooth out the cell.

Region of Interest Selection

The threshold drop produces many ROIs per cell and only one must be used for measurements. To select the best ROI per cell a ranking system was developed based on the pixel intensity inside the ROI and the shape of the ROI itself, where the ranking is defined by Equation 16.

$$Rank = \frac{RawIntDen}{Area} * Solidity^2 \quad (16)$$

Solidity is a measure of shape for the ROI where a higher solidity is better. Solidity is defined as the amount of area a convex hull adds divided by the initial area, see in Figure 31. Convex hull is like wrapping a string around the object and finding the shortest possible perimeter. "RawIntDen" is the summation of all pixel values and dividing by the area is essentially looking for the mean, except area is scaled in microns. The mean is calculated using the number of pixels and not the actual distance. This gives less weight to the area, but still influences the rating.

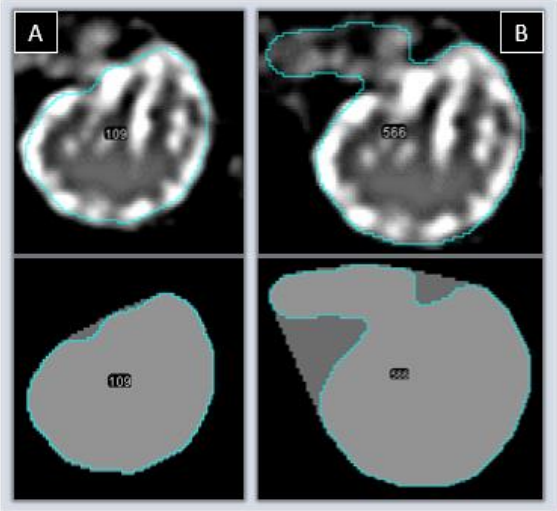

Figure 31. Solidity Comparison of ROIs.
A) High and B) low solidity object. Darker grey shows the added area convex hull creates.

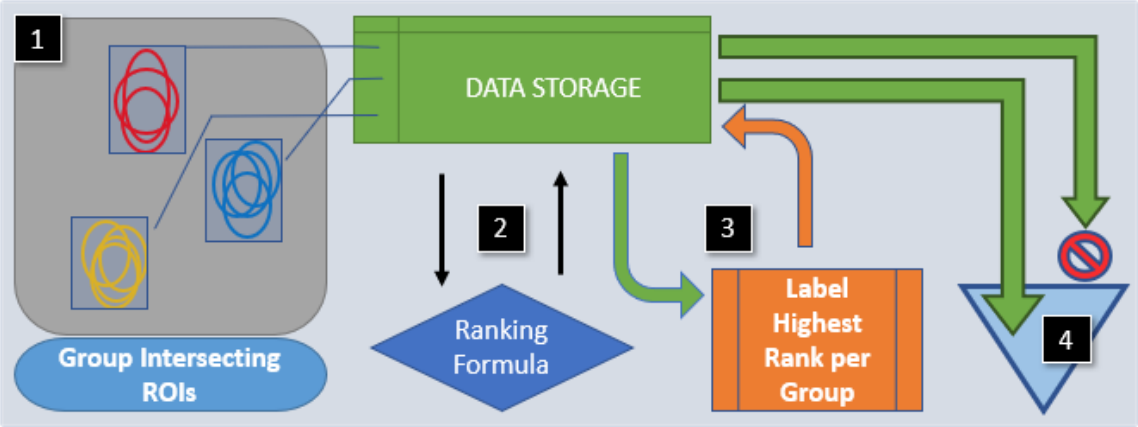

Figure 32. Single ROI Selection Flowchart. 1) ROIs are grouped by if they intersect. Grouping information stored in a table. 2) The ranking formula gives a value to each ROI based on shape and content. 3) Pulls ranking and grouping data. Labels each group with the ROI that has the highest rank. 4) ROIs labeled 'Good' aren't deleted, leaving one ROI per cell.

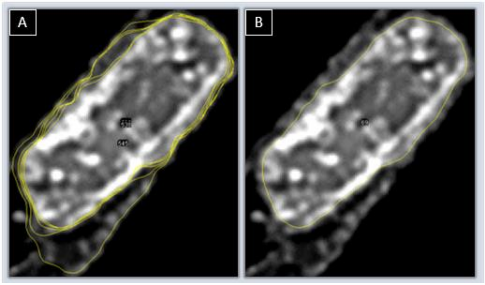

Figure 33. Example of ROI Selection. A) Before and B) after the selection process.

The first stage (Figure 32.1) starts by measuring the first ROIs center coordinates. For each following ROI, if an ROI shares the same center coordinates is labeled with the group number and set to 'used'. The next iteration goes to the second ROI and performs the same action, unless the ROI is labeled as 'used', then it is skipped. The second stage (Figure 32.2) is independent of the first stage's actions and ranks each ROI using Equation 16 above. The third stage (Figure 32.3) looks at each group and labels the ROI with the highest rank "Good ROI" and all others as "Bad ROI". The last stage (Figure 32.4) deletes all "Bad ROIs" and retains the "Good ROIs" (Figure 33B).

Filtering

Sometimes an ROI will not be grouped properly because it is outside of the reference ROI's center coordinates, seen in Figure 34 These ROIs are always smaller because they were prematurely captured in the threshold drop and only encompass a part of the cell. To get

around this all ROIs are “Combined” and immediately split to combine the mis-grouped ROI to the others of the cell. A workaround for this would be to “AND” the two ROIs together, which results in only the shared area of the two ROIS. If the result’s area is more than 0, then they intersect. This method isn’t used though because the program would take a significant time to finish and the filtering method has worked so far.

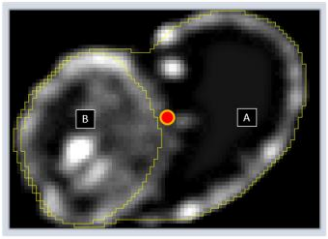

Figure 34. Potential ROI Mis-Grouping.
A) Reference ROI with the center coordinates marked by the red circle. B) ROI that wouldn’t be grouped with the reference

The second filter removes “Tails” or parts of an ROI that shouldn’t be there, seen in Figure 35. To do this an image of the same size has every value set to ‘0’ and each ROI is transcribed as a ‘1’ value. Since the image is now binary a watershed command is used to split any possible ROI’s tails off. “Analyze Particles” is used as a filter by eliminating objects smaller than 25um in area. Instead of outputting ROIs with “Analyze Particles” it outputs a mask with the objects that got through. Since watershed will split some cells down the middle the masked image goes through a set of maximum followed by minimum filters to recombine them and a median filter to smooth the cut edge. “Analyze Particles” is then used to convert the masked image back into ROIs.

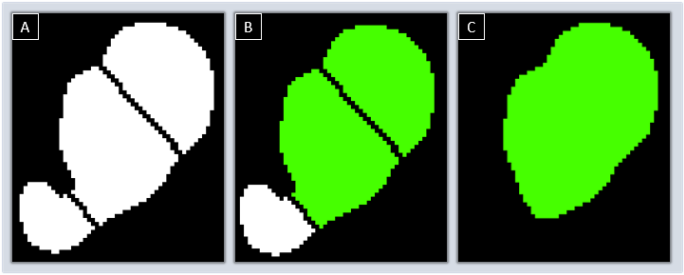

Figure 35. Second Filter to Remove 'Tails'.
A) An ROI that was masked and watershed. The watershed cut off the tail, but also split the cell. B) The filter only selects objects above a set size to remove tails, but not split cells. C) Cell is recombined and edges are smoothed with a median filter.

The final filter is made to cleanup any mistakes based on the ROIs content. It’s possible a bad ROI will make it through the other filters and redundancies programmed in the other parts. If that happens this filter is meant to catch them with a set of parameters. If any ROI falls within Equation 17’s range, then they are deleted. Where variable R is roundness, the inverse of aspect

ratio. M is the mean pixel intensity, A is the area of the ROI and S is the solidity of the ROI. The original raw image is used for the pixel-values measurements.

$$(S < 0.9\ AND\ M < 25)\ OR\ (A < 50)\ OR\ (R < 0.4\ AND\ M < 100)\ OR\ (M < 20) \quad (17)$$

The resulting ROIs are visually inspected to ensure the program is working correctly. Any obscure or ROIs on the edge of the image are deleted.

3.7.7 p21 Variable Slice Measurement

This measurement macro was developed to be used after the "Binary Threshold Drop" program in the sense it uses the ROIs obtained. Prior methods of p21 measurement were to first combine the stacked images by either a max or summed projection. That methods do not produce accurate measurements because background p21 expression would compound on each other for both a max and summed projection, as seen in Figure 36.

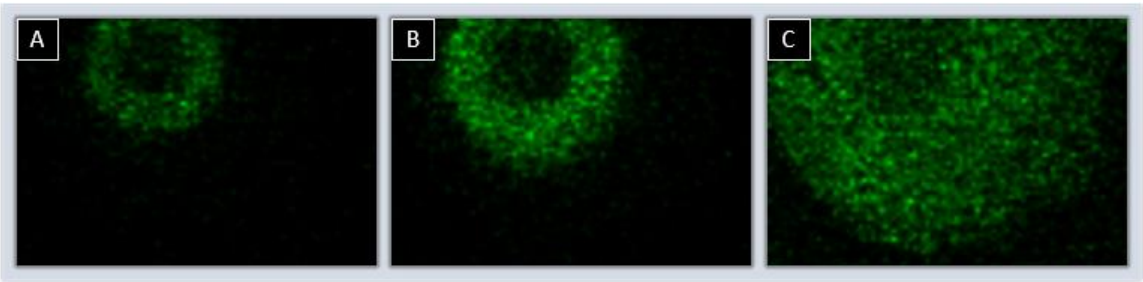

Figure 36. p21 Variability Between Slices in Z-Stack. A) Up +1 µm from reference B) Reference start slice C) Down -1 µm from reference slice.

To get around poor measurements each Hoechst's channel slice is analyzed for each cell and the slice with the greatest difference between the outer edge and the middle is selected. A properly stained Hoechst nucleus will look as if it is hollow when looking at a slice going directly through the middle, Figure 37. If the slice is looking at the bottom of the nucleus it will look

more plateau like than that of the middle, and if used as p21 measurement, then p21 underneath the nucleus will be measured as well, distorting results.

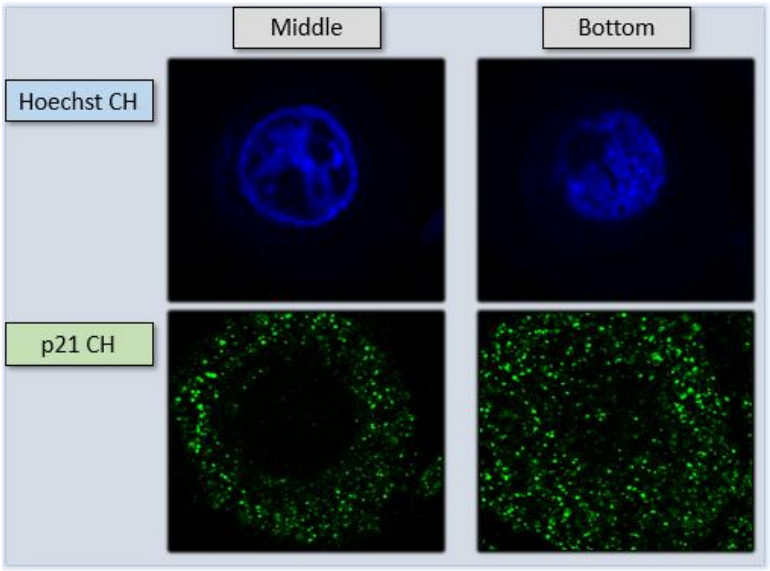

Figure 37. Hoechst is the identifier of the correct slice. Middle Hoechst is more hollow than the bottom, the indication of the correct slice for measurement. The bottom of the nucleus looks plateau like and if p21 is to be measured from this slice it will result in capturing p21 underneath the nucleus, not inside.

The short macro starts by saving the ROIS obtained from the Binary Threshold Drop program in the opened image's directory for storage and future failure analysis. The Hoechst channel is measured for the mean and shape descriptors and copied into an Excel file for data analysis. The Hoechst channel then goes through a loop where each slice for each cell has the Roi measured, then shrunk by 2um and measured again. The biggest difference between those two measurements of each slice is recorded in to a table as the ideal measurement slice. The p21 channel is then opened and the indexed ideal slice is used to measure each cell's nuclear p21 content. Another loop uses the same slice number that was recorded into the table to measure what the mean pixel value is immediately outside of the nucleus, seen in Figure 38 D. The table is then copied and pasted into the same Excel file for analysis. The macro finishes up by measuring the Ethidium Homodimer-1 channel only for the mean and max to assess dead cells.

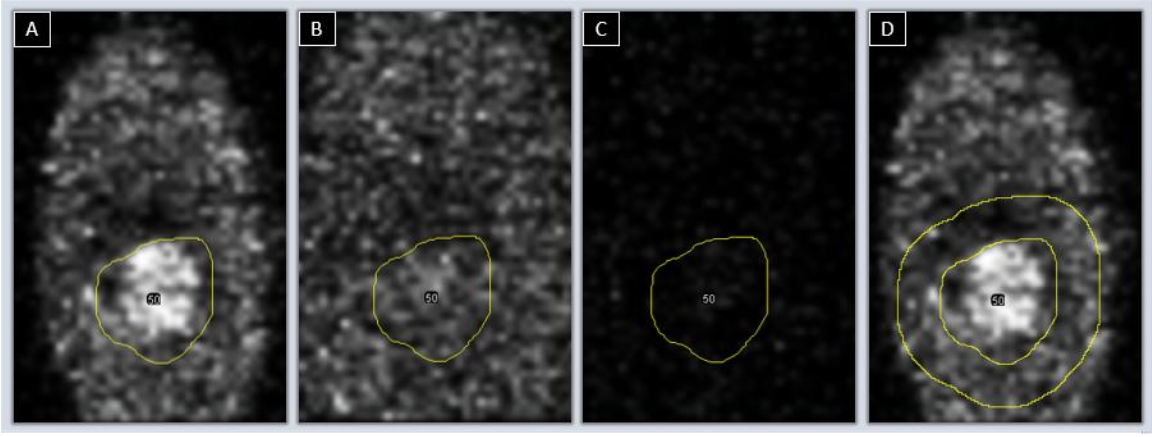

Figure 38. p21 Channel Slice Selection for Measurement. A) Up 1um from reference B) Reference start slice C) Down 1 µm from reference D) Slice that was determined ideal by the Hoechst Channel. Band around to measure expression immediately outside of the nucleus.

3.7.8 fSM Donut ROI measure

The fSM Donut ROI was created to measure cytoplasmic fluorescent sphingomyelin (fSM) while excluding the region the nucleus would be in, hence the 'Donut' name.

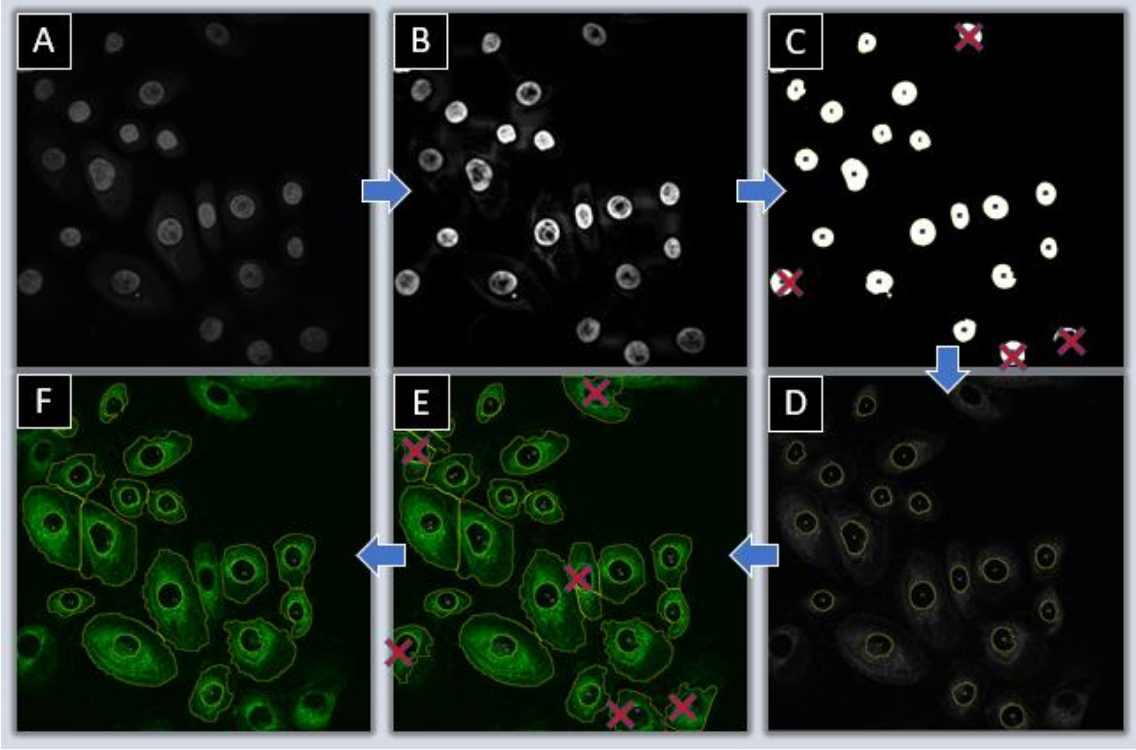

Figure 39. fSM Donut ROI Measure Flowchart. A) Hoechst Channel grey-scale. B) Processed image. C) ROI acquisiton of nuclei. D) Nuclei ROI on fSM channel. E) Cytoplasm ROI acquired. F) Nuclei ROI subtracted out of the cytoplasm ROI leaving behind a donut-shaped ROI of the cytoplasm.

The first part finds the nuclei ROI with the same method as 3.7.1, Figure 39[A-C]. ROIs near the border, and broken or incomplete ROIs are deleted, Figure 39[C]. The Hoechst channel is closed, fSM channel is opened, and the nuclei ROIs are combined and inverted, Figure 39[D]. The cytoplasm ROI is found with similar methods as 3.7.1, Figure 39[E]. Finally, the inverted nuclei ROI is 'AND' with every ROI, leaving behind a donut-shaped ROI for each cell, Figure 39[F]. At this point ROI's can be measured.

3.7.9 fSM Rotation measure

Using the donut-shaped ROIs 3.7.8 found, this macro measures where the fSM is located in the cell. The macro creates a straight-line plot profile from the center of the ROI outwards and only measures values outside of the nucleus, but inside the cytoplasm every 6 degrees for 360 degrees.

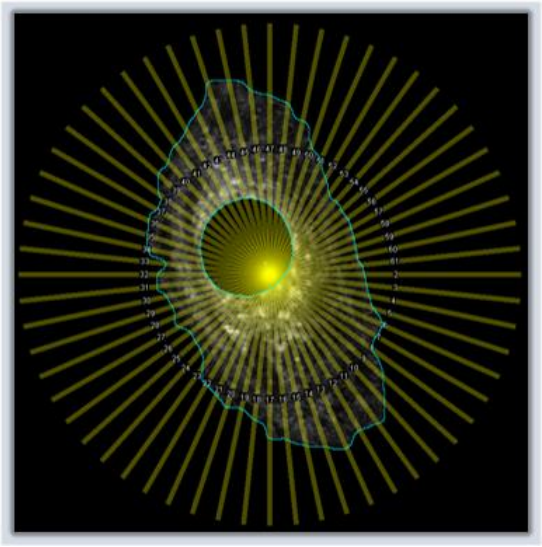

Figure 40. fSM Rotation. 200um line measures values every 6 degrees

Every value outside of the ROI is set to 0 using the 'Clear Outside' command. The measured lines are output as arrays into a '.CSV' file where a MATLAB code developed by Stephanie Switalski removes all '0' values from the array and interpolates to 100 data points to become a percent distance from nucleus to cytoplasm. The percent-distance data was then

averaged across each percent to form one array for each cell. Use of this macro can be seen in section 4.8 Fluorescent Sphingomyelin Distribution Time Study.

Chapter 4: Summary of Experiments

This chapter details each experiment that occurred while investigating sphingomyelin and the interesting effects that happened to keratinocytes when this lipid was exogenously added in culture. To be as transparent as possible, experiments nor data were omitted. Any data transformation performed was applied equally and appropriately to conjugate data sets to minimize bias at all costs. The summary of all experiments performed is found in Table 2.

Table 2. Summary of Experiments by Category.

Experiments		Goal	Macro	Imaging Method	Ref.
Poly(D-Lysine) Qualification	PDL Qual. Pilot	Assess dead cell adhesion & cytotoxicity with PDL. Develop large area image analysis methods.	3.7.1	20x & 10x stitch	4.1
	EthD-1 Qual.	Assess EthD-1 washout from permeabilization. Develop image correction automation.	3.7.2	40x	4.2
	PDL Qual. 2	Find optimal PDL conc. & incubation times	3.7.2 3.7.3	10x stitch with 3 layer z-stack	4.3
	PDL Qual. 3	Full evaluation of p21, EthD-1 & Hoechst with PDL	3.7.2 3.7.3 3.7.4	10x stitch with 6 layer z-stack	4.4
p21 Analytics of live and dead KRT	p21 Expression 1	Validate p21 expression ratios of previous experiments. Improve sample size with 10x stitches	3.7.2 3.7.3	10x stitch with 3 layer z-stack	4.5
	p21 Expression 2	Gather more samples to back first experiment. Improve sample quality with 40x instead of 10x	3.7.5 3.7.6 3.7.7	40x stitch with 3 layer z-stack	4.6
	p21 Expression 3	Qualitative analysis of high definition images	N/A	100x high definition images	4.7
fSM Distribution	fSM Distribution over time	Quantify where fSM is located within the cell over time points	3.7.8 3.7.9	60x	4.8
	Live Cell fSM Distribution over time	Quantify fSM distribution for a group of cells over a long period of time	3.7.10	60x & 100x time lapse	4.9

Throughout experiments it was very apparent that whenever UV was introduced, there were less cells in comparison to UV negative conjugates. When cells died from UV or become apoptotic, they detached and subsequently were aspirated off whenever liquid in the cell culture plates was replaced or removed. Liquid replacement occurs in nearly every step in both the culture and staining processes. Poly (D-Lysine) is an attachment factor that has been shown to leave more dead and apoptotic cells attached. Using this attachment factor has allowed for the analysis of dead and apoptotic cells to try and figure out how sphingomyelin alters p21 content in the nucleus and cytoplasm. The coating had to be qualified first to find the optimal concentration and incubation times, which is labeled as 'Poly(D-lysine) Qualification' in Table 2 below.

After qualification, the main experiment was performed to gather data and find optimal image acquisition and analysis methods for observation of 'p21 content of live and dead cells'. All three experiments had the same staining procedure and experimental setup. The first experiment, 'p21 Expression 1' used stitched images in a 3x3x3 matrix each acquired at a 10x magnification to view a large number of cells with 3 depths to choose from for accurate measurement. The second experiment had the same experimental parameters as the first experiment except with 40x magnification to get higher definition stitches at the cost of sample size. Both methods had the same results but using the 40x had less problems due to an unlevel stage. The 10x covered more area, and because of this the unlevel stage affected the quality of the stitches more. The last experiment in the series was a qualitative analysis of high definition 100x magnification images.

The last set of experiments quantified the molecular dynamics of fluorescently tagged sphingomyelin (fSM) over time. The first experiment measured the location of fSM in cells fixed at different time points, where a novel idea was used of taking measurements in straight lines

from the edge of the nucleus to the edge of the cytoplasm every 6 degrees, for 360 degrees for every cell. The last experiment observed a group of living cells at the time of adding fSM to the culture and where the fSM travels an extended period of time to try and determine where sphingomyelin is trafficked to.

4.1 Pilot Poly-D-Lysine Qualification

4.1.1 Summary and Goals

Previous experiments conducted in the lab always show a large decrease in cell population when culture plates were exposed to ultraviolet radiation. The population decrease is from programmed cellular death, apoptosis, due to irreversible genetic damage from the UVB [1]. When cells die they detach from the culture plate, and they cannot be analyzed with confocal microscopy. Poly-D-Lysine (PDL) was tested to verify if it helps with keratinocyte adhesion. If PDL helps adhesion, more dead and apoptotic cells would remain and could be evaluated for p21 content.

The goal of this experiment was a pilot study to evaluate if PDL offers greater attachment of dead and apoptotic cells than culture plates without PDL. Two 8-well culture plates were used, one with PDL and one without PDL as a control. Three dilutions of hydrogen peroxide [6%, 3%, 1%] were used to induce cell death. Ethidium homodimer-1 was used to identify cells that were dead while Hoechst was used to identify all cells. PDL manufacturer, Sigma-Aldrich suggested a 100ug/ml concentration to be incubated on the cell culture plate for 5 minutes followed by drying in a sterile environment for an hour [69].

The secondary goal of the experiment was to verify that PDL does not induce apoptosis. This was evaluated by comparing dead cell percent between control cell culture plates with PDL to without.

Confocal images were quantified using ImageJ macro 3.7.1 and analyzed in Excel. Cell attachment was evaluated by comparing percent dead cells of the population over the varying hydrogen peroxide concentrations between coated and non-coated culture plates.

4.1.2 Results

Table 3, shows that for every Hydrogen Peroxide concentration, there were a higher number of dead-labeled cells on the PDL coated plate in comparison to its conjugate, except for one of the wells without treatment. The total number of cells, Figure 42, vary quite a bit between images, so the percentage of dead to alive cells was used in analysis.

Table 3. Results of Pilot Poly-D-Lysine Qualification.

Dead Cells (#)		Total Cells (#)		Percent Dead Cells		Treatment (%H2O2)
Coated	Control	Coated	Control	Coated	Control	Hydrogen Peroxide
116	33	118	48	98.3	68.8	6%
130	44	135	178	96.3	24.7	6%
134	11	160	291	83.8	3.8	3%
18	5	222	242	8.1	2.1	3%
19	4	150	185	12.7	2.2	1%
87	67	110	184	79.1	36.4	1%
2	39	148	120	1.4	32.5	0%
40	3	128	139	31.3	2.2	0%

Figure 41 graphs that percentage for each well. A simple linear trendline was used to compare and evaluate how many dead cells were left attached between coated and uncoated cell culture plates.

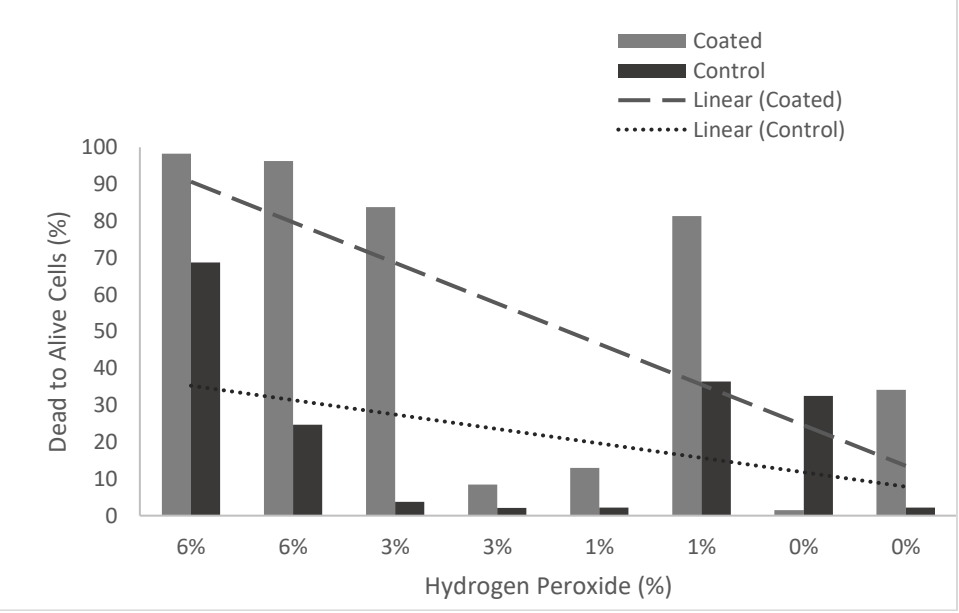

Figure 41. Dead Cells Comparison. Cell culture plate coated with Poly-D-Lysine or not coated as control. Percent dead cells to respective total.

Figure 42 shows the variability between images in terms of cell count. Both images are the same treatment in the same well number, but Figure 42 A has the PDL coating and B does not. For the cell to be counted as 'Dead' a threshold was set where every cell with at least one pixel above a value of 33 is counted, out of an 85-value maximum.

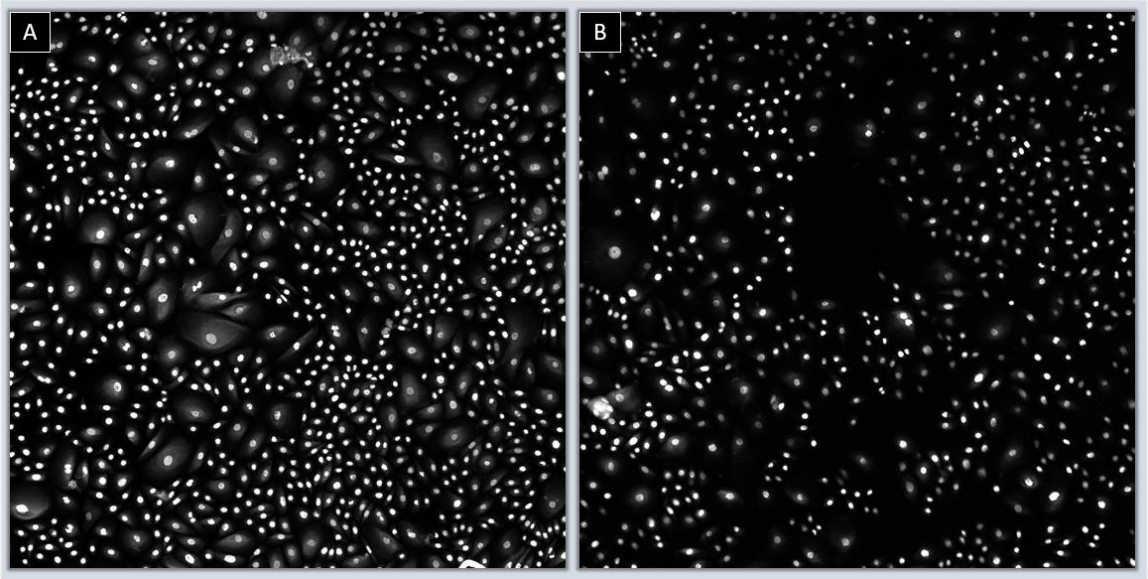

Figure 42. Population Variability. Samples of the same treatment and well position. A) Poly-D-Lysine coated cell culture plate, (well 4: 3% H_2O_2). B) Uncoated cell culture plate, (well 4: 3% H_2O_2). 10x images with enhanced contrast to 2% saturated pixels for better clarity.

4.1.3 Discussion

Since this is a pilot study and has a low number of replicates, statistical analysis cannot be used, but it is evident, that plates coated with PDL had a higher number of cells, and of those, there was a higher percent of dead cells. Another experiment was needed to test different concentrations and incubation times of PDL on the plates to find the optimal keratinocyte adhesion. It was found that when taking large stitched images, a portion of the image could be out of focus,

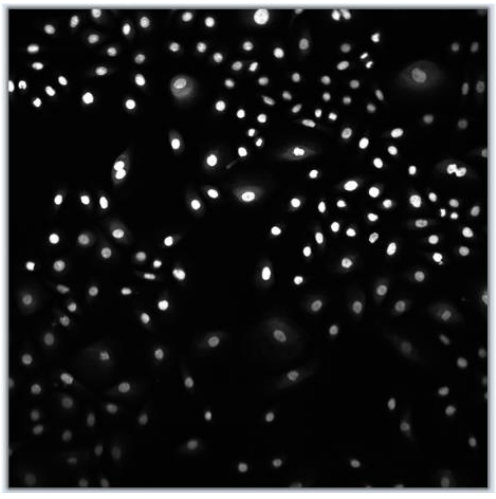

Figure 43. Example of Unlevel Stage. Causes out of focus cells seen on the bottom.

seen in Figure 43. This is due to the microscope stage being unlevel, and when the stage moved the layer of cells became out of focus. The Hoechst image tilt correction macro in section 3.7.2 was developed to adjust out of focus images to acquire more ROIs.

4.2 Ethidium with Permeabilization Qualification

4.2.1 Summary and Goals

Ethidium Homodimer-1 infiltrates cells to stain nuclear protein, but to do so the membrane must be compromised for the stain to reach the nucleus. Permeabilization is necessary if a p21 stain is going to be used in the future, but it is possible the permeabilization will make holes in healthy cells and have EthD-1 infiltrate.

The goal of this experiment was to evaluate if permeabilizing the membrane will cause EthD-1 to infiltrate healthy cells. Assessment was done qualitatively in terms of brightness and location of the EthD-1 stain

4.2.2 Results

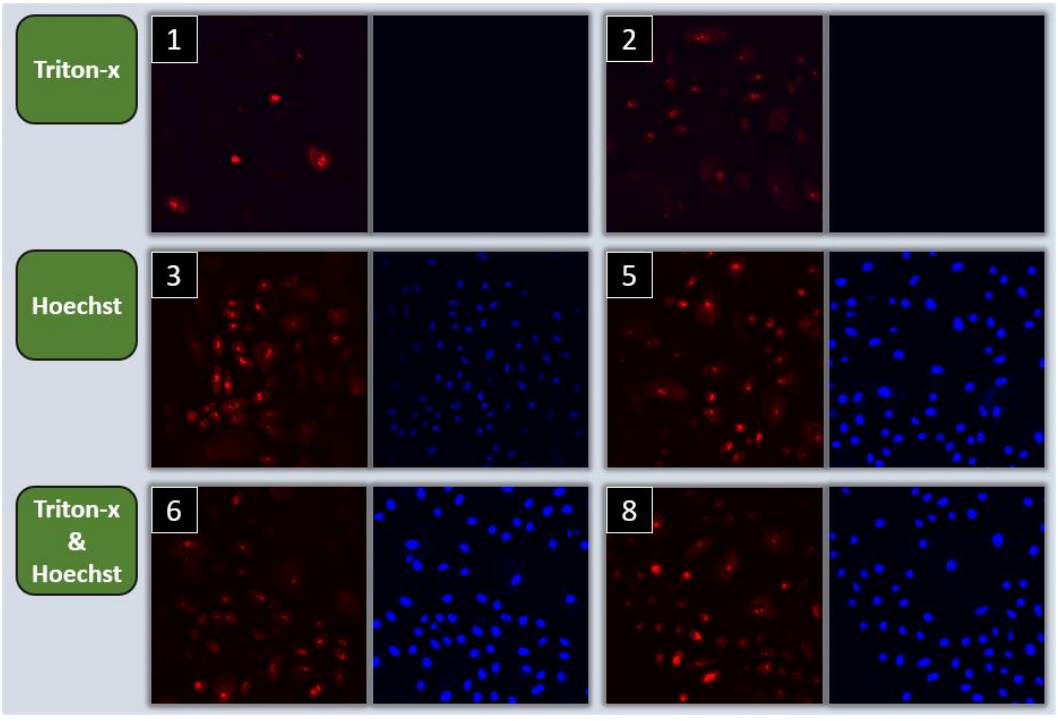

Figure 44. Treatment Groups. Representative Ethidium Homodimer-1 and Hoehcst images. Number associated corresponds to well number.

Figure 44 shows two sample locations for each treatment group. Well 1 and 2 of Figure 44 depict the control of not adding a Hoechst stain. Well 3 and 5 are the same treatment as the Pilot PDL Qualification experiment without permeabilization. Wells 6 and 8 shown are the test treatment of adding Triton X-100 to permeabilize the membrane. There was only a very slight noticeable decrease in brightness when adding Triton X-100.

4.2.3 Discussion

There was not a noticeable difference in image quality when adding the permeabilization reagent, Triton X-100. The slight decrease in brightness is probably because the added permeabilization created more holes in dead cell's membrane. The holes could let more flow of PBS into the cell during the washing steps.

When needed, the Hoechst Tilt Correction macro was used. It was concluded that Triton X-100 would not damage image quality when used in conjunction with EthD-1. This would allow for the combined use of EthD-1 with stains that require a permeabilized cell, like the p21 stain.

4.3 Poly-D-Lysine Qualification 2

4.3.1 Summary and Goals

The primary goal of this experiment was to test different concentrations and incubation times to see which conditions would result in a higher percent of dead cells. It was found that there were roughly the same number of live cells in the pilot study when comparing between a coated and uncoated PDL culture plate. To find out if the coating held on to more dead cells, the percent dead was used as the defining parameter. Again, total dead cell count could not be used as a quantified variable for the comparison between treatments, due to the variability of cell

coverage between images. The dead cell count was normalized to the total cells present in each image, as a percent.

The secondary goal was introducing ultraviolet radiation to make sure UV did not affect the coating. Testing this parameter will be merely qualitative and acknowledging adverse effects.

The experimental setup was comprised of four 8-well cell culture plates. Plate 1 was a control with no coating. Plate 2 had a concentration of 100ug/ml and was incubated for 5 minutes, the same as the pilot study. Plate 3 had the same concentration of 100ug/ml, but was incubated for 30 minutes. The final plate had a concentration of 200ug/ml, the stock solution, with a 30-minute incubation time. All plates were dried for at least 2 hours before seeding keratinocytes. One day after a 35mJ exposure of UV, the cells were fixed with PFA and stained with Ethidium homodimer-1 to detect dead cells, and Hoechst to detect all cells.

Image acquisition consisted of taking three 10x stitched images of varying depths in the middle of each well. Each stitched image was a 3x3 matrix of 10X images, while depth varied 4um above and below the first image. Taking multiple depths of images allowed for image correction since a portion of each image was out of focus and combined will give a full image.

4.3.2 Results

Figure 45 shows the variability of cell coverage in the corresponding well of each plate. Each image displays the Hoechst channel in grey-scale. Several samples were unable to be used, which resulted in only a reduction of the number of samples that were able to be imaged. Well loss was due to evaporation of the well's liquid while in the refrigerator.

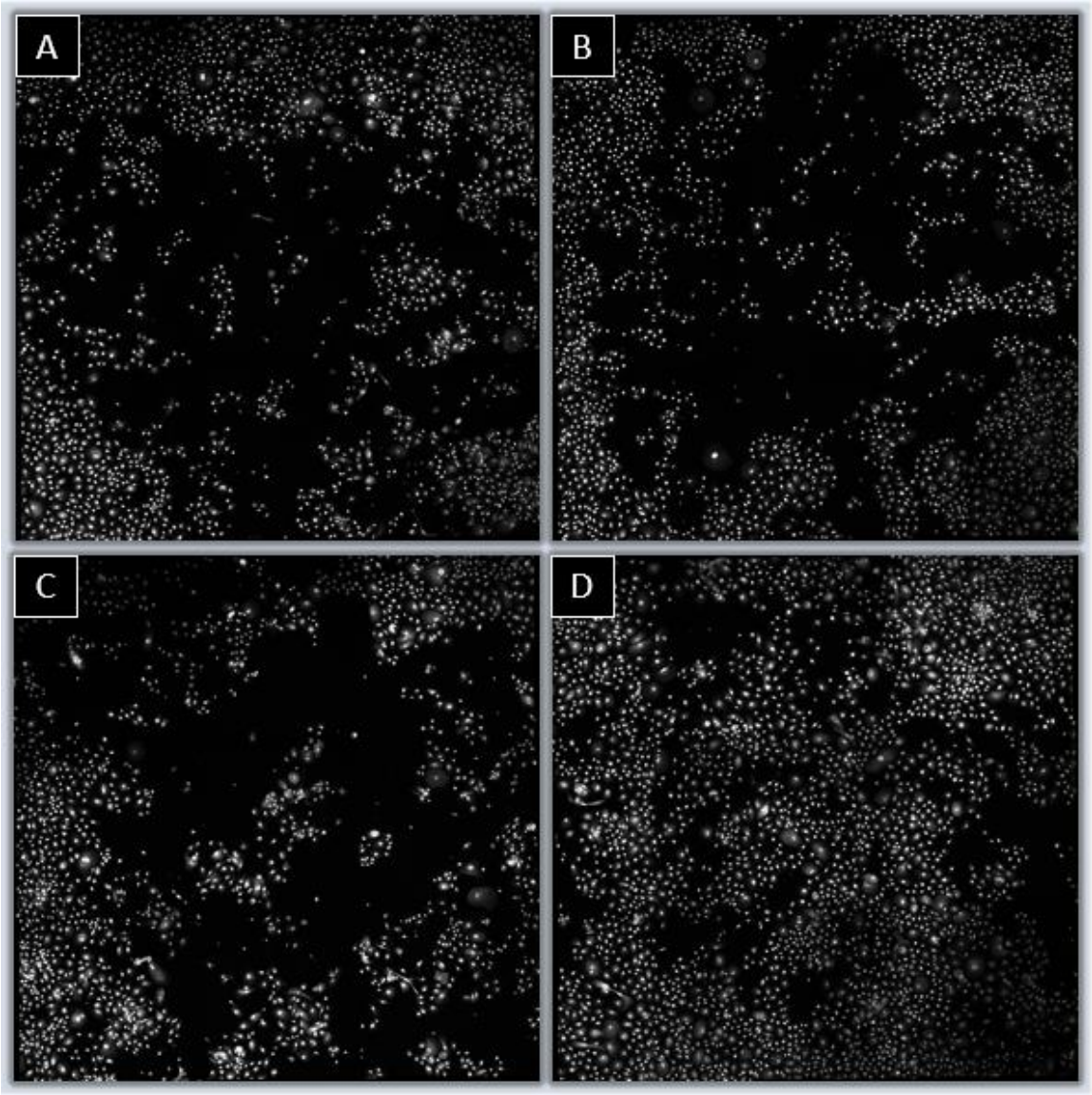

Figure 45. 8-Well Variability. Well 4 between all treatments A) Uncoated. B) 100 ug/ml & 5 min incubation. C) 100 ug/ml 30 min incubation D) 200 ug/ml 30 min incubation. Images taken in the middle of the well where cells are the least populated.

Figure 46 depicts the variability of the Ethidium Homodimer-1 stain. Figure 46B was considered ideal where EthD-1 labels the dead cells as small localized and bright orbs. However, in addition to the dead cells, Figure 46A&C show disordered, non-symmetric and jagged objects that were remnants of detached cells that were killed by the UVB.

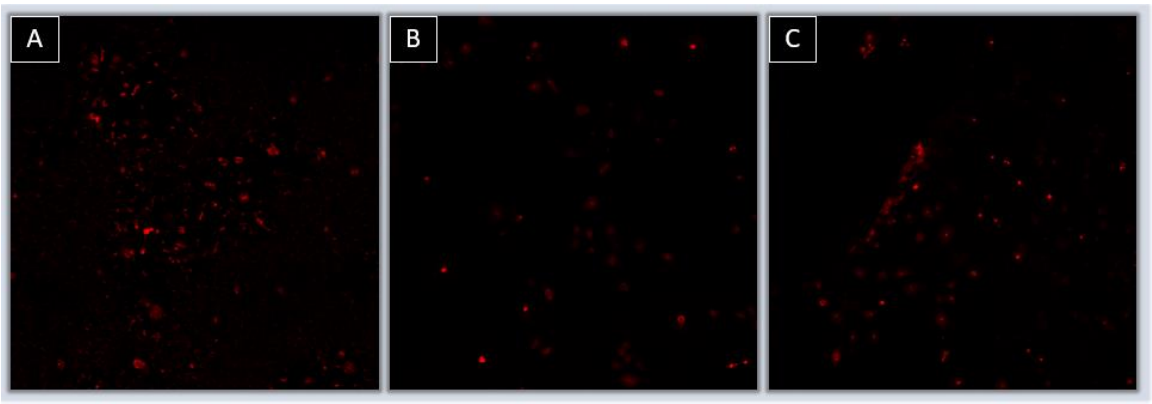

Figure 46. Ethidium Homodimer-1 Variability Between Wells. Same cell culture plate of 100 ug/ml 30 min incubation. A) Well 2, B) Well 3, C) Well 5.

4.3.3 Discussion

Figure 45 does show that there are more cells in the last image of the 200 ug/ml concentration of PDL; however, application of the coating at this concentration was significantly harder to work with. The higher concentration made the PDL solution very viscous and would not spread out over the well, instead it balled up.

This experiment ended up being more about resolving experimental procedures than if the coating worked. It was found that when introducing UVB there was not a homogenous spread of cells between wells. Some wells looked as if they received more UVB exposure, like in Figure 46A well 2. All that was left were proteins that attached to the coating and were stained /with the EthD-1, coming up looking like debris and not individual orbs that we would hope to see in Figure 46B. Due to this variability a switch from 8-well plates to 1-well plates occurred for all following experiments.

Another major problem was the loss of wells due to evaporation, Figure 47. When the plates were stored in the refrigerator, the wells tended to dry out. Cell culture plates also tended to have the glass bottom crack because they were fragile. To remedy these problems the 'Cell Culture Plate Holder' was developed and can be found in Appendix A.1. The device was designed to hold the plates throughout the staining process so the bottom did not break. It also

had a lid with soft foam to gently apply pressure to the top of the culture plates to reduce evaporation when stored in the refrigerator.

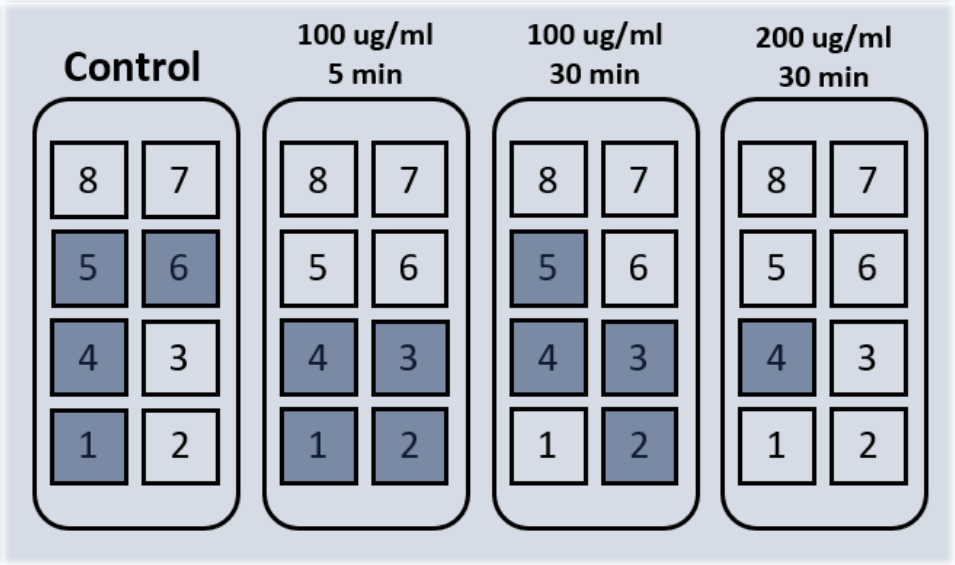

Figure 47. Missing Wells. Representation of the four 8-well plates used. Darker wells signify being full of liquid, all others were missing liquid.

It was decided to use the 100 ug/ml concentration with an incubation time of 30 minutes. The higher concentration would not be used due to difficulty with its application to culture plates. The next experiment with PDL used 1-well plates to reduce potential UV refraction from the walls. Seen in Figure 48 and detailed in Appendix A.1, the 'Cell Culture Plate Holder' was developed to reduce sample loss from cracking and evaporation, Figure 47. The p21 stain protocol that had been used before in the lab was introduced to the PDL and EthD-1 protocols as the final qualification step to observe any sort of adverse effects.

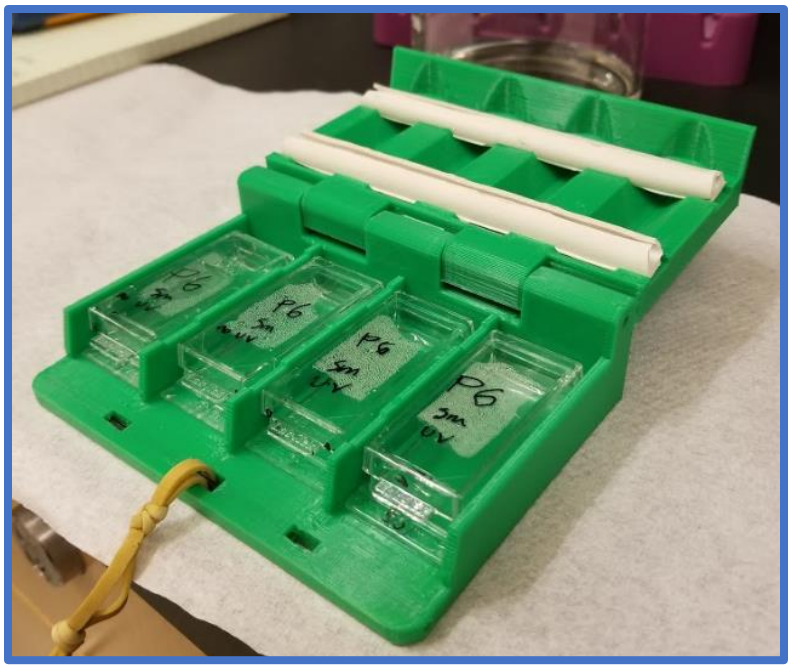

Figure 48. Cell Culture Plate Holder.

4.4 Poly-D-Lysine Qualification 3

4.4.1 Summary and Goals

The goal of the final PDL qualification was to evaluate if there were any differences when adding p21 primary and secondary stains, with Hoechst and EthD-1, between coated and uncoated plates. Nuclear p21 expression was measured by using the Image Processing technique discussed in 3.7.4 to find nuclear ROIs. Preprocessing was done using 3.7.3 to normalize the local contrast.

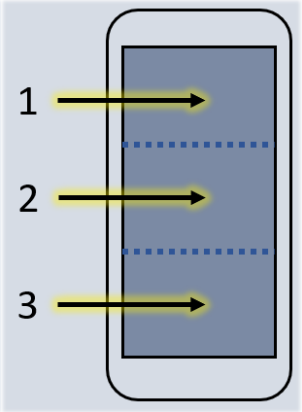

Figure 49. Zones in 1-Well Plates

Experimentation switched to 1-well plates since 8-well plates had large variation between wells in terms of cell death, most likely due to uneven irradiation of UVB. The 1-well plates were split into three distinct numbered zones, which can be seen in Figure 49. For each zone a stitched image was recorded in a 3x3 matrix of 10x images. Three stitched images were taken at 3 different heights to create a z-stack to capture all nuclei in focus.

4.4.2 Results

Table 4 depicts results of the experiment split into respective zones. There is a large variability of total cells between zones, but when summed together, were quite close between the control (n=2860) & PDL (n=2591). The number of dead cells was much higher when using the PDL coating, except for 'Zone 3' where the control was similar in count its respective PDL coating, Figure 50A. Normalizing dead cells to the total, as a percentage, gave the coating a significantly higher percentage of dead cells than that of the control for two out of three zones. Interestingly, there was slightly more, though non-significant, p21 expression in the PDL cases.

Table 4. Results of PDL Qualification 3

	Zone							
	1		2		3		All	
	Control	PDL	Control	PDL	Control	PDL	Control	PDL
Total (#)	927	521	862	1564	1061	506	2850	2591
Dead (#)	86	157	94	166	134	144	314	467
Dead (%)	9.28	30.13	10.9	10.61	12.63	28.46	11.02	18.02
Mean P21 (rel)	381.4	446.35	410.49	453.1	401.08	458.12	398.87	452.68

Figure 50 illustrates the impact of the PDL coating on cellular adherence. Zone 2's dead cell percentage appear to be similar to the control but is due to an abnormally higher number of total cells, which can be seen in Figure 50B. Figure 50A Zone 2 PDL has similar dead cell counts to other treatment zones. There was not any statistical significance between treatments in relative nuclear p21 expression. A Two-Sample Proportion test found significance of percent-dead cells between treatments of Zone 1($z=-10.19$, $p<0.001$), Zone 3 ($z=-7.67$, $p<0.001$) and when summing treatments ($z=-7.36$, $p<0.001$).

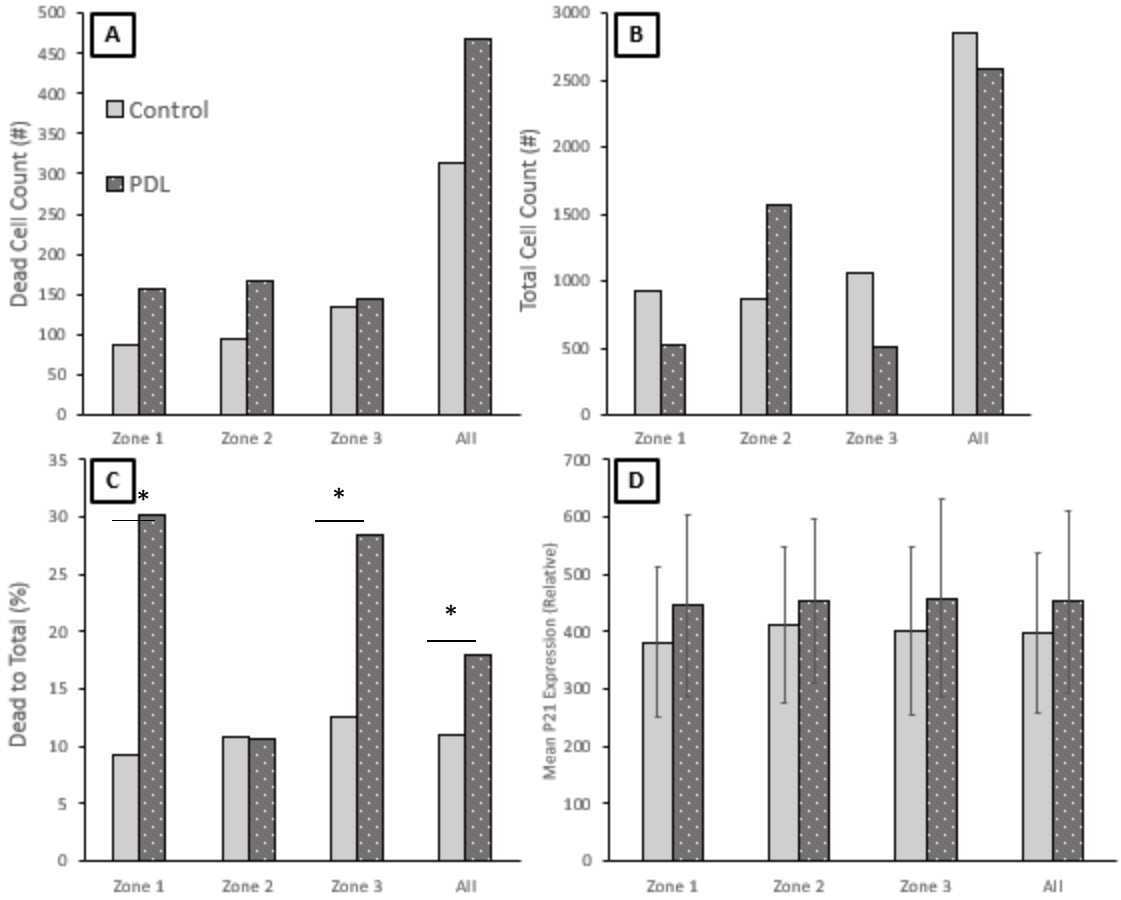

Figure 50. Plotted Results. Split into corresponding zones and together A) Number of dead cells present in each image. B) Total cells per image. C) Dead count normalized to total as a percent. D) Mean p21 expression inside the nucleus for each image. Mean p21 expression for all zones calculated by weighted average. One image per zone per treatment. (*=p<0.001)

4.4.3 Discussion

It is evident by Figure 50 A&B that there are more dead cells captured with the PDL coating. Zone 1 and 3 had significantly more percent-dead cells in PDL treated cases than that of uncoated cases, Figure 50C. Zone 2 of the PDL cases did not have more percent-dead cells, but it did have a higher count of dead cells, Figure 50A. Totaling live and dead cells, Zone 2 of PDL also had more total-cells than all other zones for both cases, Figure 50B. In terms of cells per image, there were still large variations even with the larger sample size.

There was not any significance of nuclear p21 expression between any treatments or zones. The trend of the PDL coated culture plates having slightly more expression could be attributed to normal experimental variation.

Future experiments used these same techniques but introduced sphingomyelin to test the UVB protective qualities. The coating allowed for analyzing of dead cells to try and determine their cause of death. The content of p21 in the dead cells could explain what SM is doing to the cell leading it to death.

4.5 p21 Expression of SM Treated KRT 1

4.5.1 Summary and Goals

The goal of this experiment was to use the now qualified Poly-D-Lysine coating to observe nuclear p21 expression of cells treated with sphingomyelin and UVB. Nuclear p21 expression has been already been evaluated for keratinocytes treated with SM and UVB in the lab, but not with the PDL coating, much larger sample size, and automated image processing analysis. Due to the nature of the PDL, it was found in previous experiments that it could retain dead cells better than without the coating. Ethidium homodimer-1 indicated which cells were dead in order to analyze their p21 expression.

Eight 1-well plates were split into 4 treatment groups of: UV+SM+, UV+SM-, UV-SM+ and UV-SM-. SM+ cases were incubated in SM for 1 hour, and UV+ cases were immediately exposed to UV after the incubation period. All cases were fixed with paraformaldehyde 1 day after UV+ cases were exposed to UV. All plates were stained with Ethidium Homodimer-1, Hoechst, and p21 primary and secondary. The staining protocol can be found in the Appendix.

During the second experiment, it was found in literature that cytoplasmic p21 activity could be a potential factor indicating tumorigenic tendencies, so images were reprocessed using the newer program ‘3.7.6 Binary Threshold Drop’. The program measures p21 activity 6um away

from the edge of the nucleus. Since the program uses scaled units no optimization was needed for the different magnifications.

4.5.2 Results

Figure 51 illustrates the p21 expression of dead cells in both the nucleus and 6 µm outside of the nucleus in the cytoplasm. UV-SM- and UV+SM+ both had large variations between plates, but the other two treatment groups had similar means.

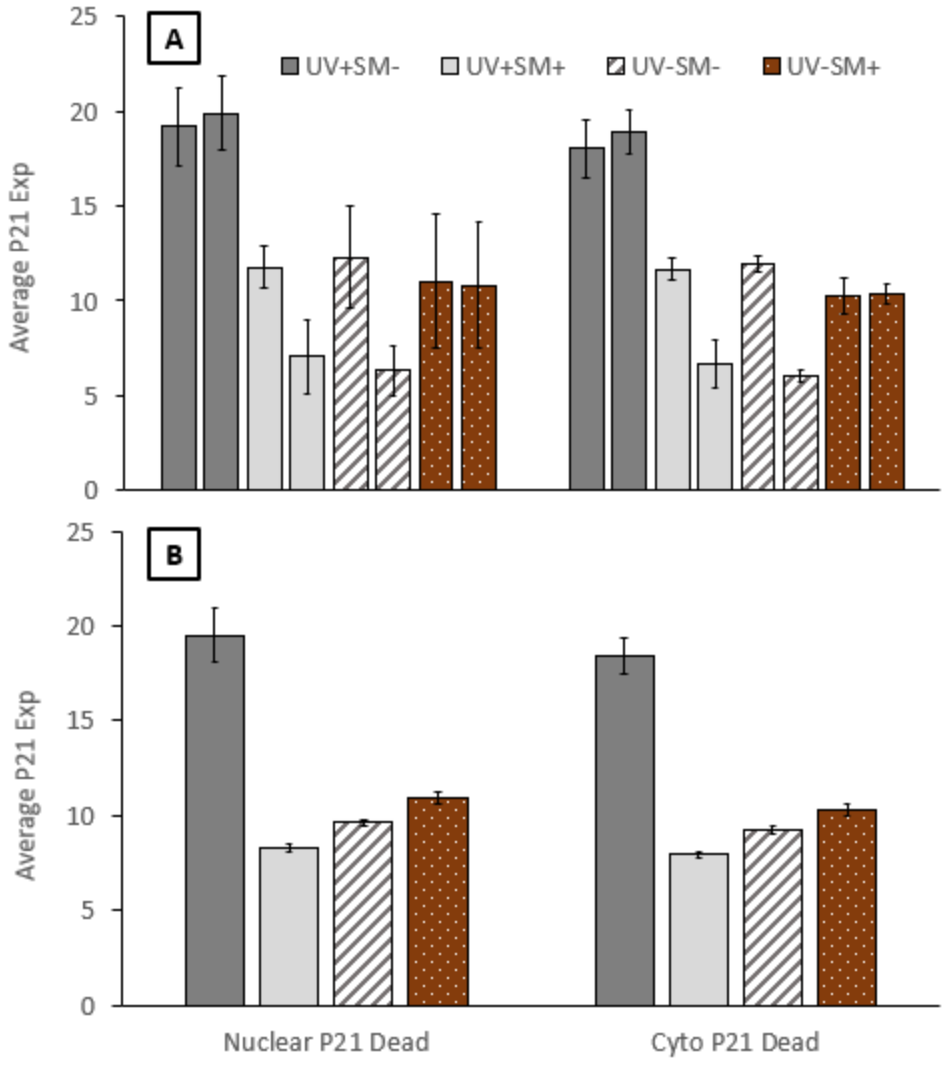

Figure 51. p21 Expression in Dead Cells, Exp 1. Average nuclear and cytoplasmic p21 expression of cells that stained positive as dead with Ethidium Homodimer-1. A) Expression of each cell culture plate with 2 plates for each treatment. Plates displayed as paired and in order as 'Plate A' followed by 'Plate B'.

UV+SM-: A(n=331); B(n=256), UV+SM+: A(n=231); B(n=667), UV-SM-: A(n=125); B(n=103), UV-SM+: A(n=71); B(n=87). B) Plates combined into treatment groups. 99% confidence interval for both graphs.

Figure 52[A] depicts the nuclear and cytoplasmic p21 expression for each treatment group. Figure 52 only displays the top 90% of the data where the cells were ranked by the average Hoechst intensity inside the nucleus. The top 90% was used to filter out-of-focus Hoechst ROI's, indicated by a very low Hoechst mean. Figure 52[B] depicts the number of cells, as a percent of the total, that have more nuclear than cytoplasmic p21 expression. Figure 52[C] shows the average area of the nucleus per treatment, where both UV cases had much higher areas. Figure 52[D] shows the number of cells that had a mean nuclear p21 expression higher than a specified threshold value of '20' out of '255', the 8-bit scale max.

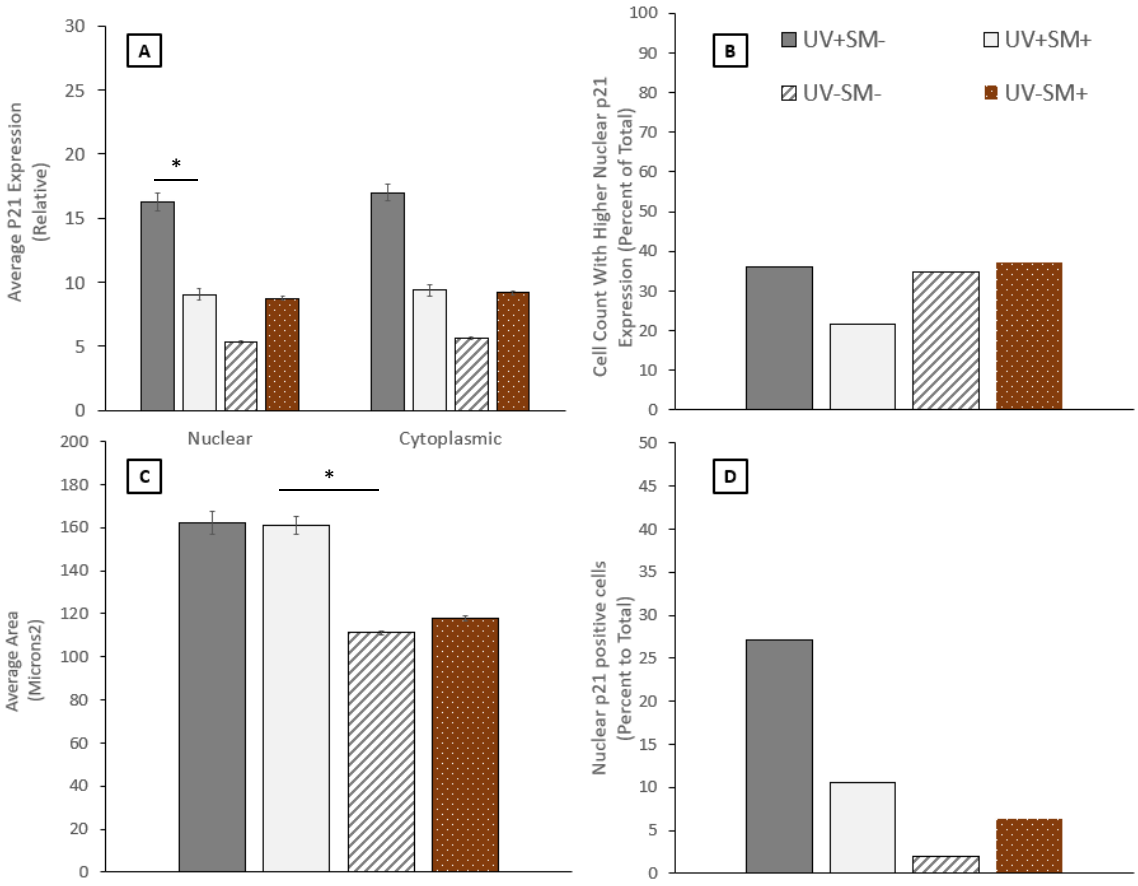

Figure 52. Nuclear and Cytoplasmic p21 Expression and Nucleus Area, Exp 1. Top 90% of all cells based on Hoechst channel intensity. A) Average nuclear and cytoplasmic p21 expression per treatment. B) Percent of cells with more nuclear p21 expresion than cytoplasmic. C) Average area of all cells per

treatment. D) Percent of cells with nuclear p21 expression above a grey-level mean value of 20, out of a 255 max scale. UV+SM-(n=2,947), UV+SM+(n=4,996), UV-SM-(n=27,180), UV-SM+(n=21,837). (*=p<.01)

Figure 53 categorizes each cell as either 'cytoplasmic-dominant', 'nuclear-dominant', or 'neutral' based on the difference between the nuclear and cytoplasmic p21 expression. The 'difference' is a simple subtraction of nuclear p21 by cytoplasmic p21 for each cell to obtain a distribution. To classify the cell, the UV-SM- 'difference' distribution was used to set threshold points. Within 95% of the data was considered 'neutral', while anything below was 'cytoplasmic dominant' and anything above was 'nuclear dominant'.

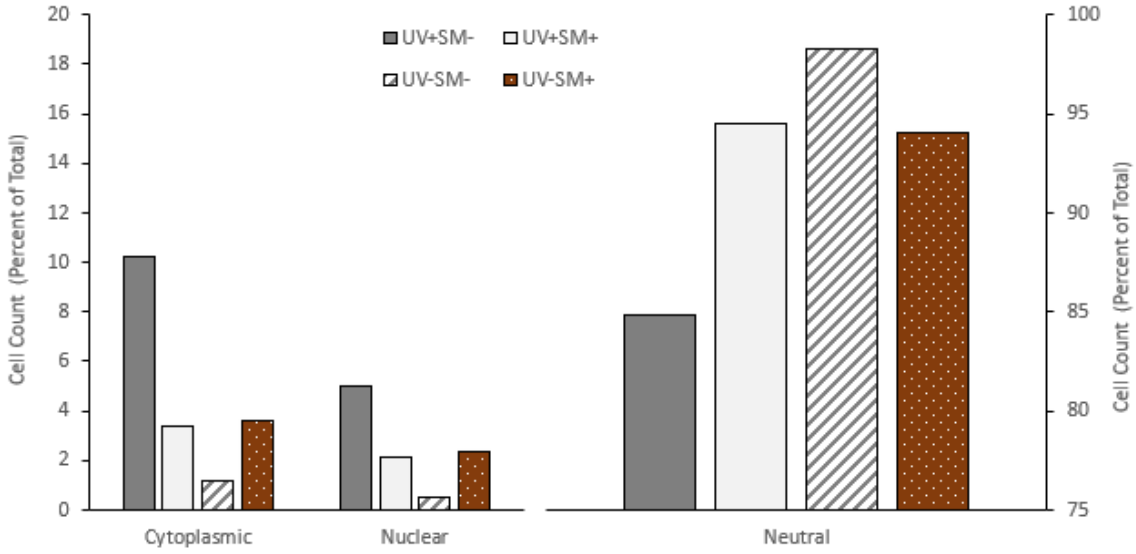

Figure 53. p21 Localization Dominance, Exp 1. Using the difference between the nuclear and cytoplasmic p21 expression, cells were categorized as either cytoplasmic dominant, nuclear dominant, or neutral. The UV-SM- distribution was used as the threshold where anything outside of 95% of the data was either cytoplasmic or nuclear dominant and anything within was considered neutral. UV+SM-(n=2,947), UV+SM+(n=4,996), UV-SM-(n=27,180), UV-SM+(n=21,837).

Figure 54 graphs both the living and dead cell distributions for each treatment group. Nuclear and cytoplasmic p21 distributions were transformed to be more normal by applying the natural logarithm. The y-axis represents what the proportion of p21 is between the nucleus and cytoplasm for each cell. The proportion was calculated as 'ln-nuclear' mean divided by the sum of the 'ln-nuclear' mean and 'ln-cytoplasmic' mean. The x-axis, 'p21 intensity', was a way to

determine what each cell was expressing in both the nucleus and cytoplasm as a single number, per cell.

$$\frac{LN(X)-Median(LN(UV-SM-))}{StdDev(LN(UV-SM-))} = Z\ Score(X) \quad (18)$$

The UV-SM- median and standard deviation were found for both the 'ln-cytoplasmic' and 'ln-nuclear' p21 distributions. For each treatment group, the median obtained from UV-SM- data was subtracted, followed by divided by the standard deviation for each cell resulting in a Z-score for both the ln-cytoplasmic and ln-nuclear p21 distributions, Equation 18.

The ln-cytoplasmic and ln-nuclear Z-score distributions were then averaged together to find the 'p21 intensity'. This method was found to result in more normally distributed data, as opposed to just averaging ln-cytoplasmic and ln-nuclear p21. Figure 54 graphs the proportion by the 'p21 intensity' described above.

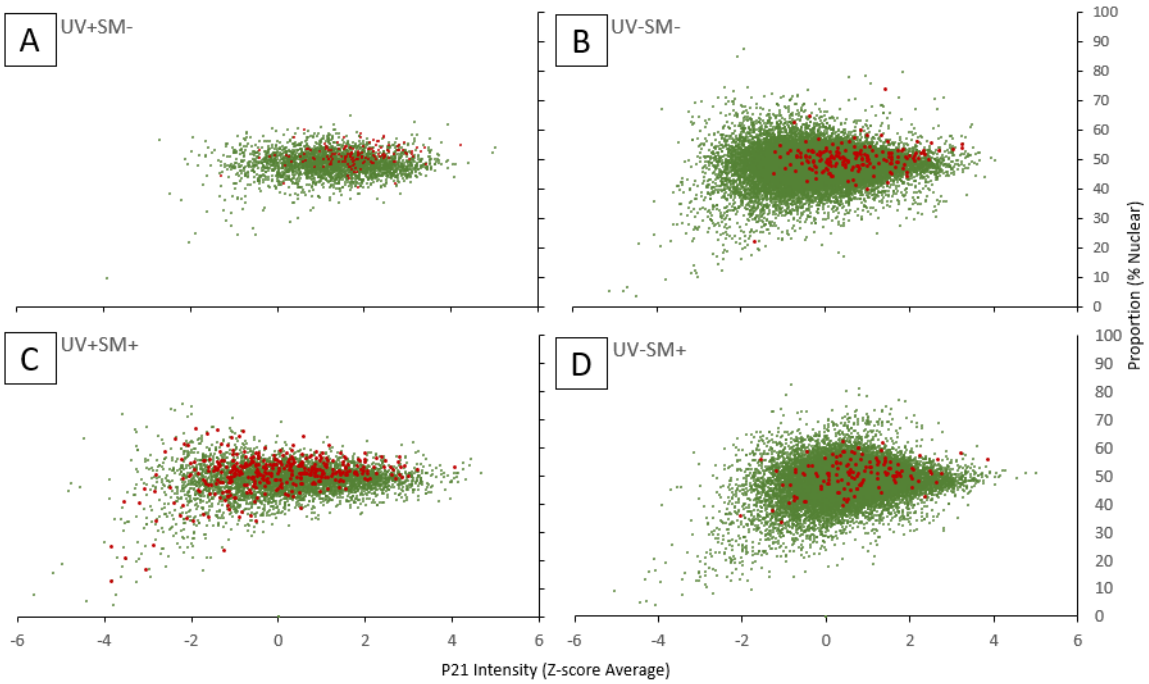

Figure 54. Dead & Alive Proportion versus p21 Intensity Distribution, Exp 1.Green points represent living cells, while red are dead. Red points enlarged by 1 pt to visualize. A) UV+SM-: Alive(n=2,947), Dead (n=154). B) UV-SM-: Alive(n=27,180), Dead(n=183). C) UV+SM+: Alive(n=4,996), Dead(n=381). D) UV-SM+: Alive(n=21,837), Dead(n=135).

Figure 55 represents a radar graph of the same data seen in Figure 54, but each cell was categorized based off of 'p21 proportion' and 'p21 intensity'. The UV-SM- 'p21 proportion' distribution was used as a baseline guide in determining p21 proportion. Cytoplasmic proportion was classified as; high: less than the 10th percentile, medium: 10th to the 25th percentile and low: 25th to the 40th. Neither nuclear nor cytoplasmic proportion was classified as balanced: 40th to 60th percentile. Nuclear expression was classified as; low: 60th to 75th percentile, medium: 75th to 90th percentile, and high: more than the 90th percentile.

To categorize cells based on the 'p21 intensity', they were classified as low, medium and high, where low: less than mean + StdDev, medium: between low and mean + 2.5* Stddev, and high as above the medium cutoff.

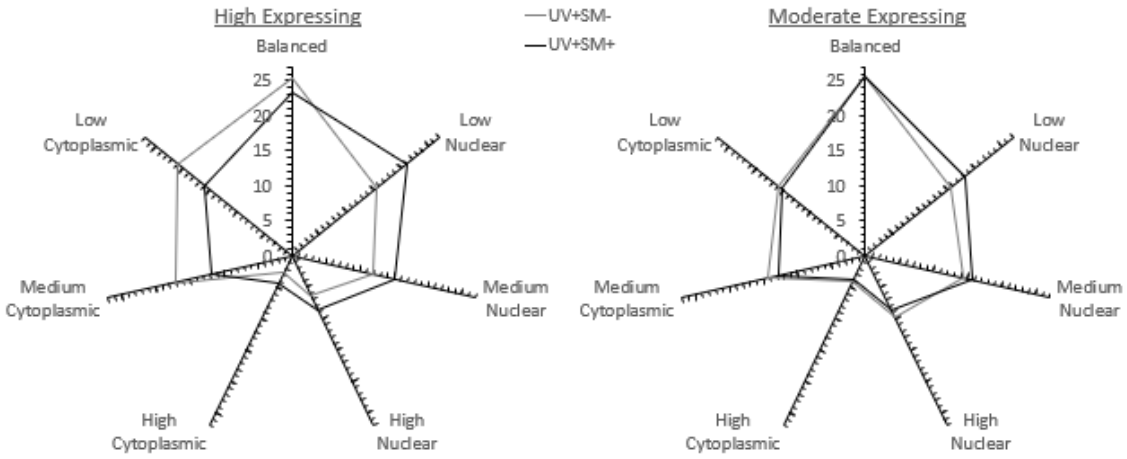

Figure 55. Comparison of p21 Proportion in High and Moderate Expressing Cells, Exp 1. Cells grouped by proportion of nuclear to cytoplasmic p21 expression. High expressing cells; UV+SM-(n=987), UV+SM+(n=680). Moderate expressing cells; UV+SM-(n=871), UV+SM+(n=878).

Of the highest expressing cells, UV+SM- has more medium and low cytoplasmic cells than UV+SM+, while UV+SM+ has more low, medium and high nuclear cells with a slightly higher high cytoplasmic. Of the moderate expressing cells there is less difference, but UV+SM- still shows more low and medium cytoplasmic cell proportions, while UV+SM+ still has more

medium and low nuclear proportion cells. In general, there is a shift of cells going more towards nuclear expression when SM is added, in UV cases.

Table 5. Proportion and Intensity Classification, Exp 1. Data represented as count of cells within each class. Cells cannot be in more than 1 class.

Proportion:	High Cyto <10th			10th< Moderate Cyto <25th			25th< Low Cyto <40th			40th< Balanced <60th			60th< Low Nuclear <75th			75th< Moderate Nuclear <90th			90th< High Nuclear		
Intensity:	Low	Moderate	High	Low	Moderate	High	Low	Moderate	High	Low	Moderate	High	Low	Moderate	High	Low	Moderate	High	Low	Moderate	High
UV+SM-	93	36	27	150	126	169	164	140	205	234	224	250	170	135	155	173	125	118	105	85	63
UV+SM+	431	33	29	480	112	80	432	135	109	600	225	158	451	160	143	540	138	103	496	75	58
UV-SM-	2523	138	57	3606	388	83	3405	490	182	4419	796	221	3334	592	151	3571	397	109	2519	138	61
UV-SM+	2543	357	96	2249	729	244	1726	826	368	2037	1103	560	1554	832	315	1902	972	285	2236	726	168

4.5.3 Discussion

The primary goal of this study was to determine if keratinocytes treated with sphingomyelin (SM+/SM-) prior to ultraviolet exposure (UV+/UV-) would have lower nuclear expression of the damage marker protein p21 twenty-four hours after UV. This was shown in Figure 52A where cells exposed to UV had more p21 located in the nucleus of untreated cells than that of those treated with SM. The number of cells with higher nuclear p21 content was also higher in the UV+SM- case, Figure 52D.

The secondary goal was to analyze p21 expression of dead cells to try and determine if SM had an effect. Figure 51 shows a similar trend to live cells in Figure 52. Interestingly, looking at Figure 54, UV+SM+ has many more dead cells at low p21 intensities, when compared to UV+SM-, this may suggest that SM causes cells to go more towards an apoptotic path at lower levels of p21.

The third goal of analyzing cytoplasmic p21 was added after realizing in the following experiment that p21 in the cytoplasm was higher in UV+SM- cases in comparison to UV+SM+. All images were reprocessed using the more accurate algorithm of the 'Binary Threshold Drop' combined with the 'p21 Variable Slice Measurement'. Figure 53 and Figure 55 visualize different ways to see cytoplasmic activity relative to each cell. Figure 53 is a simplistic representation, but only has 3 groups and does not differentiate between expression. Figure 55 does do this and is definitely apparent that without SM, KRTs exposed to UV (UV+SM-) had more high and

moderate expressing cells lean more cytoplasmic than nuclear, whereas when incubating with SM first seemed to keep p21 in the nucleus. Figure 55 represents 'high expressing' as a percent of the 'total high expressing' cells in that treatment and is done the same with the moderately expressing cells graph. Take note than UV+SM- still has much higher counts of cells with high expression of p21 regardless of location, seen in Figure 52[A&D].

Due to large images a portion of the image may be in focus while the other portion is not. Figure 56[B&C] has a LUT applied to the stitched image to help visualize the error where each stitch of the image is in focus for the top right, but the bottom left is out of focus measuring the coverglass. Numerically the error can be seen in Figure 56[A&D] where there is a wave like pattern occurring that is easily seen by looking at the minimum values. This wave-like pattern is occurring because ImageJ measures each ROI in the order of starting in the top left, traveling across and repeating, ending in the bottom right. The graph's x-axis is the order of measurement, replicating what is being seen in the image. A correctly leveled stage would not have the wave-like pattern seen in minimum values. To still use the data each cell's p21 value would have to be relative to that cell only, which is where measuring the cytoplasmic activity can be used and the relative difference be evaluated.

The original images were reanalyzed using a new algorithm mostly eliminating the error. The algorithm uses the quality of the Hoechst channel to determine the best slice to use and can be found in 3.7.7 p21 Variable Slice Measurement. Figures displayed were made by using the updated algorithm.

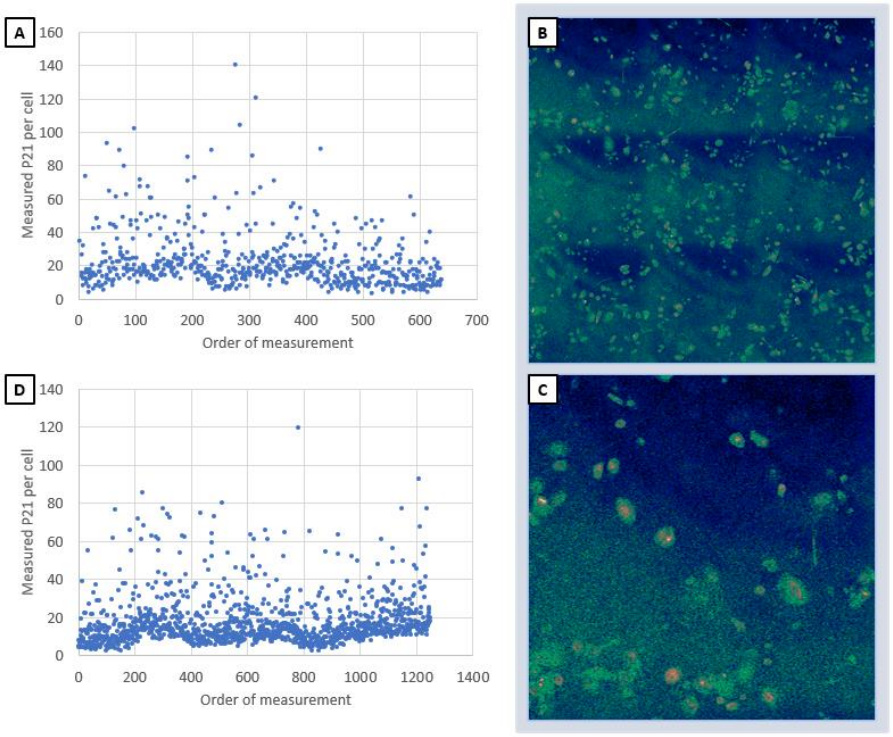

Figure 56. Unlevel Confocal Stage. A) and D) are two zones in the UV+SM+ treatment group graphed by mean Nuclear p21 and the location. The order of measurement is line by line from top to bottom. B) is UV+SM+ zone 4 plate B and C) is the top left most image that created the stitch. A 3-3-2 RGB LUT was used to help visualize the off-balance.

To account for this error in following experiments the image stitch used a higher magnification of 40x, instead of 10x. Z-stacks were also taken at 1 um differences (-1, 0, +1) rather than 4 um (-4, 0, +4).

4.6 p21 Expression of SM Treated KRT 2

4.6.1 Summary and Goals

The first experiment produced results similar to those others in the lab had found, but it also had large variability in the p21 images due to the combination of an unlevel stage and large 10x stitched images. The area of the 10x images were so large in physical size that a portion of the image was in focus and the other portion was not. Instead, the out-of-focus portion would capture the cover plate reflection of the laser and take inaccurate readings. To get around this 40x images were used instead, with everything else remaining the same.

The primary goal of this experiment was to gather more data of the same exact experimental setup, but with the 40x images to make sure the process is robust. Main attributes to be looked at are nuclear and cytoplasmic p21 concentrations of living and dead cells.

There were eight 1-well plates split between the 4 treatment groups of UV+SM+, UV+SM-, UV-SM- and UV-SM+. All cells were stained the same way with Hoechst, p21 (1° & 2°) and Ethidium Homodimer-1 to see nuclei, p21 content and if the cell was dead, respectively.

4.6.2 Results

Figure 57 displays p21 expression in cells that were marked dead with Ethidium homodimer-1. Figure 57A compared scatterplots between cells in treatment groups where the y-axis is the average p21 expression in the nucleus and the x-axis is the average cytoplasmic p21 expression. UV+SM+ has a higher max p21 expression, but UV+SM- has more cells that are high expressing. There appears to be a relationship between nuclear and cytoplasmic p21, but UV+SM- has some cells that do not follow that relationship where they are more cytoplasmic-dominant than nuclear-dominant. Figure 57B displays the percent of cells that have nuclear p21

expression above a threshold of 20(grey-value intensity) out of a 255 scale-max. UV+SM+ has more cells above the threshold while UV+SM- has the least. Figure 57C is the nuclear and cytoplasmic p21 expression of all of the dead cells. Figure 57D are also the nuclear and cytoplasmic p21 expressions of dead cells, but only of cells that had more than 20 (grey-value intensity) threshold applied, like in Figure 57B. UV+SM- has the lowest p21 expression in the nucleus and cytoplasm, whereas UV+SM+ has the most. It is evident that for dead cells, UV+SM- samples have more cells expressing nuclear p21, but of those thresholded cells, UV+SM+ have higher expression cells.

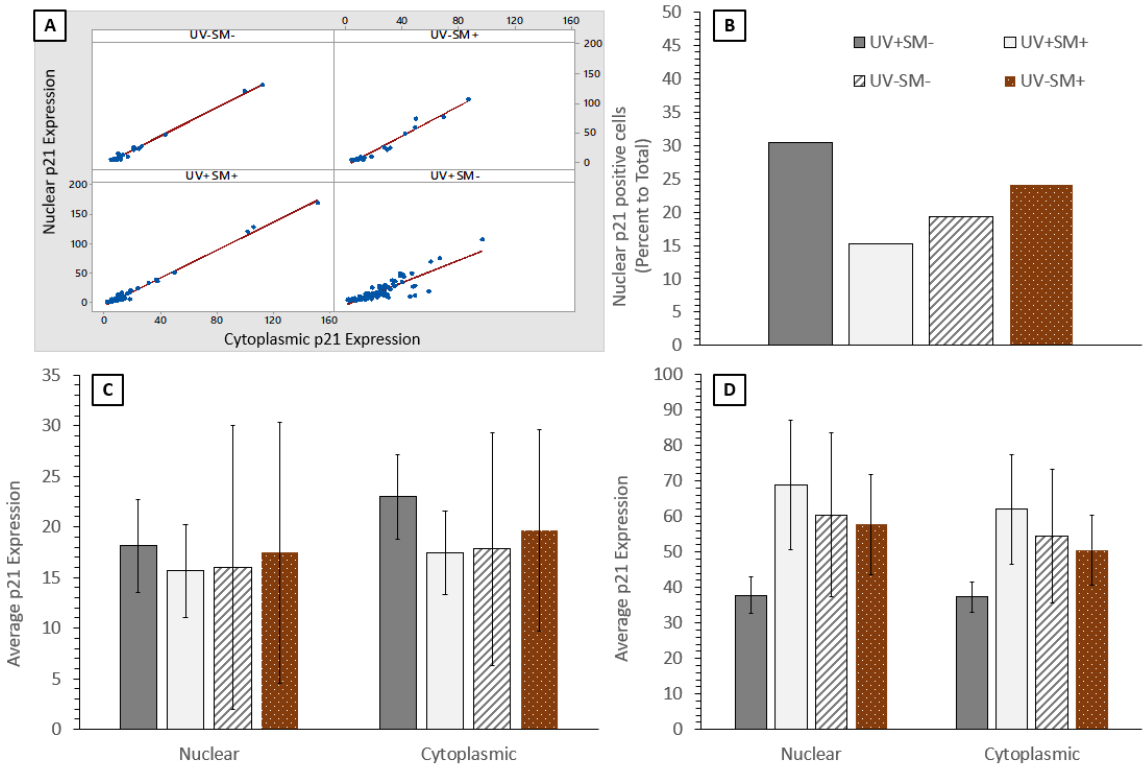

Figure 57. p21 Expression in Dead Cells, Exp 2. Top 90% of data based on Hoechst Channel mean. A) Scatter plots of each treatment nuclear by cytoplasmic p21 expression per cell. B) Percent of cells with nuclear p21 expression above the grey-value mean of 20, of a 255 scale-max. C) Nuclear and cytoplasmic p21 expression. (UV+SM-, n=92), (UV+SM+, n=59), (UV-SM-, n=31) & (UV-SM+, n=29). D) Nuclear and cytoplasmic p21 expression of cells with nuclear p21 means higher than 20 (grey-value intensity) of a 255 scale-max. (UV+SM-, n=28), (UV+SM+, n=9), (UV-SM-, n=6), (UV-SM+, n=7).

Figure 58[A] shows mean nuclear and cytoplasmic p21 expression for each treatment group. Like Figure 52, Figure 58 only displays the top 90% of the data where the cells were

ranked by the average Hoechst intensity inside the nucleus. The top 90% was used to filter out-of-focus Hoechst ROI's, indicated by a very low Hoechst mean. Figure 58[B] shows the percent of cells that have more nuclear than cytoplasmic p21 expression. Figure 58[C] shows the average area of the nucleus per treatment, where both UV cases had much higher areas, the same trend seen in Figure 52[C] of the previous experiment. Figure 52[D] shows the number of cells that had a mean nuclear p21 expression higher than a specified threshold value of '20' out of '255', the 8-bit scale max.

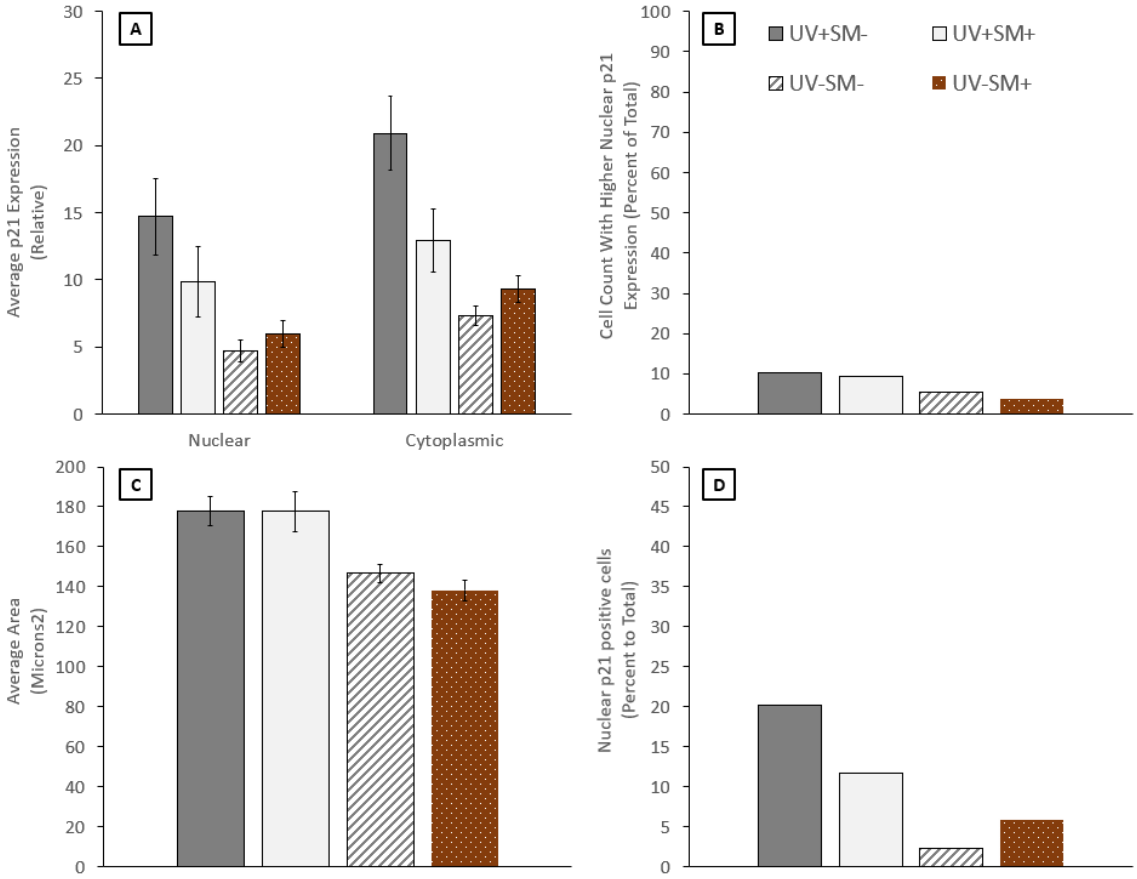

Figure 58. Nuclear and Cytoplasmic p21 Expression and Nucleus Area. Top 90% of data based on Hoechst Channel mean. A) Average p21 expression per treatment. B) Percent of cells with more nuclear p21 expresion than cytoplasmic. C) Average area of all cells per treatment. D) Percent of cells with nuclear p21 expression above a grey-level mean value of 20, out of a 255 max scale. UV+SM-(n=282), UV+SM+(n=324), UV-SM-(n=949), UV-SM+(n=790). (*=p<.01)

In the same way as Figure 53 in the previous experiment, Figure 59 categorized each cell as either 'cytoplasmic-dominant', 'nuclear-dominant', or 'neutral' based on the difference

between the nuclear and cytoplasmic p21 expression. The 'difference' is a simple subtraction of nuclear p21 by cytoplasmic p21 for each cell to obtain a distribution. To classify the cell, the UV-SM- 'difference' distribution was used to set threshold points. Within 95% of the data was considered 'neutral', while anything below was 'cytoplasmic dominant' and anything above was 'nuclear dominant'.

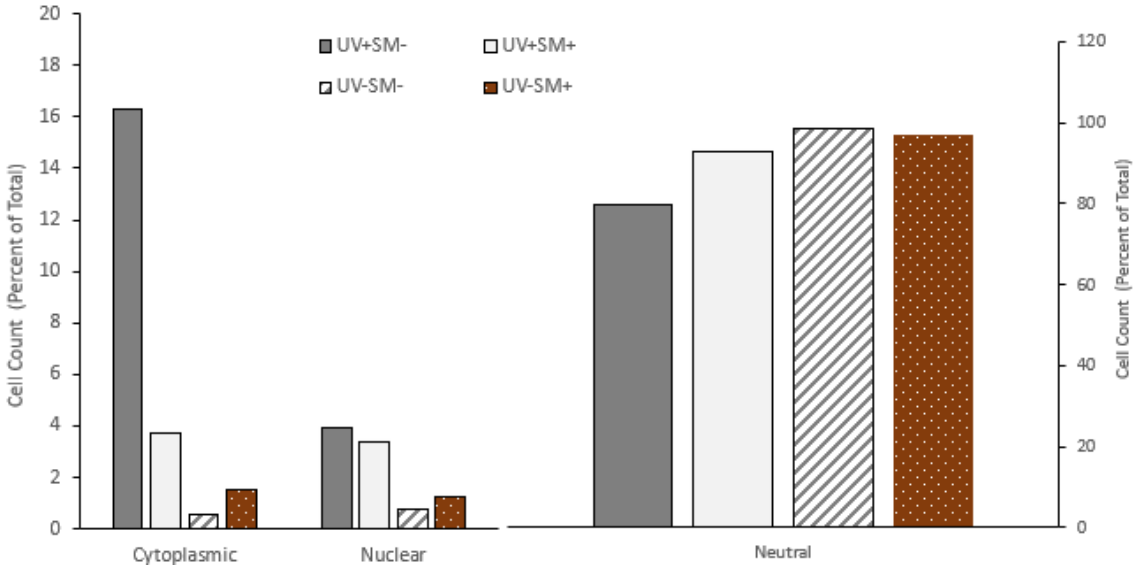

Figure 59. p21 Localization Dominance, Exp 2. Using the difference between the nuclear and cytoplasmic p21 expression, cells were categorized as either cytoplasmic dominant, nuclear dominant, or neutral. The UV-SM- distribution was used as the threshold where anything outside of 95% of the data was either cytoplasmic or nuclear dominant and anything within was considered neutral.

Figure 60 represents the living and dead cells in regards to 'p21 proportion' of nuclear and cytoplasmic p21 by the 'p21 intensity' using the same methods described in the previous experiment of the same graph, Figure 54. The only difference is that the 'p21 proportion' distributions went through a Johnson transform, based off of UV-SM- proportion data, to improve normality. UV+SM+ looks to have a similar spread to UV+SM-, but more centrally located at a lower average p21 intensity.

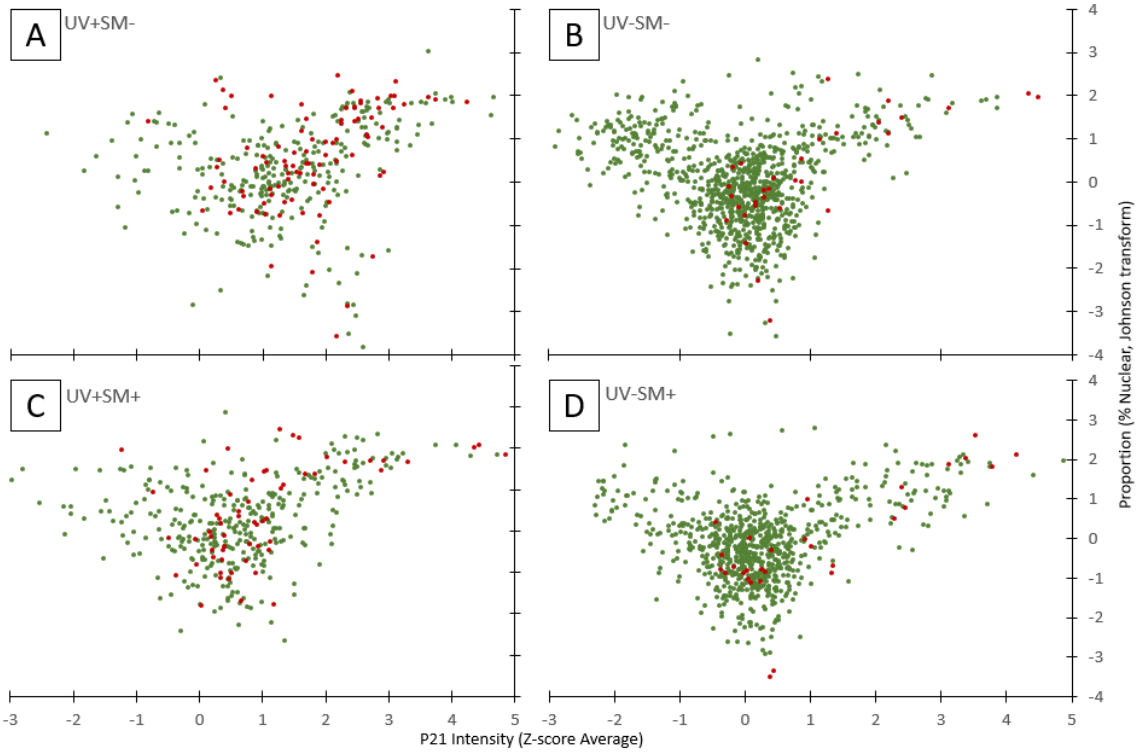

Figure 60. Dead & Alive Proportion versus p21 Intensity Distribution, Exp 2. Green points represent living cells, while red are dead. A Johnson Transform was used on proportion data to make the distribution more normal. A) UV+SM-: Alive(n=282), Dead(n=92). B) UV-SM-: Alive(n=949), Dead(n=31). C) UV+SM+: Alive(n=324), Dead(n=59). D) UV-SM+: Alive(n=790), Dead(n=29).

Using the same method of classification used in the previous experiment, both treatments see similar trends compared to the last experiment, Figure 55. In high expressing cells, UV+SM+ had more cells with high cytoplasmic proportion, but less cells with high nuclear proportion, when compared to UV+SM+. In the moderate expressing cells, UV+SM+ definitely had a higher number of cells expressing medium and high nuclear proportions of p21, while UV+SM- had only slightly more cells with low cytoplasmic proportions.

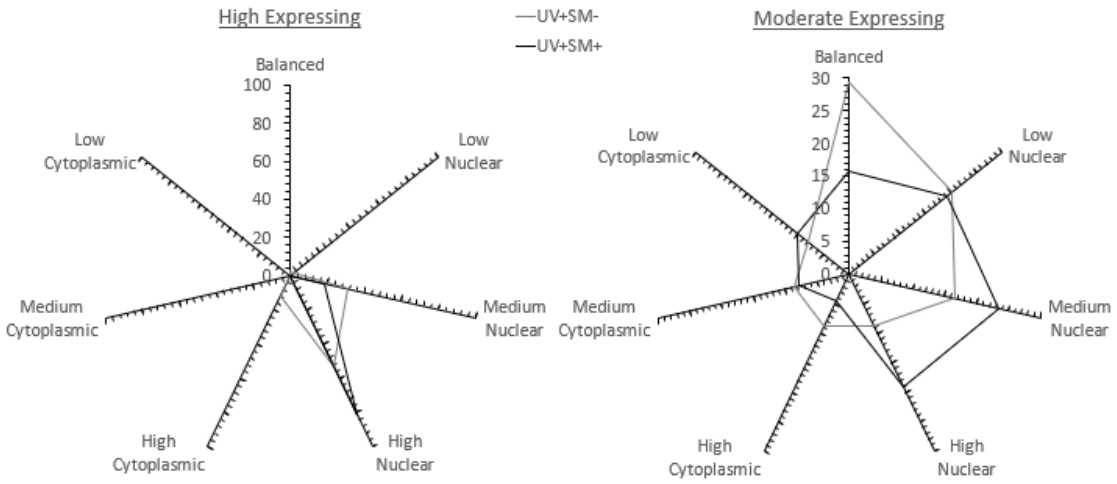

Figure 61. Comparison of p21 Proportion in High and Moderate Expressing Cells, Exp 2. Baseline threshold based off of UV-SM- distributions. Cells grouped by proportion of nuclear to cytoplasmic p21 expression. High expressing cells; UV+SM-(n=51), UV+SM+(n=27). Moderate expressing cells; UV+SM-(n=139), UV+SM+(n=89).

4.6.3 Discussion

The purpose of this experiment was to gather more data using 40x magnification rather than 10x for the stitched images for better resolution and to test how robust the image processing program was. All other methods of staining, image acquisition, image processing and data analysis were left the same as the first experiment.

When comparing localization dominance, seen in Figure 59, with Figure 53 of the last experiment, there are similar trends, but UV+SM- had many more cytoplasmic dominant cells than before. This could be because of the higher resolution allowing for more accurate nuclei borders.

Comparing dead cells between experiments also shows similar trends where they reflect living cells p21 content, Figure 57 & Figure 51. The error bars of Figure 57 represent the 95% confidence interval. They are so large most likely due to the low dead population numbers and the natural tendency of these cells to have a wide variation of p21 content. The high sample

number the first experiment had seems to almost be a necessity to understand what these cells are doing, however 40x magnification still allows for more accurate ROI labeling.

Distributions found in Figure 60 & Figure 54 show similar trends of UV+SM- centering around high p21 intensities when compared to UV+SM+. It is visualized much easier in the first experiment opposed to this experiment. To go around this problem, each cell was classified into proportion classes of nuclear to cytoplasmic p21 and average intensity classes, which can be found in Figure 61 and Figure 55 for the second and first experiments, respectively. Both graphs between the experiments look different, but both show that UV+SM+ has more nuclear dominant cells, while UV+SM- has more cytoplasmic dominant cells. Interestingly, UV+SM+ has less nuclear dominant cells than UV+SM- compared to their respective total populations, Exp. 2 (Figure 57[B] & Figure 58[D]) and Exp1(Figure 51[B] & Figure 52[D]).

This procedure seems to give the most accurate results, but it would be beneficial to take twice as many images of UV+ plates than UV- plates to acquire more data, or possibly use 25x magnification with high resolution. Regardless, both experiments show similar trends in the processed data.

4.7 p21 Expression of SM Treated KRT 3

4.7.1 Summary and Goals

The purpose of this experiment was to acquire high definition images of the cells with the same exact protocol of staining to obtain qualitative data, opposed to every other experiment focusing on quantitative data. The images were evaluated by finding differences between treatments in terms of p21 distribution and localization, to pair with the quantitative results of the first two experiments. Cells were stained with ethidium homodimer-1 to see dead cells, along with the p21-AF488 probe. Cells were not stained with Hoechst since the 405nm was

not functioning. Instead brightfield images were used to see the nuclei and subcellular structures. The images were obtained with a 100X magnification objective with up to 2x zoom.

It was found that ethidium homodimer-1 (EthD-1) could be used to identify some subcellular structures. Not all images had EthD-1 acting this way. Plot profiles were used to compliment the qualitative image with a quantitative representation. A plot profile measures each pixel on a user-defined line to output a plot of intensity versus distance. The plots were overlaid on the image to show differences of pixel intensity that are difficult to distinguish visually.

4.7.2 Results

Figure 62 shows high p21 expression in the cytoplasm of a UV+SM- cell. The arrow is pointing to the same p21 that was in a vesicle-like structure at the edge of the cytoplasm. The orange ellipse indicates an accumulation of p21 within the nucleus, but between the nucleolus and nuclear envelope, pointed out by the black and yellow arrow, respectively. This may have been a flow of p21 that transcripted and subsequently was traveling out of the nucleus towards the cytoplasm.

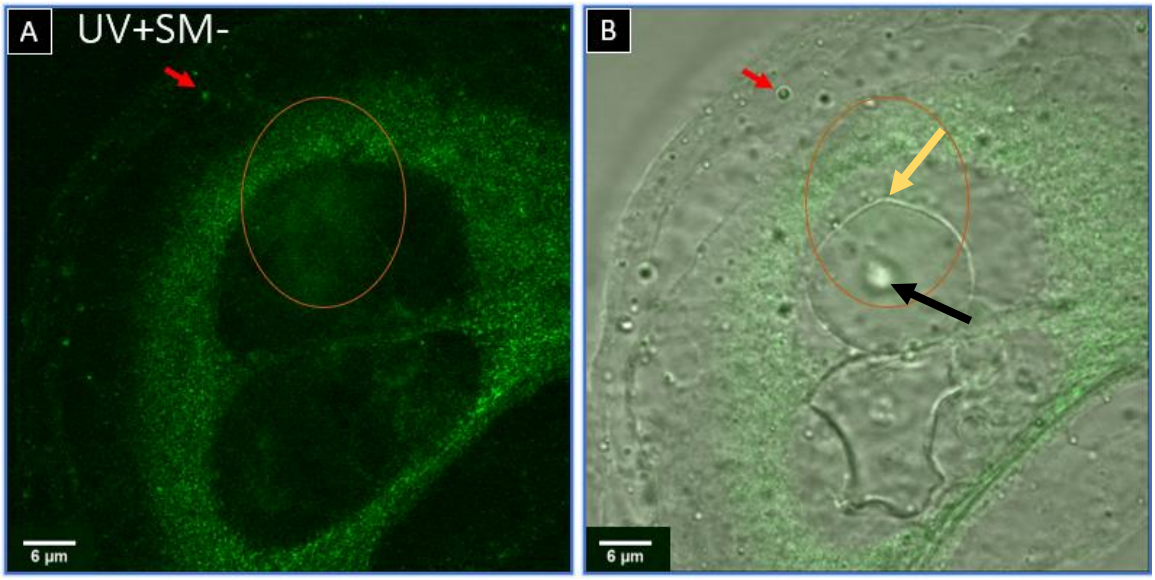

Figure 62. Dividing KRT, UV+SM-. A) p21 channel. Ellipse indicates an interesting accumulation of p21. Red arrow points to a vacuole with p21 inside. B) brightfield and p21 channel overlay. Red arrow and circle are in the same location as the left, for reference. Yellow arrow points to the nuclear envelope while the black arrow points to the nucleolus. Image Reference: A2

Figure 63 looks at another UV+SM- cell but with high nuclear expression. Figure 63[A] shows the p21 channel with a greyscale LUT and a plot profile following the yellow line. It was observed that this cell had a noticeable decline in p21 activity immediately outside of the nucleus, but showed higher p21 activity towards the plasma membrane. Figure 63[B] is the raw p21 channel. Figure 63[C] is the brightfield image. Figure 63[D] is the EthD-1 channel with contrast enhancements. The ROI seen in all images was made using this channel. Plot profiles in all figures were created in Excel and smoothed. Ethidium homodimer-1 channels were used as structure identifiers to complement brightfield, when looking at residuals left behind.

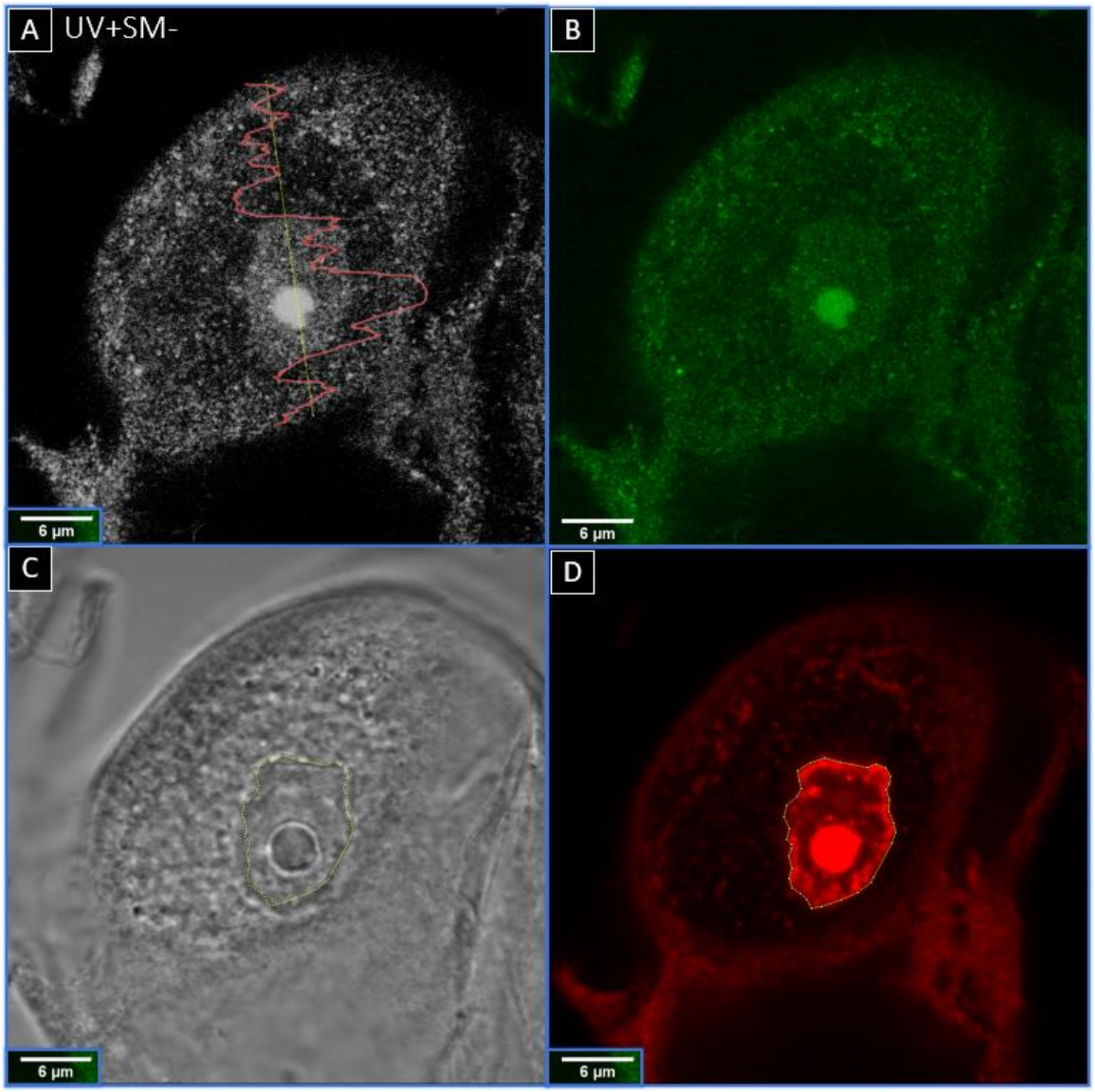

Figure 63. Dead KRT, High Expression, UV+SM- A) p21 channel, greyscale, contrast enhanced. Red line is the plot profile of the yellow line. B) p21 channel without modifications. C) Brightfield image. D) Ethidium homodimer-1 channel allowed for the ROI of the nucleus. Hoechst could not be used due to excitation laser not working. Image Reference: A3

Figure 64 takes many more plot profiles down the center of UV+SM- cells. Starting from the nucleus and working out, there seems to have been 3 distinct regions of p21 expression labeled as the nucleus, endoplasmic reticulum, and plasma membrane. The nucleus region is the area that has the lowest intensity towards the center of the cell. The endoplasmic reticulum, or what is presumed to be the endoplasmic reticulum, is adjacent to the nucleus region. The plasma membrane is the outermost region of the cell.

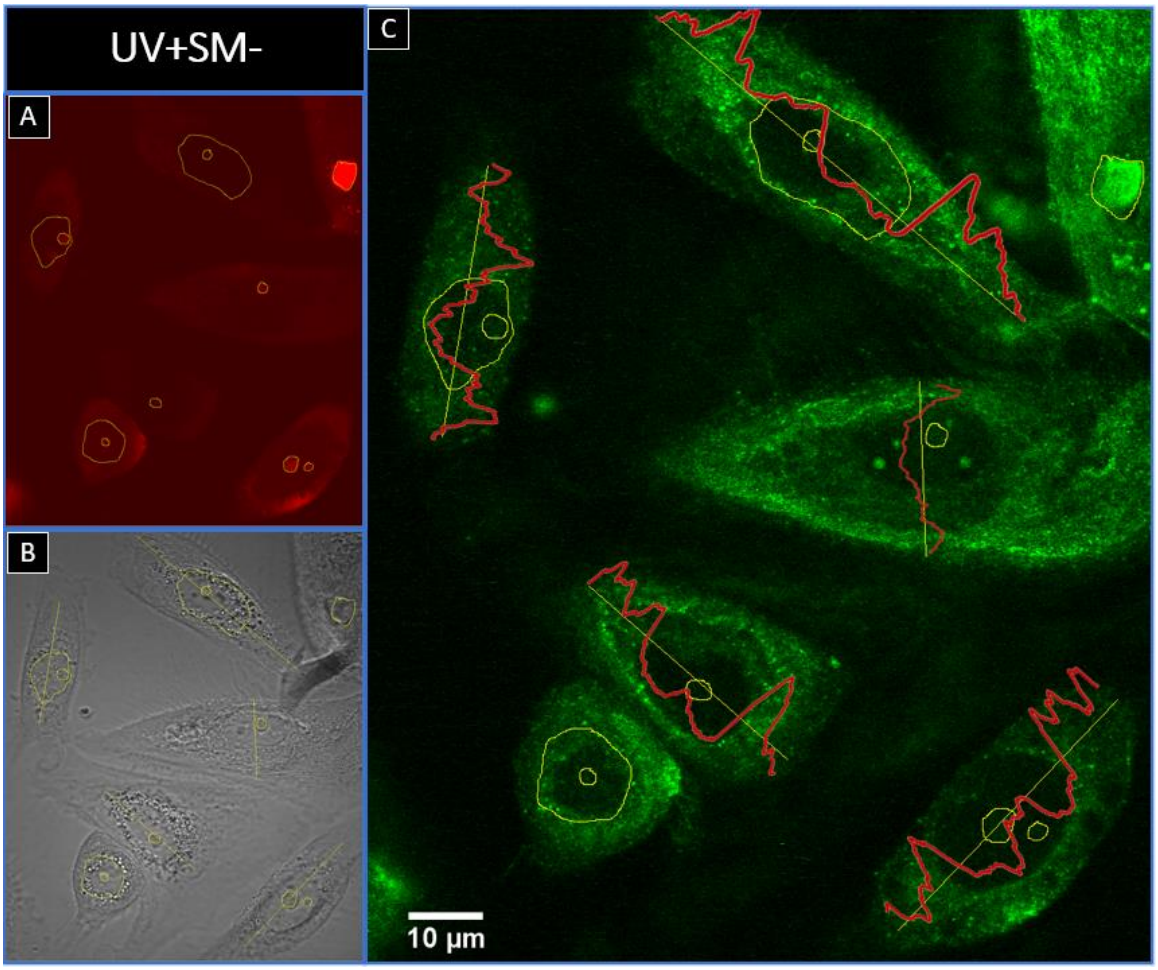

Figure 64. Grouping of KRT, UV+SM-. A) EthD-1 channel used for nuclear envelope and nucleolus identification. B) Brightfield with ROIs overlaid and plot profile lines. C) p21 channel, slightly enhanced contrast. Red lines are plot profiles of the yellow lines. Image Reference: B4

Figure 65 shows a group of UV+SM+ cells where two were dead. Pointed out by the white arrows in Figure 65[B], the bright red orbs of the EthD-1 channel signify a dead cell. Figure 65[C] is the brightfield channel and Figure 65[D] is an overlay of all the channels.

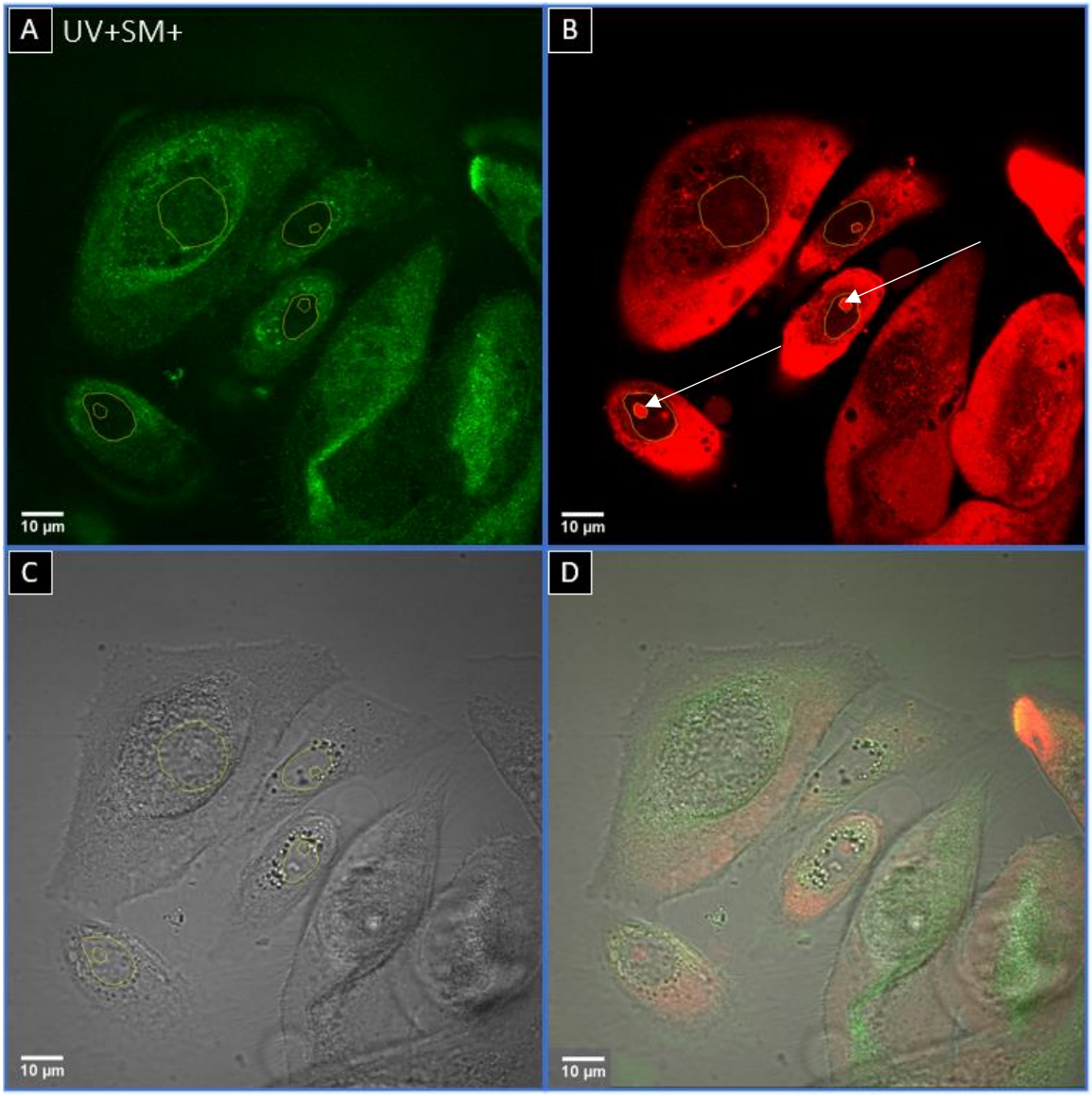

Figure 65. Grouped up KRT, UV+SM+ Larger circles indicate nuclear envelope, smaller circles indicate nucleolus. White arrows are pointing to bright EthD-1 staining, indicating a dead cell. A) p21 channel. B)EthD-1 channel. Image heavily modified in contrast and max value in order to see the structures. C) Brightfield. D) Overlay of all three channels. Image Reference: A4

Figure 66 are plot profiles of three UV+SM+ cells. Figure 65[A], the EthD-1 channel, was used to create ROIs around the nucleus of two out of three cells. Interestingly, the middle cell did not have any EthD-1 at all, possibly indicating different levels of permeabilization immediately before fixation of the cells. The two outer cells look similar to the UV+SM- cells that had low p21 immediately outside of the nuclear envelope, but had increased farther away from the nucleus. The middle one, however, had the opposite occur where there was high expression

immediately outside of the nuclear envelope and decreased farther away from the nucleus. There may be a correlation between EthD-1 not entering at all and p21 closer to the nucleus.

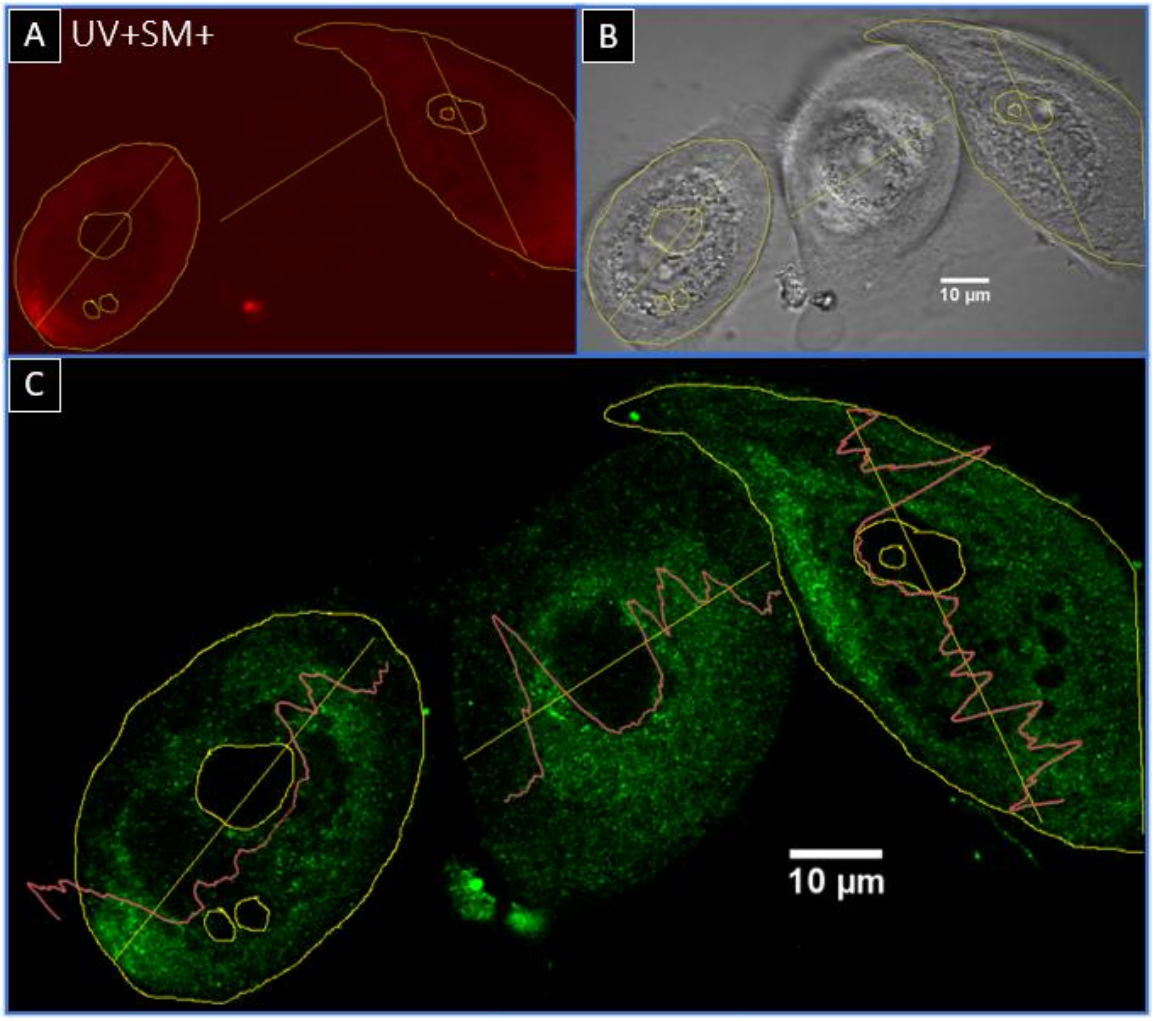

Figure 66. Three KRTs, UV+SM+.A) EthD-1 heavily contrast enhanced to see nuclear envelope. ROIS were found using this channel. B) Brightfield with ROI's overlayed. C) p21 channel, slight contrast enhancement. Red lines indicate plot profile of the yellow lines. Image Reference: A1

Figure 67 shows a dead UV+SM+ cell that had high nuclear expression. Dead cells were indicated by the infiltration of EthD-1 into the nucleus. When comparing to the high nuclear p21 UV+SM- cell in Figure 63, the plot profile seems to show less of a decline immediately outside of the nucleus when SM is added. The decline also extends for a shorter distance with the SM case, and the p21 that is in the cytoplasm looks uniformly distributed.

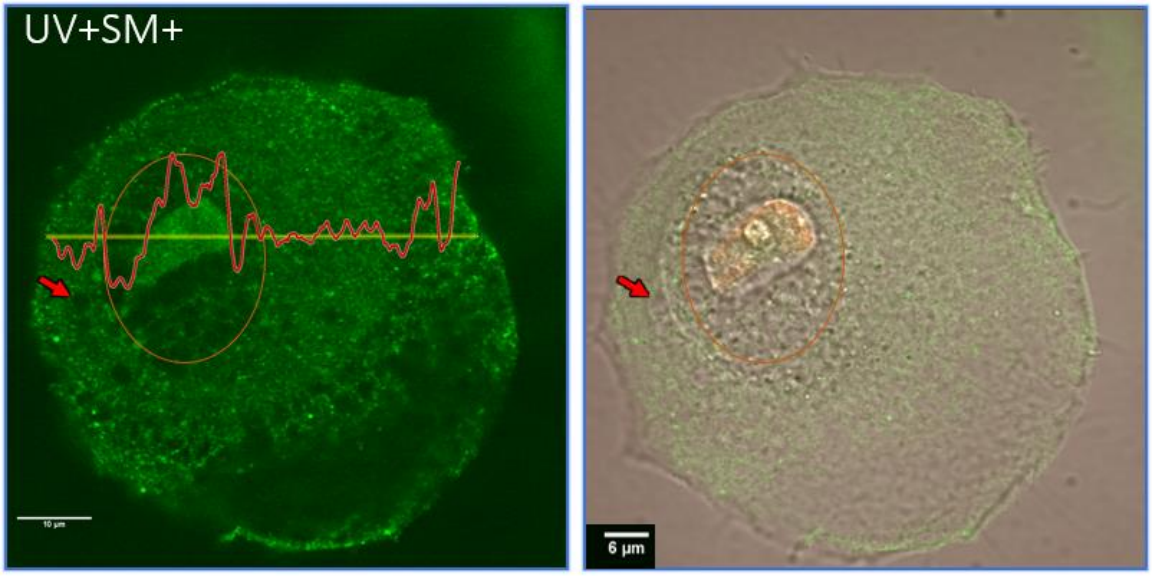

Figure 67. Dead KRT, UV+SM+. Left, p21 channel, slightly enhanced. Right, p21, EthD-1 and brightfield overlayed. Circle indicates rough estimation of the nuclear envelope. Red arrow pointing in the same sport, for reference. Image Reference: A3

Figure 68 is a representation of what the majority of the cells in the UV-SM- case looked like: if there was p21 at all, it was fairly uniform throughout the cell. Interestingly, there is a dip immediately outside of the nucleus, indicated as between the two dashed blue lines. However, when comparing nuclear and cytoplasmic peaks, they were very close.

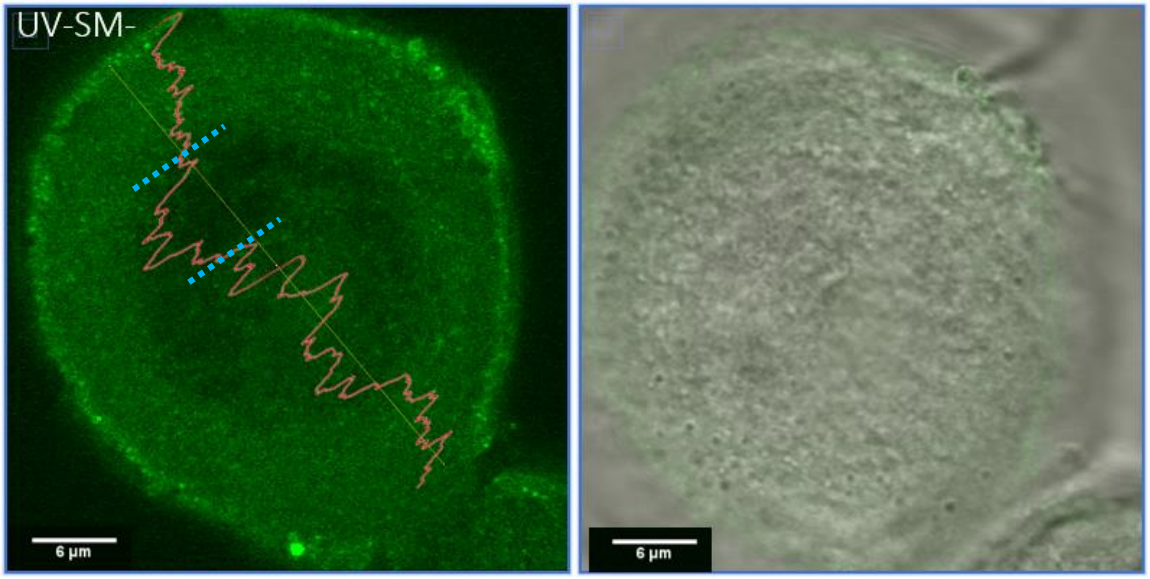

Figure 68. Low expressing KRT, UV-SM-. Left, p21. Red line is plot profile of the yellow line. Right, brightfield with p21 channel overlaid.

Figure 69 is the comparison of the UV+SM+ and UV+SM- treatment between a nuclear-dominant cell and a cytoplasmic-dominant cell. Comparing the nuclear-dominant, the UV+SM+ cell had a very high nuclear expression opposed to cytoplasmic, while the UV+SM- cell had nuclear expression just shy of the cytoplasmic. UV+SM- also seemed to have a more erratic distribution. The cytoplasmic-dominant cells were very similar to each other with the only noticeable difference being that UV+SM- looks to have a higher cytoplasmic mean of p21

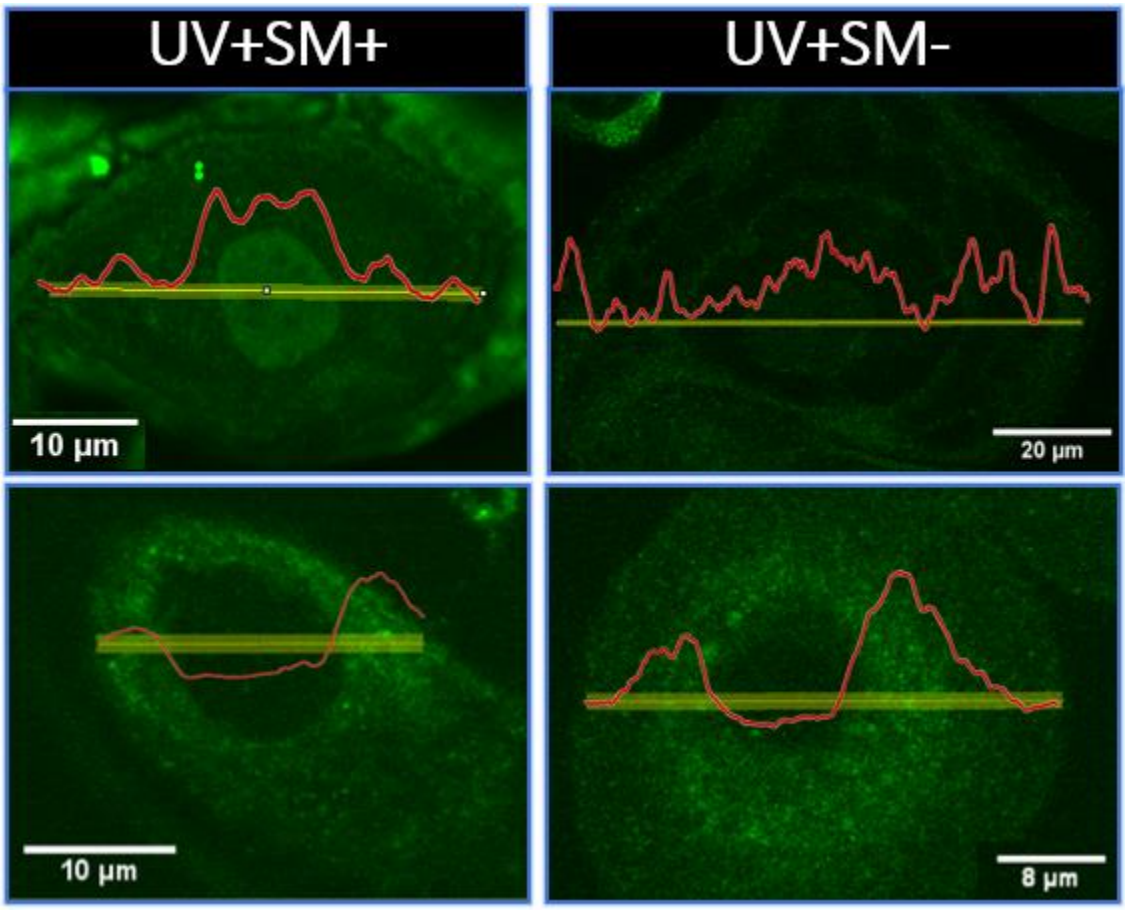

Figure 69. Side-by-Side of UV+SM-&UV+SM+. Top images would be considered nuclear dominant, while the bottom would be cytoplasmic dominant, in the case of p21 localization.

Figure 70 are images from the previous experiment, where similar trends were noticed. When looking at the plot profile of a nuclear expressing UV+SM- cell, Figure 70[1B], the dip immediately outside of the nucleus, yellow arrow, followed by an increase as the plot profile was closer to the plasma membrane, white arrow, was noticed. However, when observing the

plot profiles of nuclear expressing UV+SM+ cells, Figure 70[2A&2B], they both had only a slight increase from the nuclear envelope to the plasma membrane. Figure 70[1A], a non-nuclear expressing UV+SM- cell, had a major increase of p21 from the nuclear envelope to plasma membrane. Figure 70[1C&2C] were groups of cells in the p21 channel with a LUT applied. The LUT colors high values with orange shades, while low expressing values are green. It can be seen that the UV+SM- group of cells has much more p21 concentrated towards the plasma membrane, while the UV+SM+ group of cells had p21 more uniform, with some spots concentrated toward the plasma membrane.

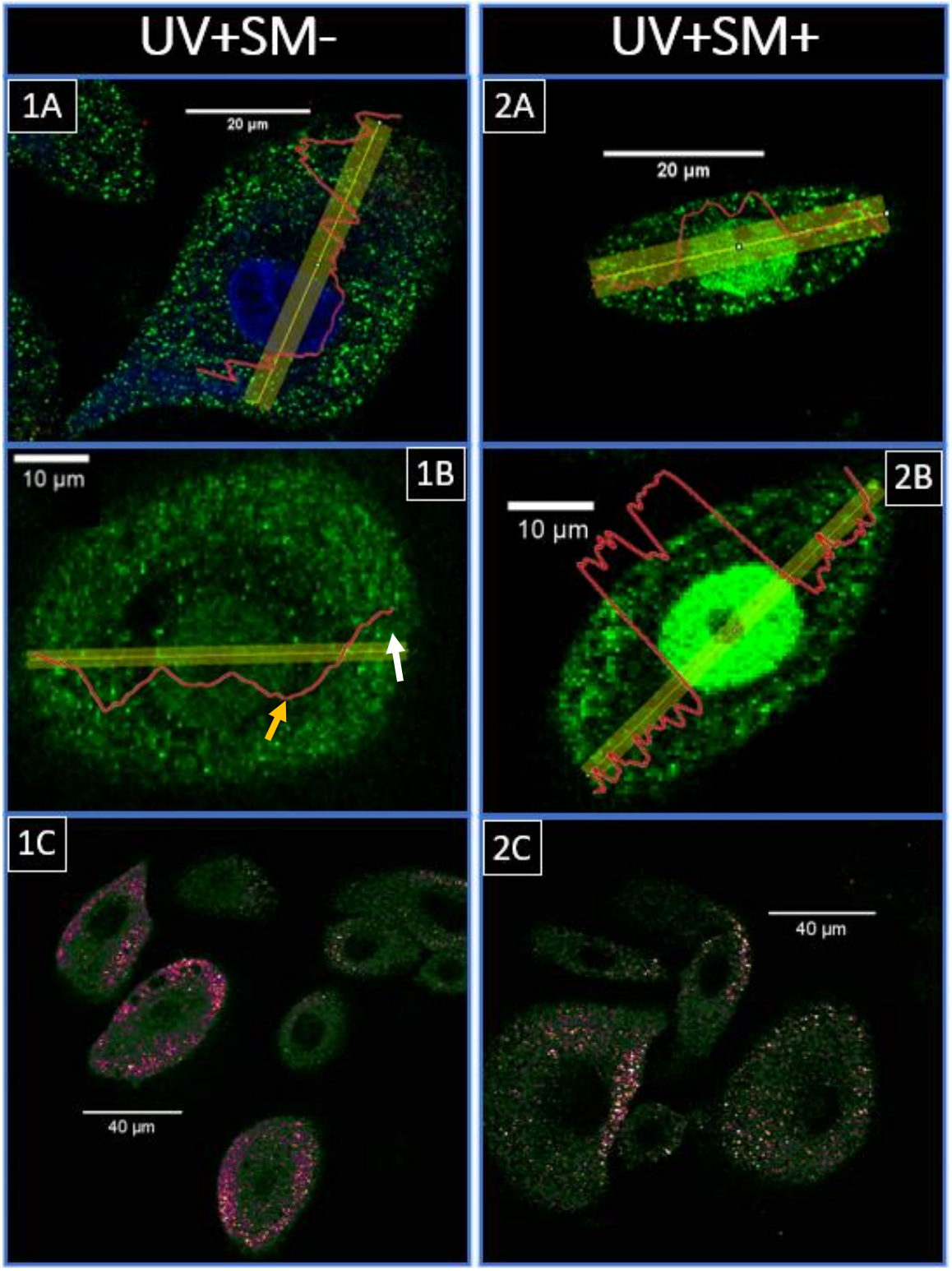

Figure 70. Similar analysis using Exp 2. Images. Top four images showing how p21 outside of the nucleus is more uniform in UV+SM+ cases, when compared to UV+SM-. Bottom two images are zoomed out in a random grouping of KRTs with a 'blue orange icb' LUT applied to see the highest value pixels.

4.7.3 Discussion

The goal of this study was to take high resolution, 100x magnification and high-quality images of cells within the four respective treatments: UV+SM+, UV-SM-, UV+SM- and UV-SM+. Unfortunately, the 405nm excitation laser was not working at the time, so Hoechst could not be seen. Fortunately, when the EthD-1 channel had the contrast significantly enhanced, it would sometimes unveil structures within the cell that EthD-1 could not penetrate into. This is apparent in Figure 66[A] where there was a slight fluorescence in the cytoplasm, but no penetration into the nuclear envelope, defining the boarder.

When comparing the location of p21 between UV+SM+ and UV+SM-, it appears as if UV+SM- KRTs had more cytoplasmic p21 towards the plasma membrane, Figure 64[C], Figure 63. Whereas, UV+SM+ KRTs had quite a few cells where cytoplasmic p21 was closer to the nucleus, Figure 66 & Figure 67.

Dead cells of the two treatments also had that similar effect. UV+SM+, Figure 67, had an almost uniform distribution along the plot profile line directly outside of the nucleus. On the other hand, UV+SM-, Figure 63[A], had a dip outside of the nucleus, where the endoplasmic reticulum may be and regains intensity when reaching the plasma membrane.

Regardless, data in the last two experiments shows that the proportion of p21 in UV+SM- KRTs favored cytoplasmic localization while the UV+SM+ KRTs favored nuclear localization. This means that cytoplasmic p21 in UV+SM+ KRTs had very low intensity compared to the UV+SM- KRTs. Even though p21 was more uniformly distributed closer to the nucleus in UV+SM+, UV+SM- had significant increases in p21 the further away from the nucleus.

Performing the analysis on the images from experiment 2, Figure 70, shows the same sort of trend where UV+SM- KRTs have a slope of p21 intensity starting at a low intensity from the nucleus. UV+SM+ has the same uniform p21 distribution immediately outside of the

nucleus. In addition, the bottom two images of Figure 70 have a LUT applied where orange pixels are the highest intensity. UV+SM- orange pixels are much more localized cloaser to the plasma membrane, while UV+SM+ are more distributed evenly in the cytoplasm.

4.8 Fluorescent Sphingomyelin Distribution Time Study

4.8.1 Summary

In order to understand how and what sphingomyelin is doing to protect KRTs from UV, we investigated where SM is located in the cell and how it fluctuates over time. KRTs with exogenous fluorescently tagged sphingomyelin (fSM) can be used to follow the lipid as it is transported throughout the cell. The fSM used was a short chain NBD C6-sphingomyelin lipid attached with a fluorescent tag that excites under 488 nm light.

This experiment was performed jointly with Stephanie Switalski. For this study KRTs were incubated in fSM for an hour, followed by replacing with fresh media. One plate of KRTs were fixed and stained with Hoechst immediately following the incubation period, while the other plates were fixed at; 1, 2, 4, 6, 9 and 12 hours after, Table 6. Fixation and Stain Schedule.

The primary goal was to see how fSM intensity shifted over time in the cytoplasm. The donut ROI macro was used to accomplish this, found in 3.7.8 fSM Donut ROI measure. The secondary goal was to see how the distribution of fSM shifted throughout the cell over time. Macro in Section 3.7.9 fSM Rotation measure was used for this part.

The tertiary goal was to see if there was a difference in the staining process while performing under red light, versus normal light. The donut ROI data was used to compare fSM accumulation in the cytoplasm between cases.

Table 6. Fixation and Stain Schedule.

Time (Hours)

Specimen	-1	0	1	2	3	4	5	6	7	8	9	10	11	12
0		Fix & H												
1			Fix & H											
2				Fix & H										
4						Fix & H								
6								Fix & H						
9											Fix & H			
12														Fix & H
1 Bleached			Fix & H											
fSM	Media													

4.8.2 Results

Figure 71 shows the fSM intensity in the cytoplasm for each cell for each time point. Using ANOVA at a 99% CI, the 0hr was significantly different than every other time point. The 1hr was significantly different than every time point, except for the 6hr. 1hr-bleached was significantly different from the 1hr, showing that the fluorescent lights can cause significant bleaching during the staining process. An ANOVA, or analysis of variance, tests to see if the means between two or more groups are significantly different, or not, but won't say which groups are different. A Tukey Test can be done after the ANOVA to find exactly which groups are significantly different from each other, pairwise.

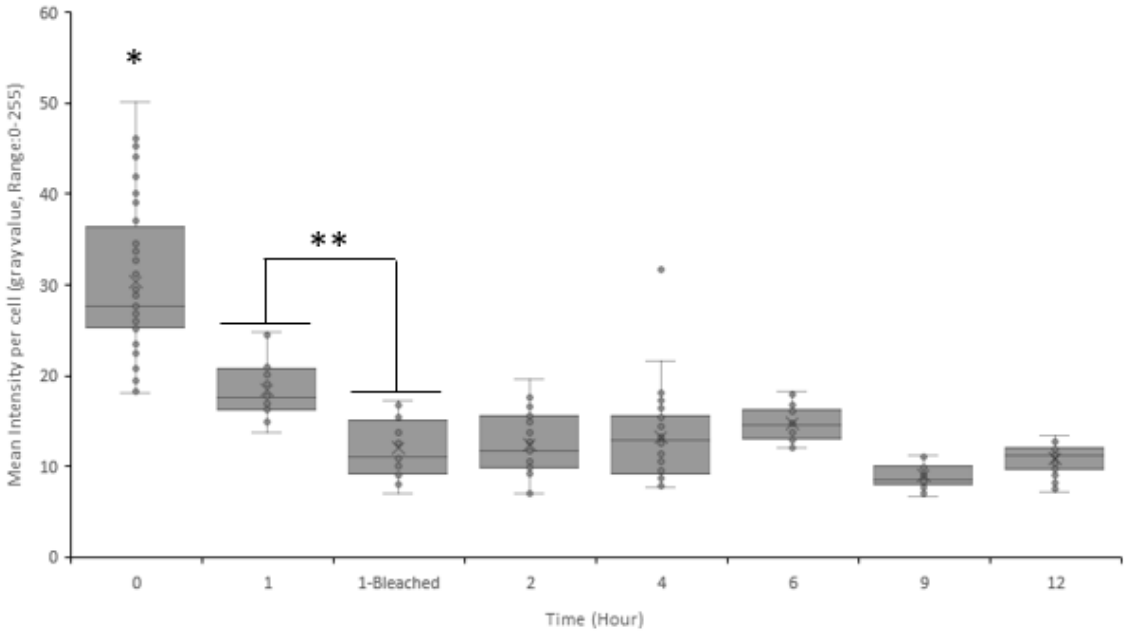

Figure 71. Cytoplasmic fSM intensity over time. KRTs fixed at different times following the 1 hour incubation period of fSM. Mean cytoplasmic intensity found by using the 'donut' method described in 3.7.8 fSM Donut ROI measure. 0hr(n=40), 1hr(n=16), 2hr(n=29), 4hr(n=36), 6hr(n=22), 9hr(n=35), 12hr(n=65) and 1hr-Bleached(n=32). (*= (p<.01))

Table 7 were the results of the Tukey Test showing which time points were significantly different, at a 99% CI. If a time point shares a grouping letter, that means they are not significantly different.

Table 7. Tukey Test, 99% CI of Figure 71. Cytoplasmic fSM intensity over time. 1.1 is the photobleached 1hr case.

Hour	N	Mean	Grouping			
0.0	40	30.35	A			
1.0	16	18.365		B		
6.0	22	14.698		B	C	
4.0	36	13.238			C	D
2.0	29	12.433			C	D	E
1.1	32	12.001			C	D	E
12.0	65	10.878				D	E
9.0	35	8.959					E

Means that do not share a letter are significantly different.

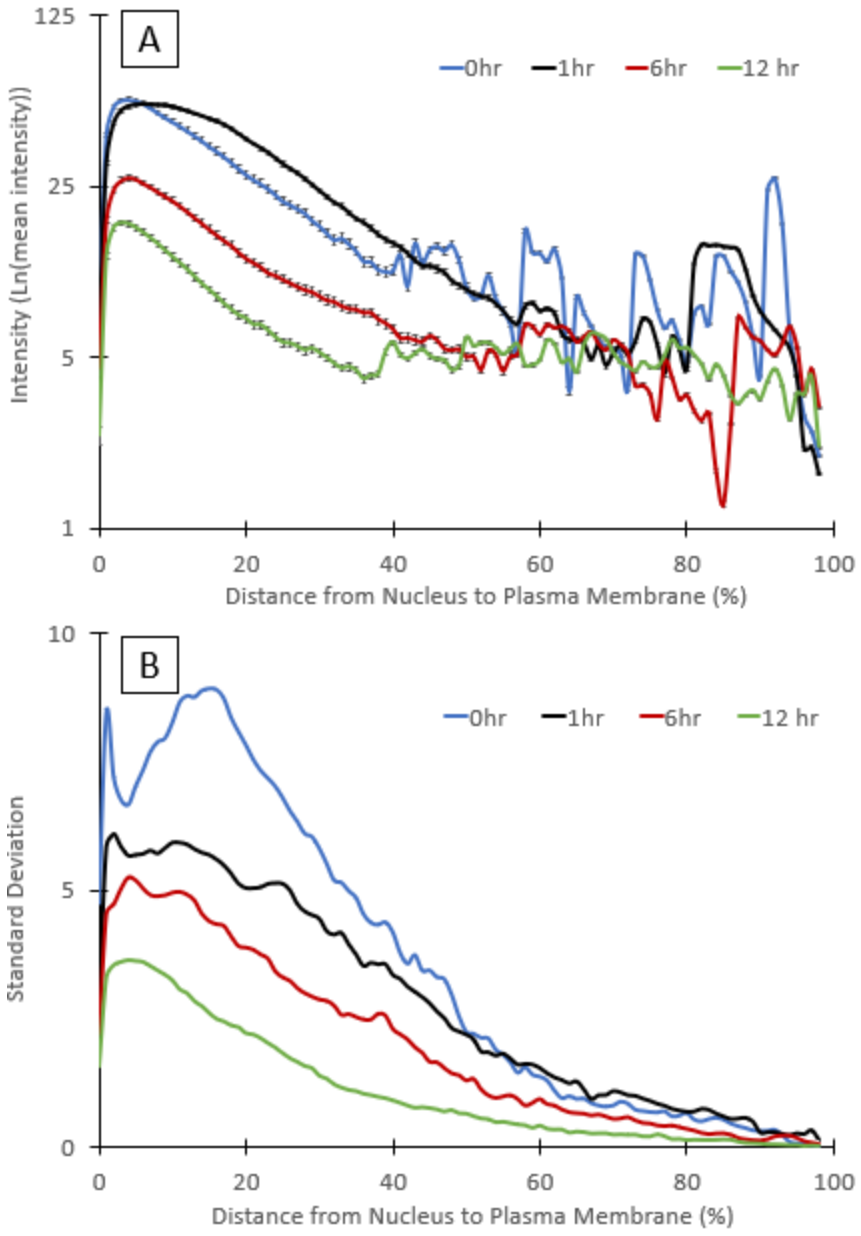

Figure 72. fSM Intensity Between the Nuclear Envelope and Plasma Membrane. Distance from nuclear envelope to plasma membrane respresented as a percentage. A) Mean Intensity on a log-normal scale. B) Plotting the standard deviation. 0hr(n=37), 1hr(n=15), 6hr(n=26), 12hr(n=64).

To quantitatively determine fSM distribution changing with time post incubation, the rotation data was averaged across all cells for each treatment group. Figure 72 hows a decrease in intensity as time goes on. Standard error was found across every percentage point for all 61 plot profile lines of a cell resulting in a 1x100 array per cell. The standard error array was then

averaged across all cells in the treatment group, resulting in a 1x100 array for each time point. The average standard error was then plotted to see how gray value variation changes over time, as seen in Figure 72.

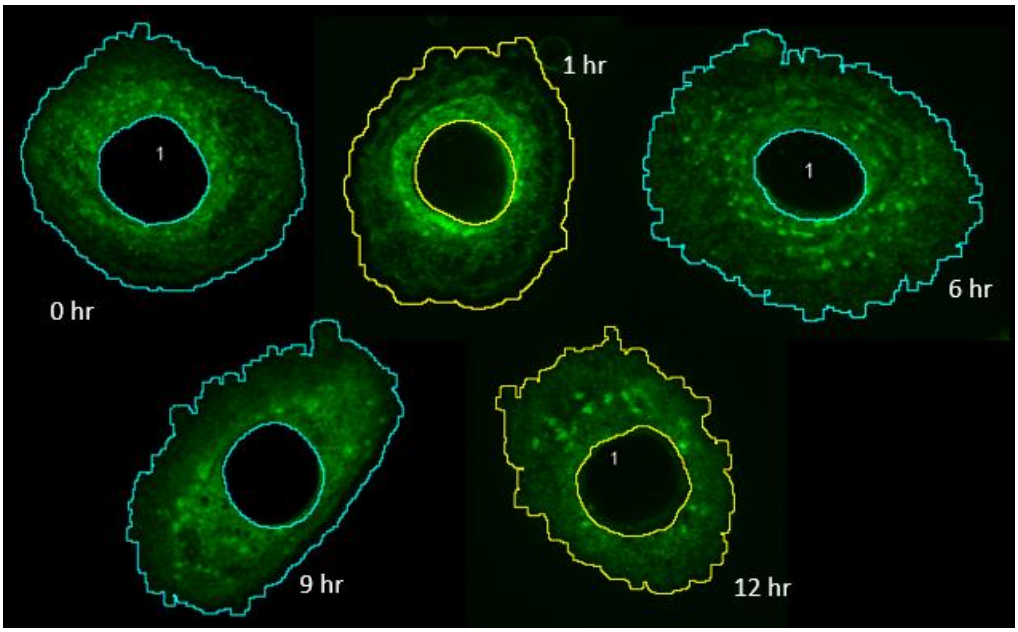

Figure 73. Representative Cells of Each Time Point. Each cell shown had it's respective mean normalized to the mean of the 1hr time point.

Observing Figure 73,Figure 73. Representative Cells of Each Time Point.there is a clear change in fSM distribution from the 0hr to 12hr time point. At 0hr, the fSM signal was diffuse but concentrated towards the nucleus. At 1 hour, there was a clear concentration of fSM surrounding the nucleus, with the rest of the cytoplasm containing less signal. There was still fSM concentration around the nucleus at the 6hr, but signal had also started to diffuse out towards the cell edge. There was also the formation of 'packets', which were small areas of high fSM signal. This trend continues in the 9 and 12hr images, with an increase in packets of signal and non-packeted signal becoming more diffuse through the cell.

4.8.3 Discussion

Image processing methods and data analysis allowed for the quantification of fluorescent sphingomyelin trafficking throughout the cell over time with the use of confocal microscopy and ImageJ.

The primary goals of this experiment were two-fold: to investigate the trafficking patterns of fSM and to find a way of quantifying the movement. Using confocal microscopy, the movement of the fluorescent lipid can be tracked over time. Image analysis using ImageJ was successful in identifying the different distributions of fSM as the lipid was processed by KRT. Despite slight limitations involving statistical analysis, this experiment was successful in identifying how keratinocytes traffic fSM through time and in creating an image processing method to measure it.

A decrease in intensity was found between the photobleached plate, which used fluorescent lights, and the red-light data, which did not use fluorescent lights. This supports the hypothesis that fluorescent lights can photobleach fSM. However, experiments performed by other members of the lab have corrected for fluorescent light photobleached samples with slightly increased laser power. While using red lights did prevent photobleaching, it also caused some difficulties while performing the methods, such as the low-light conditions it created. More experimenting should be done to determine if the effects of fluorescent light photobleaching are severe enough to warrant the extra effort of using the red-light lamps.

The decrease in the fSM channel intensity may be attributed to several different theories. The first being that the cells are expelling fSM out through the membrane due to saturation during the 1 hour of incubation. The second is that the cells are converting the fSM into derivatives like ceramide and in that process the fluorescent tag is lost and no longer

fluoresces. The third is that the fluorescent tag on the fSM is being cleaved or loses its intensity as time goes on.

Average standard error of the cell rotation was used to quantify how the cell's intensity changed as time goes on by distance from the nucleus to the membrane, Figure 72. fSM Intensity Between the Nuclear Envelope and Plasma Membrane. Qualitative data shows a possible theory as to what may be happening in the cell Figure 73.

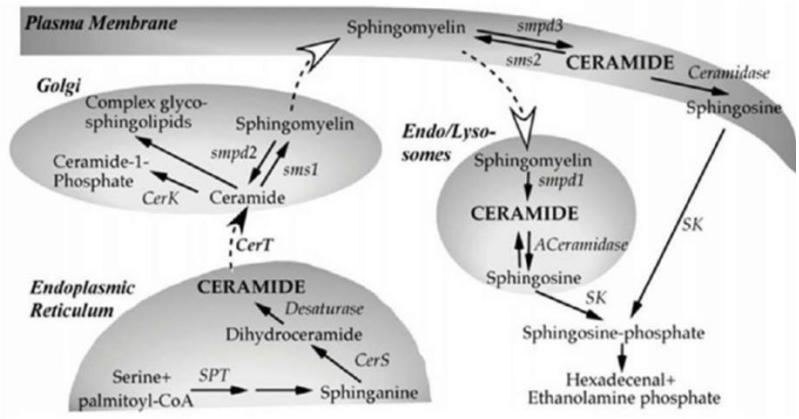

Figure 74. Potential fSM trafficking explanation [70].

Figure 74 depicts a possible pathway fSM is trafficked throughout the cell. It is theorized that at hour 0 fSM is in the middle of being trafficked towards the endoplasmic reticulum (ER) seen as the high variation between 10% and 20%. At hour 1 the variation decreases and appears as if the majority of intensity is located around the nucleus showing a possible accumulation in the ER. As time goes on variation and intensity decrease while images no longer show any high fSM concentrations around the nucleus. Figure 74 shows fSM can turn into SM metabolites at many different steps which could be why there is a decrease in fSM intensity in the overall cell and specifically the ER. Excess fSM could be expelled through the membrane to restore the cell to an equilibrium balance.

4.9 Fluorescent Sphingomyelin Live Cell Distribution Dynamics

4.9.1 Summary and Goals

With the development of the confocal incubator, seen in Figure 75 and documented in Appendix A.2, allowed for observing fSM in KRTs and how the lipid moves throughout the cell over time. The incubator keeps the temperature of the cell culture plate at 37C, to keep cells in physiologically relevant conditions over a long period for imaging. Previous lab member, Rebecca Kandell, experimented with fSM in living cells, but found that temperature was a major limiting factor that affected how long you could image the cells [67].

The goal of this study was to evaluate how well the incubator works in terms of ambient air temperature near the cell culture plate, and image quality. A digital multimeter with a temperature probe was used to measure air temperature. The secondary goal was finding an optimal image acquisition and/or image processing method. Establishing the appropriate method is necessary since fSM was left on during a part of the imaging causing an extremely bright and saturated plasma membrane, in relation to the dim subcellular fSM.

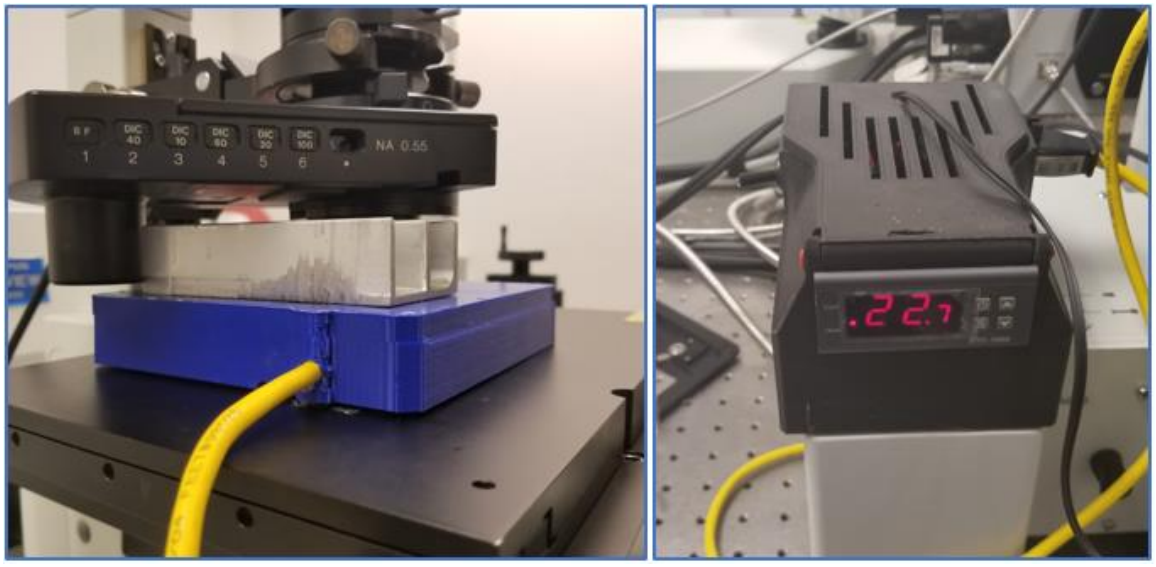

Figure 75. Confocal Microscope Live Cell Incubator.

4.9.2 Results

A macro was created to reduce the intensity of the plasma membrane localized fSM since it washed out fSM within the cells, Figure 76. Each image in the series had the minimum value subtracted from every pixel to line up the minimum with every image. Then, each image had a natural logarithm transform to improve normality and peak histogram values aligned, ignoring saturated. The square root was taken to reduce distance between high and low values more so than between two low values. Gamma corrections were then done to isolate higher expressing values from surrounding noise. After each step a linear scale was applied to equalize the histogram from 0 to 4095 (12-bit scale). The 12-bit scale was used to give the lower values more bandwidth, whereas starting in 8-bit scale (0-255) lower expressions would be binned too close together.

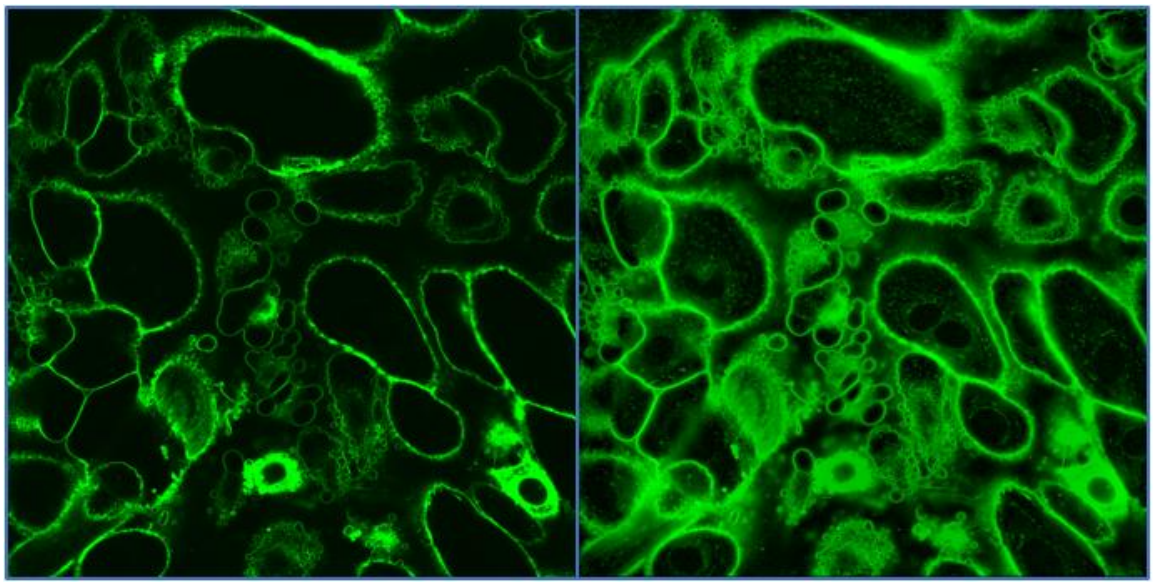

Figure 76. Live fSM Image Correction. Left, raw image acquired with the confocal microscope. Edges were nearly completely saturated, while subcellular fSM was nearly invisible to the eye. Right, after a natural-log transform, square root and gamma correction to unveil the subcellular fSM.

Figure 77 shows some interesting events that were observed after adding fSM to the KRT media. The yellow arrows are pointing to major events involving fSM that most KRTs had at the plasma membrane. fSM bubbles were quickly moving to the cell membrane, collapsing and

entering the cell. The graphs to the right in Figure 77 are plot profiles of the yellow line in the image. The red arrow follows an fSM signal traveling towards the nuclear envelope.

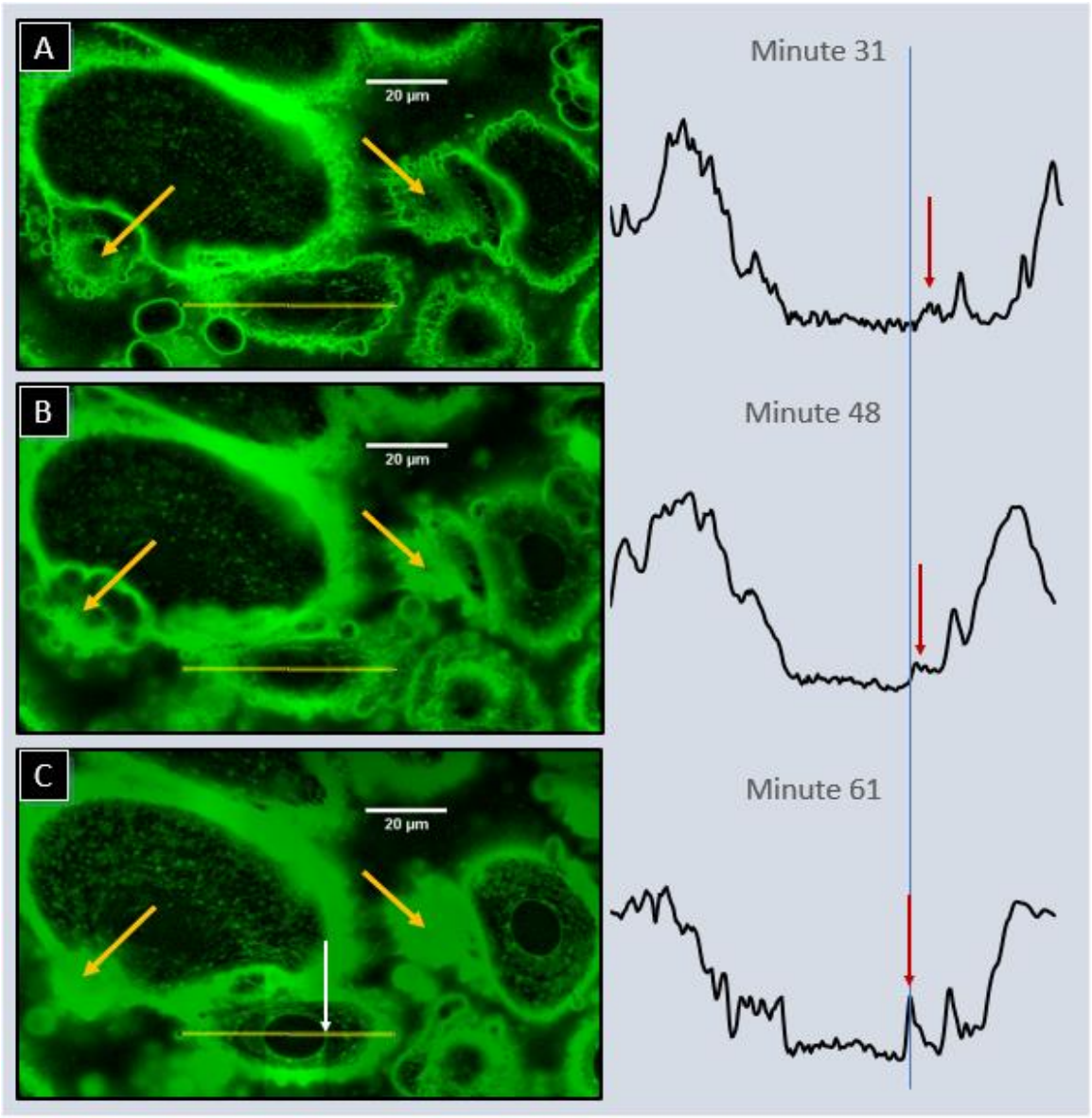

Figure 77. fSM entering KRTs over 30 minutes. Plots to the right represent the plot profile of the yellow line over time. Vertical blue line aligns plot profiles to a moving signal. White arrow in the last image points to where the blue line is, the nuclear envelope. Yellow arrows pointing to similar large events. A) 31-minute after replacing KRT media with the fSM infused KRT media. B) 48 minutes after and C) 61 minutes after.

Figure 78 was the first image taken after adding fSM. The image quality was not as good as the previous figure because imaging parameters were being adjusted to find the correct amount of plasma membrane fSM saturation to subcellular fSM visibility. Here, the plasma

membrane fSM was not saturated, in turn giving the low subcellular expressions very low bandwidth in the PMT. Before the confocal microscope could be set to scan, fSM was already inside cells, according to this image. It is possible that it could be an artifact of some sort of reflectance. Even when adjusting the image with the method described in Figure 76. Live fSM Image Correction. Subcellular fSM was visually much lower in comparison to Figure 77.

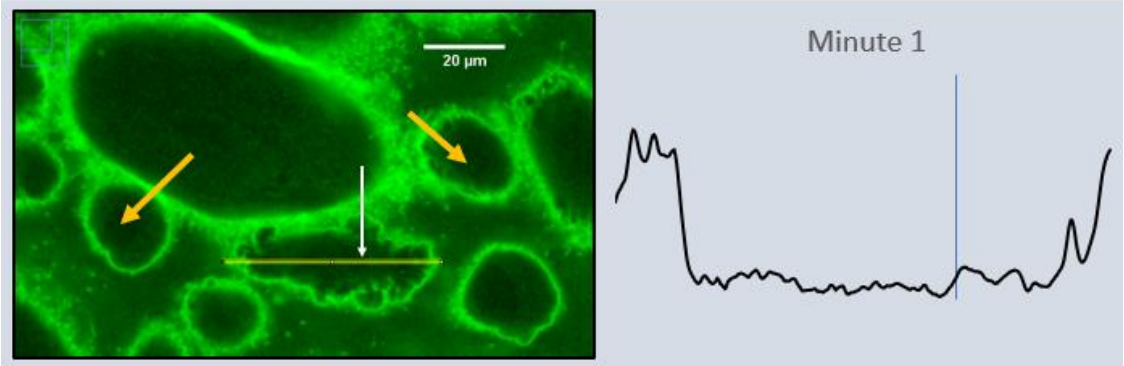

Figure 78. First Image after adding fSM. Adjusted image, 1 minute after replacing KRT media with fSM/KRT media solution. Yellow arrows pointing to the same cells in the previous figure. White arrow pointing to the same nuclear envelope as well. Blue line in plot profile lines up with the white line in the image.

Using the reflectance channel, Figure 79, the same plot profile line used in Figure 77 was used to measure the values of reflected light. The graph to the right compares the two channels intensities on the line, where some structures line up, like the plasma membrane.

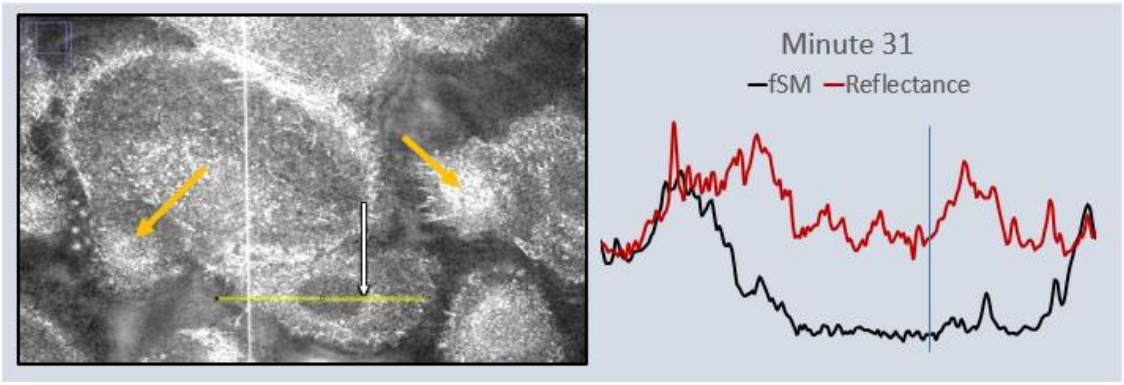

Figure 79. Comparing Reflection Image. Adjusted reflectance channel, 31 minutes after replacing KRT media with fSM/KRT media solution. Yellow arrows pointing to the same cells in the previous figure. White arrow pointing to the same nuclear envelope as well. Blue line in plot profile lines up with the white line in the image.

4.9.3 Discussion

The goal of this experiment was to test how well the incubator worked in terms of image quality and ambient air temperature next to the cell culture plate, while the secondary goal was establishing an appropriate acquisition and image processing method.

Ambient air temperature was able to get to 34°C, 3 degrees less than body temperature, but right on target for skin temperature. Incubator temperature fluctuated 3 degrees passed the setpoint with a slow decline back to the setpoint, indicating the heating source is too powerful with a simple switched relay. Future revisions implementing a full PID relay adjusting current. Right now, a variable resistor can be used to suppress the rate at which temperature increases, potentially limiting how far temperature goes passed the setpoint. Since the heating plate is above the culture plate and heat rises, two L-brackets can be fastened against the plate to try and deliver heat at lower temperatures, as well as retain heat while the relay is off.

It was found that the switching on and off of the temperature relay along with the slow cooling and fast heating caused the coverglass to expand and retract on the micron level, causing cells to go in and out of focus. This occurred much more severely when the top of the culture plate was removed at minute 61. Watching time lapses after minute 61, it looked as if the cells were beating like a heart, but in reality, the cover glass expanding in higher temperature pushed the cells up, while the cooling pulled the cells down towards the objective. To remedy this problem, the temperature probe for the incubator will be moved closer to the heating element as well as keeping the lid on the cell culture plate when imaging.

When image acquisition was adjusted, image quality was enhanced. Laser power was gradually reduced in order to reduce photobleaching, something Rebecca Kandell observed in a very similar experiment set-up using fSM [67]. Laser power was able to get to 2% to sustain

measurements of subcellular fSM, while the PMT was around 700. Though, it still took image processing to unveil subcellular fSM.

To remedy the intense plasma membrane fSM, two fSM channels could be created in FluoView. One channel could have a high PMT voltage to see the subcellular interactions, while the second channel could have a low PMT voltage to see the interactions outside of the cells.

Chapter 5: Discussion

5.1 Conclusion

The primary goal of this thesis was to investigate why SM-incubated KRTs have less nuclear p21 after UV exposure, as opposed to UV-exposed KRTs that were not incubated in SM. The first direction of investigation was examining the expression of p21 in dead KRTs. Unfortunately, dead KRTs lose their adherence to the coverglass and are discarded whenever liquid is aspirated off the cell culture plate. To remedy this, Poly(D-Lysine) was coated on cell culture plates in an effort to hold on to more dead and apoptotic cells. It was found that an incubation of 30+ minutes in 100ug/ml PDL followed by drying for 1-2 hours gave enough of an attachment factor to hold on to dead and apoptotic cells until fixation. Dead cell adherence was evaluated by using Ethidium Homodimer-1 to label dead, permeabilized cells. After the attachment factor was optimized, the dead and apoptotic cells were able to stay attached to the coverslip until fixation. This allowed the dead and apoptotic cells to go through the same staining and imaging procedure as the living cells. When dead and apoptotic cells were plotted with living cells in terms of p21 intensity, it was observed that there was a large proportion of dead and apoptotic cells that had low p21 intensity in the UV+SM+ treatment group in comparison to the UV+SM- treatment group, Figure 54.

Nearing the end of the qualification experiments, it was evident that there was much variation between KRTs coverage in the same environment, so the sample size was significantly increased to ‘paint’ a better distribution. Starting with 10x stitched images in a 3x3 matrix, the sample size was increased, but at the cost of image quality and potentially ‘missing’ the middle of nucleus, giving inaccurate results. Using the same exact process, the magnification was increased from 10x to 40x. This reduced the sample size, but improved image quality and confidence of imaging the middle of the nucleus, and not the top or bottom. At this point it was

observed that the cytoplasmic p21 in UV+SM- KRTs were higher than UV+SM+ KRTs. The Binary Threshold Drop macro served to measure nuclear and cytoplasmic p21 expression in the larger images to confirm adding SM prior to UV exposure reduced the cytoplasmic expression. It was quickly realized that there was a correlation of nuclear expression and cytoplasmic expression, so measuring every cell's cytoplasmic expression did not accurately reflect if there was more or less expression.

In the attempt of quantifying how p21 expression was different in the UV+SM- treatments when compared to the UV+SM+, it was evident that two variables were needed: where the proportion of p21 was located, and at what level of expression. When averaging the p21 expression level of the nucleus and cytoplasm between treatment groups, it did not give any new information where UV+SM- had more nuclear p21 expression than every other treatment group, but cytoplasmic p21 expression followed the same trend, Figure 58A. When averaging the nuclear/cytoplasmic proportion of p21 between treatment groups, it came out inconclusive. Low expressing populations of cells had different proportions than that of higher expressing populations, causing the average to be sporadic between samples. To separate the subpopulations based on p21 expression cells were categorized. Cytoplasmic and nuclear p21 expression values were combined to create the 'p21-intensity' variable for each cell. Cells were categorized as either low, moderate or high expressing with cutoff points created from the UV-SM- control distribution. In addition, cells were categorized from p21 proportion data as either low, moderate or high expressing of the nuclear or cytoplasmic regions. Cutoffs were created from the UV-SM- data as well. Graphing the categorized cells in radar graphs showed that of the moderate and high expressing cells the UV+SM- treatment had more cells with proportionally more cytoplasmic p21 activity, whereas the UV+SM+ treatment had more nuclear. This is interesting, because there was a higher number of nuclear expressing cells in the UV+SM-

treatment in comparison to the UV+SM+ treatment. What this means is that the UV+SM- treatment causes more cells to have elevated nuclear p21 expression than the UV+SM+ treatment, but the majority of p21 still resides in the cytoplasm.

A possible explanation of this phenomenon could be that SM is causing a reduction of p21 being translocated from the nucleus to the cytoplasm, keeping the p21 within the nucleus. SM could interfere with the lipid raft containing the appropriate signaling molecules to effectively activate Akt. Without SM, UVB causes a cascade starting with EGFR and activating Akt, pulling p21 out of the nucleus into the cytoplasm, Figure 80.

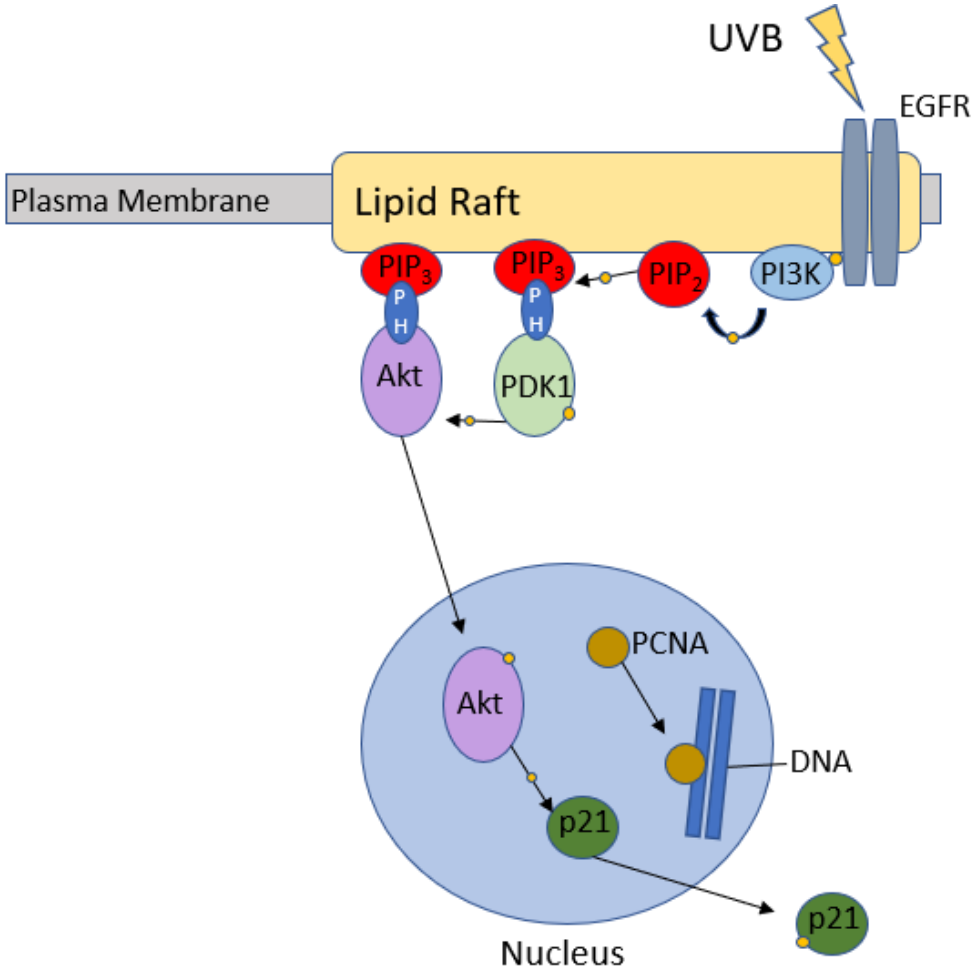

Figure 80. Potential Explanation for Cytoplasmic p21 Expression in UV+SM-.Lipid rafts made of sphingomyelin and cholesterol bring together signaling molecules for the PI3K/Akt pathway involved in pro-tumorigensis [10][46][47][48][49]. Akt and PDK1 attach to lipid rafts rich in PIP_2 and it's phosphorylated conjugate, PIP_3 by PH domains [7][60][61].

With SM, the signaling molecules within the lipid rafts responsible for activating Akt are disassociated with each other, effectively down regulating p21 being pulled out from the nucleus into the cytoplasm. It is known that a disruption of the cholesterol/SM enriched lipid rafts causes a decrease in Akt activation in many different types of cells due to signaling molecules not being in close proximity in lipid rafts for both the EGF and IGF-I receptors [12][46][50][51][52][56]. Only one study was found to add sphingomyelin when addressing Akt activation, at which they saw a decrease with SM, but an increase with C_{16} ceramide [57]. Cuijuan et al. and Megha et al. found that adding exogenous ceramide caused cholesterol to displace from lipid rafts in lipid raft membrane models [53][54]. Cuijuan et al. also increased ceramide levels in Schwann cells by adding an SMase, causing cholesterol to dissociate from lipid rafts, disrupting them[54]. It is also known that UVB causes ASM to quickly activate and convert a large portion of SM into ceramide [42][53][55].

It is hypothesized that cells within the UV+SM- treatment had a majority of the plasma membrane SM reserves quickly deplete after UV activated ASM but enough to have stable lipid rafts to assist in Akt activation. The cells within the UV+SM+ treatment had a much larger supply of SM that didn't deplete as quickly, causing the plasma membrane to still be saturated with SM, not allowing for proper lipid raft formation, resulting in a downregulation of Akt activation and keeping p21 in the nucleus, Figure 81.

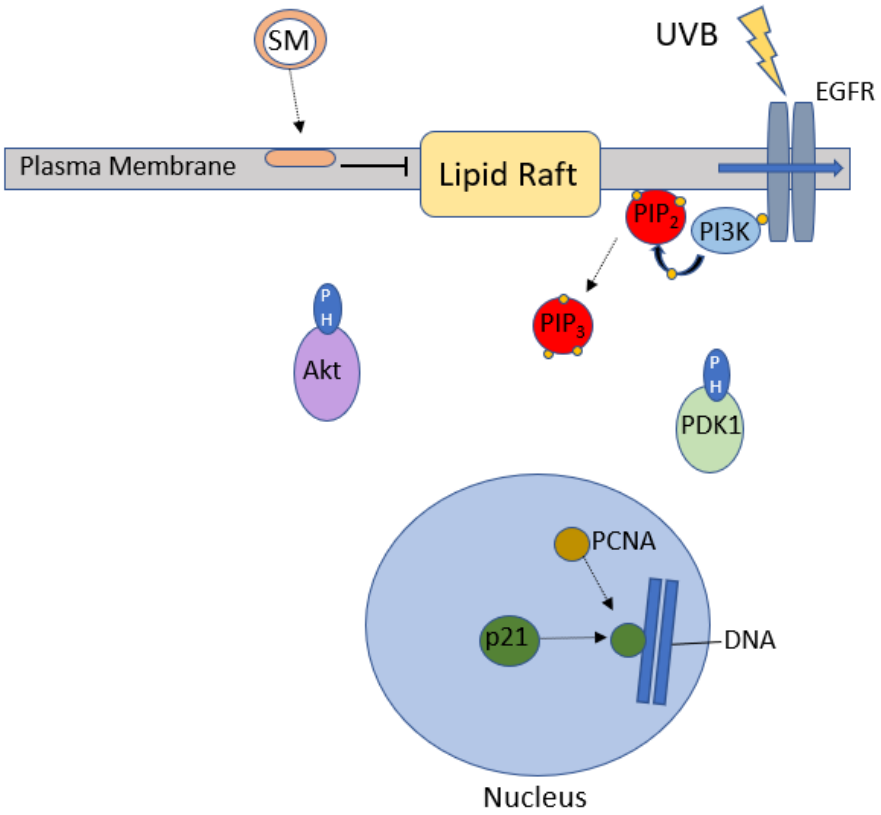

Figure 81. Excessive Exogenous SM may disrupt lipid rafts & signal transduction in UV+SM+. Disruption of the lipid raft for the PI3K/Akt pathway could cause p21 to stay in the nucleus slowing DNA damage repair and favoring apoptotic pathways due to inactivation of Akt [42][53][55][50][51].

Another hypothesis for the UV+SM+ case is that a very large amount of SM was converted to ceramide due to the abundance of SM. The ceramide then formed into many ceramide-enriched rafts, causing apoptotic signals to be amplified [42][55]. The many ceramide-enriched rafts won't allow for cholesterol/SM enriched rafts because there is not enough room on the PM and ceramide displaces cholesterol as well [42][53][55].

5.2 Limitations and Future Work

The work done in this thesis evaluated the level of p21 expression keratinocytes had when they were incubated in SM and subsequently exposed to UV. SM was incubated for an hour, at which fresh media was exchanged and cells were immediately exposed to the UV. The cells then were fixed twenty-four hours after the UV exposure. Evaluating p21 content was only

done using those parameters and setpoints. Future work of measuring p21 should consider looking at different timepoints after initial UV exposure, for example one hour, or two days after exposure. Looking at different timepoints could give different results in identifying what SM is doing to the KRTs. Continuous incubation of SM could also give different results since a cell would have a nearly infinite supply in proximity at all times. In these experiments, SM was removed before UV exposure potentially using up the cell's SM supply.

When using ImageJ to automate the measurement process, 'cytoplasmic p21' was evaluated within 6 μm, starting at the outside of the nucleus. A more sophisticated way of measuring this could be finding the cell's plasma membrane and subtracting out the nucleus to leave just the cytoplasm, similar to Section 3.7.8 fSM Donut ROI measure. However, that macro was not optimized for large images and time was a finite resource. UV+SM- cells had very high cytoplasmic p21 closer to the edges of the plasma membrane, meaning there could have been an even bigger difference when compared to UV+SM+ cells. It was also noticed that there may be some sort of dip immediately outside of the nucleus in UV+SM- cells, so a slope analysis could be performed, like in Section 3.7.9 fSM Rotation measure.

Cytoplasmic p21 content in UV+SM- cells was elevated in comparison to UV+SM+ cells, potentially hinting at a higher expression of Akt. Since Akt pulls p21 from the nucleus into the cytoplasm, its activation should be measured between the two treatment groups to see if that may be the cause.

Future researchers in the lab should look into EGFR and Akt activation following UV with and without SM to confirm why p21 stays in the nucleus when cells are incubated with SM. They should also use my same method and procedure to generate more data points to validate that SM causes p21 to stay in the nucleus.

References

[1] Z. Apalla, A. Lallas, E. Sotiriou, E. Lazaridou, and D. Ioannides, “Epidemiological trends in skin cancer,” *Dermatol. Pract. Concept.*, vol. 7, no. 2, pp. 1–6, 2017.

[2] R. Böni, C. Schuster, B. Nehrhoff, and G. Burg, “Epidemiology of skin cancer,” *Neuroendocrinol. Lett.*, vol. 23, no. SUPPL. 2, pp. 48–51, 2002.

[3] A. Katalinic, U. Kunze, and T. Schäfer, “Epidemiology of cutaneous melanoma and non-melanoma skin cancer in Schleswig-Holstein, Germany: Incidence, clinical subtypes, tumour stages and localization (epidemiology of skin cancer),” *Br. J. Dermatol.*, vol. 149, no. 6, pp. 1200–1206, 2003.

[4] R. P. Rastogi, Richa, A. Kumar, M. B. Tyagi, and R. P. Sinha, “Molecular mechanisms of ultraviolet radiation-induced DNA damage and repair,” *J. Nucleic Acids*, vol. 2010, 2010.

[5] R. P. Feehan and L. M. Shantz, “Molecular signaling cascades involved in nonmelanoma skin carcinogenesis.,” *Biochem. J.*, vol. 473, no. 19, pp. 2973–94, 2016.

[6] G. T. Bowden, “Prevention of non-melanoma skin cancer by targeting ultraviolet-B-light signalling,” *Nat. Rev. Cancer*, vol. 4, no. 1, pp. 23–35, 2004.

[7] T. Abbas and A. Dutta, “p21 in cancer: intricate networks and multiple activities.,” *Nat. Rev. Cancer*, vol. 9, no. 6, pp. 400–14, Jun. 2009.

[8] A. J. Mendez, G. Lin, D. P. Wade, R. M. Lawn, and J. F. Oram, “Membrane Lipid Domains Distinct from Cholesterol/Sphingomyelin-Rich Rafts Are Involved in the ABCA1-mediated Lipid Secretory Pathway,” *J. Biol. Chem.*, vol. 276, no. 5, pp. 3158–3166, 2001.

[9] G. Li, J. Kim, Z. Huang, J. R. St. Clair, D. A. Brown, and E. London, “Efficient replacement of plasma membrane outer leaflet phospholipids and sphingolipids in cells with exogenous lipids,” *Proc. Natl. Acad. Sci.*, vol. 113, no. 49, pp. 14025–14030, 2016.

[10] M. E. Irwin and J. L. Boerner, “Lipid raft localization of EGFR alters the response of cancer

cells to the EGFR tyrosine kinase inhibitor gefitinb," *J Cell Physiol*, vol. 226, no. 9, pp. 2316–2328, 2012.

[11] X. Chen and M. D. Resh, "Cholesterol depletion from the plasma membrane triggers ligand-independent activation of the epidermal growth factor receptor," *J. Biol. Chem.*, vol. 277, no. 51, pp. 49631–49637, 2002.

[12] K. Roepstorff, P. Thomsen, K. Sandvig, and B. Van Deurs, "Sequestration of epidermal growth factor receptors in non-caveolar lipid rafts inhibits ligand binding," *J. Biol. Chem.*, vol. 277, no. 21, pp. 18954–18960, 2002.

[13] L. Zhuang, J. Lin, M. L. Lu, K. R. Solomon, and M. R. Freeman, "Prostate Cancer Cells Cholesterol-rich Lipid Rafts Mediate Akt-regulated Survival in Cholesterol-rich Lipid Rafts Mediate Akt-regulated Survival in Prostate Cancer Cells," *Cancer Res [CANCER Res.*, vol. 62, no. 62, pp. 2227–2231, 2002.

[14] C. Peres, A. Yart, B. Perret, J. P. Salles, and P. Raynal, "Modulation of phosphoinositide 3-kinase activation by cholesterol level suggests a novel positive role for lipid rafts in lysophosphatidic acid signalling," *FEBS Lett.*, vol. 534, no. 1–3, pp. 164–168, 2003.

[15] K. Campbell, "The use of Sphingomyelin to protect against UV induced DNA damage in Human Keratinocytes," California Polytechnic State University, San Luis Obispo, California, 2015.

[16] A. Van Laethem, S. Claerhout, M. Garmyn, and P. Agostinis, "The sunburn cell: Regulation of death and survival of the keratinocyte," *Int. J. Biochem. Cell Biol.*, vol. 37, no. 8, pp. 1547–1553, 2005.

[17] H. Yousef and S. Sharma, *Anatomy, Skin (Integument), Epidermis*, vol. 25, no. 3. 2018.

[18] W. D. Losquadro, "Anatomy of the Skin and the Pathogenesis of Nonmelanoma Skin Cancer.," *Facial Plast. Surg. Clin. North Am.*, vol. 25, no. 3, pp. 283–289, Aug. 2017.

[19] A. T. Slominski, P. R. Manna, and R. C. Tuckey, “On the role of skin in the regulation of local and systemic steroidogenic activities.,” *Steroids*, vol. 103, no. 4, pp. 72–88, Nov. 2015.

[20] Michel Démarchez, “The epidermis,” *27 January*, 2011. [Online]. Available: https://biologiedelapeau.fr/spip.php?article3.

[21] P. M. Elias, D. Crumrine, A. Paller, M. Rodriguez-Martin, and M. L. Williams, “Pathogenesis of the cutaneous phenotype in inherited disorders of cholesterol metabolism: Therapeutic implications for topical treatment of these disorders,” *Dermatoendocrinol.*, vol. 3, no. 2, pp. 100–106, 2011.

[22] G. K. Menon, K. R. Feingold, A. H. Moser, B. E. Brown, and P. M. Elias, “De novo sterologenesis in the skin. 11. Regulation by cutaneous barrier requirements,” vol. 26, no. 5, pp. 418–427, 1985.

[23] F. Permatasari, B. Zhou, and D. Luo, “Epidermal barrier: Adverse and beneficial changes induced by ultraviolet B irradiation depending on the exposure dose and time (Review),” *Exp. Ther. Med.*, vol. 6, no. 2, pp. 287–292, 2013.

[24] P. M. Elias, “Stratum corneum defensive functions: An integrated view,” *J. Invest. Dermatol.*, vol. 125, no. 2, pp. 183–200, 2005.

[25] A. T. Slominski, M. A. Zmijewski, C. Skobowiat, B. Zbytek, R. M. Slominski, and J. D. Steketee, *Sensing the environment: Regulation of localand global homeostasis by the skin’s neuroendocrine system*, vol. 212. 2012.

[26] M. J. Eide *et al.*, “Identification of patients with nonmelanoma skin cancer using health maintenance organization claims data,” *Am. J. Epidemiol.*, vol. 171, no. 1, pp. 123–128, 2010.

[27] U. Leiter, T. Eigentler, and C. Garbe, “Epidemiology of skin cancer.,” *Adv. Exp. Med. Biol.*,

vol. 810, pp. 120–40, 2014.

[28] D. S. Rigel, R. J. Friedman, L. M. Dzubow, D. S. Reintgen, J.-C. Bystryn, and R. Marks, “Cancer of the Skin,” p. 728, 2005.

[29] W. De Oliveira Sousa, S. C. Ribeiro, S. C. Vieira, T. C. B. Carvalho, and A. L. Carvalho, “Metastatic basal cell carcinoma: A case report,” *Dermatol. Online J.*, vol. 9, no. 5, pp. 140–143, 2003.

[30] H. W. Rogers, M. A. Weinstock, S. R. Feldman, and B. M. Coldiron, “Incidence estimate of nonmelanoma skin cancer (keratinocyte carcinomas) in the us population, 2012,” *JAMA Dermatology*, vol. 151, no. 10, pp. 1081–1086, 2015.

[31] J. D’Orazio, S. Jarrett, A. Amaro-Ortiz, and T. Scott, “UV radiation and the skin,” *Int. J. Mol. Sci.*, vol. 14, no. 6, pp. 12222–12248, 2013.

[32] D. Roymans and H. Slegers, “Phosphatidylinositol 3-kinases in tumor progression,” *Eur. J. Biochem.*, vol. 268, no. 3, pp. 487–498, 2001.

[33] C. L. Carpenter, B. C. Duckworth, K. R. Auger, B. Cohen, B. S. Schaffhausen, and L. C. Cantley, “Purification and characterization of phosphoinositide 3-kinase from rat liver,” *J Biol Chem*, vol. 265, no. 32, pp. 19704–19711, 1990.

[34] M. Gonzales and G. T. Bowden, “The role of PI 3-kinase in the UVB-induced expression of c-fos,” *Oncogene*, vol. 21, no. 17, pp. 2721–2728, 2002.

[35] T. B. El-Abaseri and L. A. Hansen, “EGFR activation and ultraviolet light-induced skin carcinogenesis,” *J. Biomed. Biotechnol.*, vol. 2007, 2007.

[36] R. Pralhada Rao, N. Vaidyanathan, M. Rengasamy, A. Mammen Oommen, N. Somaiya, and M. R. Jagannath, “Sphingolipid Metabolic Pathway: An Overview of Major Roles Played in Human Diseases,” *J. Lipids*, vol. 2013, pp. 1–12, 2013.

[37] N. Bartke and Y. A. Hannun, “Bioactive sphingolipids: metabolism and function,” *J. Lipid*

Res., vol. 50, no. Supplement, pp. S91–S96, 2009.

[38] N. Bartke and Y. A. Hannun, "Bioactive sphingolipids: metabolism and function.," *J. Lipid Res.*, vol. 50 Suppl, no. Supplement, pp. S91-6, Apr. 2009.

[39] S. Borodzicz, K. Czarzasta, M. Kuch, and A. Cudnoch-Jedrzejewska, "Sphingolipids in cardiovascular diseases and metabolic disorders," *Lipids Health Dis.*, vol. 14, no. 1, pp. 1–8, 2015.

[40] Y. Uchida, A. Di Nardo, V. Collins, P. M. Elias, and W. M. Holleran, "De novo ceramide synthesis participates in the ultraviolet B irradiation-induced apoptosis in undifferentiated cultured human keratinocytes," *J. Invest. Dermatol.*, vol. 120, no. 4, pp. 662–669, 2003.

[41] C. MAO, "Ceramidases: regulators of cellular responses mediated by ceramide, sphingosine, and sphingosine-1-phosphate," *Biochim. Biophys. Acta - Mol. Cell Biol. Lipids*, vol. 1781, no. 9, pp. 424–434, Sep. 2008.

[42] M. Schenck, A. Carpinteiro, H. Grassmé, F. Lang, and E. Gulbins, "Ceramide: Physiological and pathophysiological aspects," *Arch. Biochem. Biophys.*, vol. 462, no. 2, pp. 171–175, 2007.

[43] C. Michel and G. Van Echten-Deckert, "Conversion of dihydroceramide to ceramide occurs at the cytosolic face of the endoplasmic reticulum," *FEBS Lett.*, vol. 416, no. 2, pp. 153–155, 1997.

[44] T. Yamaji, K. Kumagai, N. Tomishige, and K. Hanada, "Two sphingolipid transfer proteins, CERT and FAPP2: Their roles in sphingolipid metabolism," *IUBMB Life*, vol. 60, no. 8, pp. 511–518, 2008.

[45] L. Riboni, R. Bassi, A. Caminiti, A. Prinetti, P. Viani, and G. Tettamanti, "Metabolic fate of exogenous sphingosine in neuroblastoma neuro2A cells: Dose-dependence and biological

effects," *Ann. N. Y. Acad. Sci.*, vol. 845, pp. 46–56, 1998.

[46] F. Mollinedo and C. Gajate, "Lipid rafts as major platforms for signaling regulation in cancer," *Adv. Biol. Regul.*, vol. 57, pp. 130–146, 2015.

[47] L. J. Pike, "Lipid rafts: bringing order to chaos Linda," *J. Lipid Res.*, vol. 44, no. 4, pp. 655–667, 2003.

[48] P. Hazarika, M. F. Mccarty, V. G. Prieto, M. Bar-eli, and M. Duvic, "Up-regulation of Flotillin-2 Is Associated with Melanoma Progression and Modulates Expression of the Thrombin Receptor Protease Activated Receptor 1 Up-regulation of Flotillin-2 Is Associated with Melanoma Progression and Modulates Expression of the Throm," pp. 7361–7369, 2004.

[49] Y. C. Li, M. J. Park, S. K. Ye, C. W. Kim, and Y. N. Kim, "Elevated levels of cholesterol-rich lipid rafts in cancer cells are correlated with apoptosis sensitivity induced by cholesterol-depleting agents," *Am. J. Pathol.*, vol. 168, no. 4, pp. 1107–1118, 2006.

[50] D. Calay, D. Vind-Kezunovic, A. Frankart, S. Lambert, Y. Poumay, and R. Gniadecki, "Inhibition of akt signaling by exclusion from lipid rafts in normal and transformed epidermal keratinocytes," *J. Invest. Dermatol.*, vol. 130, no. 4, pp. 1136–1145, 2010.

[51] A. Mound *et al.*, "Non-senescent keratinocytes organize in plasma membrane submicrometric lipid domains enriched in sphingomyelin and involved in re-epithelialization," *Biochim. Biophys. Acta - Mol. Cell Biol. Lipids*, vol. 1862, no. 9, pp. 958–971, 2017.

[52] T. Ringerike, F. D. Blystad, F. O. Levy, I. H. Madshus, and E. Stang, "Cholesterol is important in control of EGF receptor kinase activity but EGF receptors are not concentrated in caveolae.," *J. Cell Sci.*, vol. 115, no. Pt 6, pp. 1331–1340, 2002.

[53] Megha and E. London, "Ceramide selectively displaces cholesterol from ordered lipid

domains (rafts): Implications for lipid raft structure and function," *J. Biol. Chem.*, vol. 279, no. 11, pp. 9997–10004, 2004.

[54] C. Yu, M. Alterman, and R. T. Dobrowsky, "Ceramide displaces cholesterol from lipid rafts and decreases the association of the cholesterol binding protein caveolin-1," *J. Lipid Res.*, vol. 46, no. 8, pp. 1678–1691, 2005.

[55] H. Grassmé *et al.*, "CD95 Signaling via Ceramide-rich Membrane Rafts," *J. Biol. Chem.*, vol. 276, no. 23, pp. 20589–20596, 2001.

[56] H. Huo, X. Guo, S. Hong, M. Jiang, X. Liu, and K. Liao, "Lipid rafts/caveolae are essential for insulin-like growth factor-1 receptor signaling during 3T3-L1 preadipocyte differentiation induction," *J. Biol. Chem.*, vol. 278, no. 13, pp. 11561–11569, 2003.

[57] Z. Li *et al.*, "Reducing Plasma Membrane Sphingomyelin Increases Insulin Sensitivity," *Mol. Cell. Biol.*, vol. 31, no. 20, pp. 4205–4218, 2011.

[58] Y. Xiong, G. J. Hannon, H. Zhang, D. Casso, R. Kobayashi, and D. Beach, "p21 is a universal inhibitor of cyclin kinases," *Nature*, vol. 366, no. 6456, pp. 701–704, 1993.

[59] X. Lei, B. Liu, W. Han, M. Ming, and Y. Y. He, "UVB-Induced p21 degradation promotes apoptosis of human keratinocytes," *Photochem. Photobiol. Sci.*, vol. 9, no. 12, pp. 1640–1648, 2010.

[60] W. Xia, J. Chen, and X. Zhou, "Phosphorylation / Cytoplasmic Localization of p21Cip1 / WAF1 Is Associated with HER2 / neu Overexpression and Provides a Novel Combination Predictor for Poor Prognosis in Breast Cancer Patients," *Clin. cancer Res.*, vol. 10, no. 713, pp. 3815–3824, 2004.

[61] B. P. Zhou, Y. Liao, W. Xia, B. Spohn, M. Lee, and M. Hung, "by Akt-induced phosphorylation in HER-2 / neu-overexpressing cells," vol. 3, no. March, pp. 245–252, 2001.

[62] Y. Li, D. Dowbenko, and L. A. Lasky, “AKT/PKB phosphorylation of p21Cip/WAF1 enhances protein stability of p21Cip/WAF1 and promotes cell survival,” *J. Biol. Chem.*, vol. 277, no. 13, pp. 11352–11361, 2002.

[63] a C. Lines, B. F. Sections, and C. P. Sections, “Immunofluorescence Staining Protocol,” pp. 4–5.

[64] “Immunofluorescence.”

[65] R. Y. Tsien and A. Waggoner, “Fluorophores for Confocal Microscopy,” *Handb. Biol. Confocal Microsc.*, pp. 267–279, 1995.

[66] S. Prag, “Introduction to Confocal Microscopy Introduction to Confocal Microscopy,” vol. 12, no. Supp 2, pp. 1756–1757, 2016.

[67] R. M. Kandell, “ASSESSING THE PHOTOPROTECTIVE EFFECTS OF FLUORESCENT SPHINGOMYELIN AGAINST UVB INDUCED DNA DAMAGE IN HUMAN KERATINOCYTES,” no. June, 2018.

[68] I. A.-C. David Legland, “MorphoLibJ (IJPB-plugins),” 2018. [Online]. Available: https://imagej.net/MorphoLibJ.

[69] Sigma-Aldrich, “P6407 Product Information Sheet.” [Online]. Available: https://www.sigmaaldrich.com/content/dam/sigma-aldrich/docs/Sigma/Product_Information_Sheet/1/p6407pis.pdf.

[70] P. Bossuyt, E. Louis, J.-Y. Mary, S. Vermeire, and Y. Bouhnik, *Sphingolipids as Signaling and Regulatory Molecules*, vol. 688, no. c. New York, NY: Springer New York, 2010.

APPENDICES

A. Mechanical Designs

A.1 Cell Culture Plate Holder

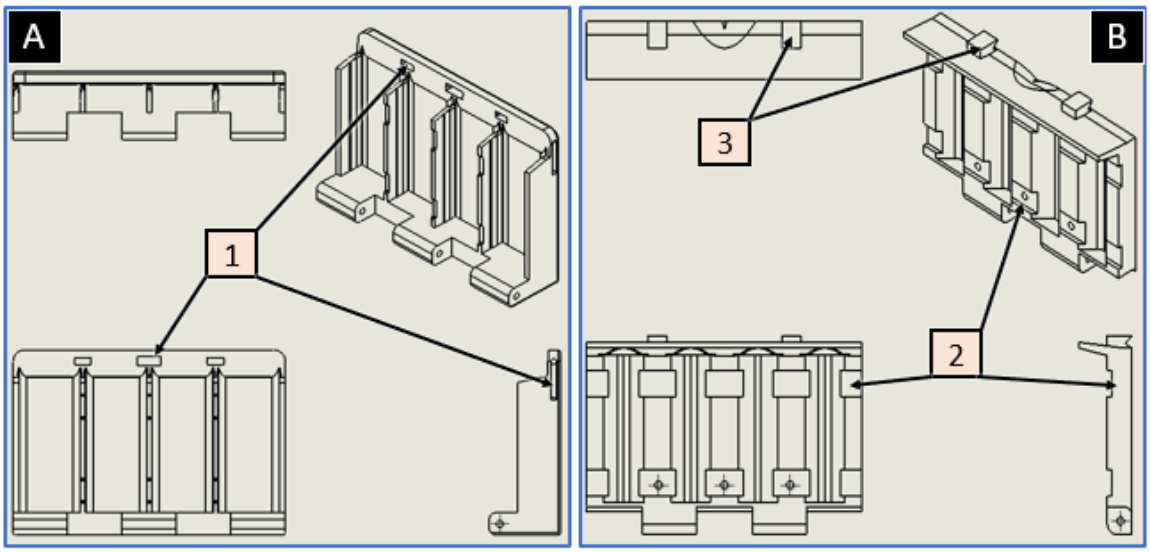

Figure 82. Schematic of the Plate Holder A) Bottom and B) Top. 1) Hole going through to fit an allen wrench. The allen wrench secures a rubber band and is also the correct size to level the microscope stage. 2) Guides cut out to place foam that gently puts force on the top of the cell culture plate's lid. 3) Extra hold points for the rubber band that keeps it closed.

The cell culture plate holder was created to reduce evaporation of liquid in the cell culture plate. It also protected the cell culture plate's fragile cover glass. Seen in Figure 82 & Figure 83, the foam inserts (2) were designed to gently push down on the top of the cell culture plate lid while in storage. It was noticed that

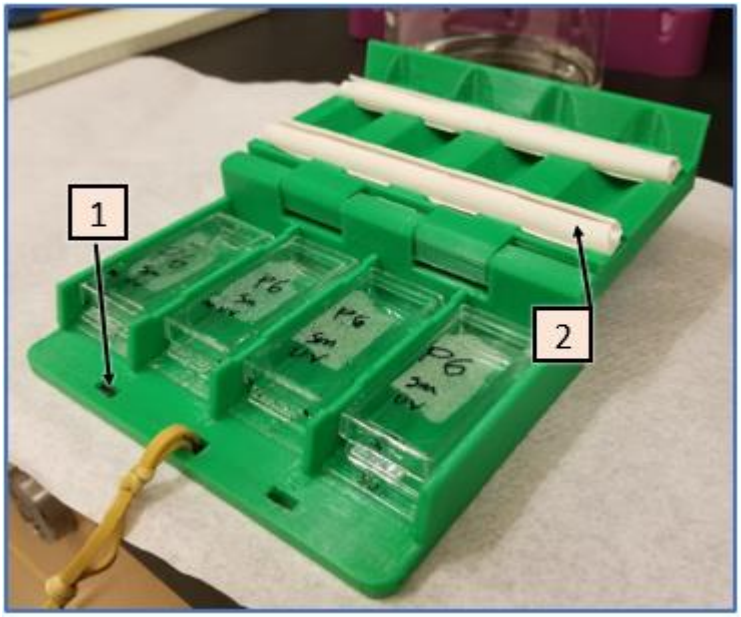

Figure 83. Cell Culture Plate Holder.

liquid evaporated very quickly when cell culture plates were stored in the refrigerator. Immobilizing the cell culture plates by keeping them in the plate holder while staining eliminated any cover glasses from breaking. An allen wrench (1) served two purposes in this design. First, it gave a rubber band a hardpoint so the lid could be kept closed. Second, the size of the allen wrench was the same size as the set screws to level the microscope stage.

A.2 Confocal Microscope Live Cell Incubator

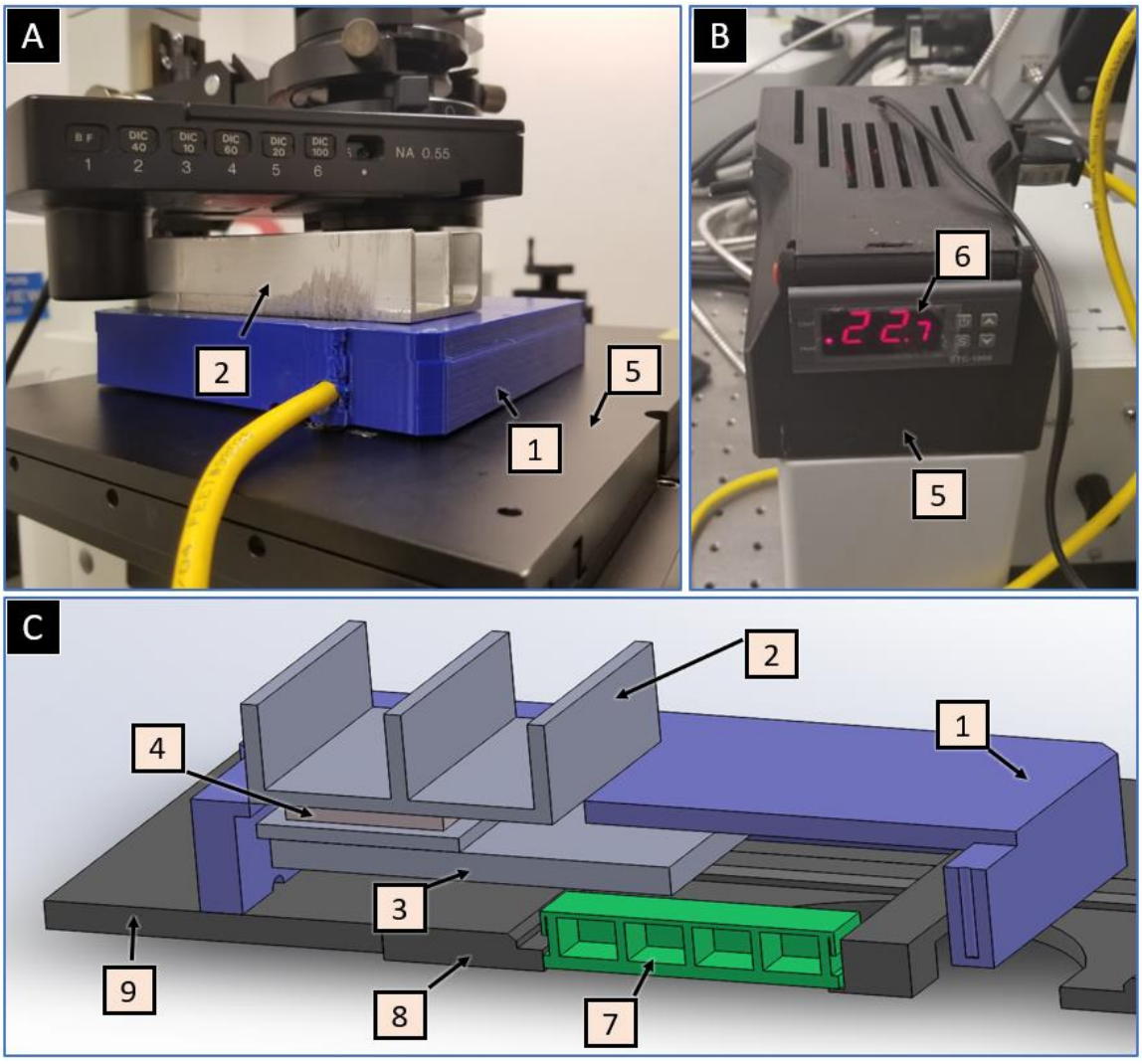

Figure 84. Confocal Microscope Live Cell Incubator. A) Incubator covering the culture plate. B) Temperature control and power supply unit. C) Cross-section view in SolidWorks of the incubator. 1) incubator body, 2) cooling block, 3) heating block, 4) Peltier unit, 5) power supply, 6) STC1000, 7) cell culture plate, 8) microscope's cell culture plate holder, 9) microscope's gantry.

The incubator was created to be a cheap alternative to OEM. The incubator only regulated temperature and not CO_2. The incubator was a simple design comprised of just a few parts and can be seen in Figure 84:

1. Incubator body – Modeled in SolidWorks and 3D printed on a cartesian FDM Prusa-type printer. ABS filament was used due to its resilience to heat. It was designed to be printed with minimal supports.
2. Cooling block – Aluminum heatsink from industrial equipment. Cut to size using an end mill.
3. Heating block – ¼" Aluminum plate cut by carbide blade.
4. Peltier unit – Two 14A units were used in series at 4.5V.

Power Unit:

5. Power Supply – ALITOVE 50W, 110V to 4.5-6.5V at 10A.
6. STC1000 – Temperature regulator relay triggered with a temperature probe.

Non-incubator parts:

7. Cell culture plate
8. Microscope's plate holder – Holds the cell culture plate in place.
9. Microscope's gantry – The part of the microscope that moves in 2 axis to find cells.

B.1 ImageJ Programs

B.1.1 Cell Viability

```
//Hoechst/DAPI ROI

run("Set Measurements...", "area mean
standard min display redirect=None
decimal=3");
run("Subtract Background...",
"rolling=50");
run("Minimum...", "radius=1");
run("Maximum...", "radius=1");
run("Gaussian Blur...", "sigma=1");
run("Subtract Background...",
"rolling=50");
run("Remove Outliers...", "radius=5
threshold=10 which=Bright");
run("Enhance Contrast", "saturated=.25");

setOption("BlackBackgroud");
run("Make Binary");
run("Dilate");
run("Fill Holes");
run("Erode");
run("Watershed");
run("Analyze Particles...", "size=40-
Infinity circularity=0.5-1.00 exclude
include add");


//opens dead stain channel

run("Open Next");

roiManager("Deselect");
roiManager("Measure");
String.copyResults();
selectWindow("Results");
run("Close");
```

B.1.2 Hoechst Image Tilt Correction

```
//Image Correction part 1
run("Set Measurements...", "area mean
standard min centroid center display
redirect=None decimal=3");
run("32-bit");
run("Subtract Background...", "rolling=50");
run("Median...", "radius=1");
run("Maximum...", "radius=1");
run("Bandpass Filter...", "filter_large=40
filter_small=4 suppress=None tolerance=5
autoscale saturate");
run("Subtract...", "value=1");
run("RGB Color");
run("Subtract Background...", "rolling=50");
run("Enhance Contrast", "saturated=.2");
run("Subtract Background...", "rolling=50");
setOption("BlackBackgroud");
run("Make Binary");
run("Dilate");
run("Fill Holes");
run("Erode");
run("Watershed");
sizeL=(1E-6);
sizeH=(9E-6);
run("Analyze Particles...", "size="+sizeL+"-
"+sizeH+" circularity=0.5-1.00 exclude
include add");
run("Clear Results");
run("Revert");
run("Select None");
array1 = newArray("0");;
for (i=1;i<roiManager("count");i++){
        array1 = Array.concat(array1,i);
        Array.print(array1);
}
roiManager("select", array1);

roiManager("Combine");
roiManager("Add");
roiManager("Delete");
run("From ROI Manager");

//Image Correction part 2

run("Revert");
run("Clear Results");
run("32-bit");
width=getWidth;
height=getHeight;

//middle
makeRectangle(3*width/8,3*height/8,width/4,
height/4);
roiManager("Add");
roiManager("Select", newArray(0,1));
roiManager("AND");
roiManager("add");
roiManager("Deselect");
roiManager("Select", 1);
roiManager("Delete");
roiManager("Select", 1);
roiManager("Measure");
roiManager("Select", 1);
roiManager("Delete");
m=getResult("Mean");
mx=getResult("XM");
my=getResult("YM");
run("Clear Results");
width=getWidth;
height=getHeight;

//top left square
makeRectangle(0,0,width/4, height/4);
roiManager("Add");
roiManager("Select", newArray(0,1));
roiManager("AND");
roiManager("add");
roiManager("Deselect");
roiManager("Select", 1);
roiManager("Delete");
```

```
roiManager("Select", 1);
roiManager("Measure");
roiManager("Select", 1);
roiManager("Delete");
a=getResult("Mean");
ax=getResult("XM");
ay=getResult("YM");
run("Clear Results");
width=getWidth;
height=getHeight;

//top right square
makeRectangle(3*width/4,0,width/4,height/4);
roiManager("Add");
roiManager("Select", newArray(0,1));
roiManager("AND");
roiManager("add");
roiManager("Deselect");
roiManager("Select", 1);
roiManager("Delete");
roiManager("Select", 1);
roiManager("Measure");
roiManager("Select", 1);
roiManager("Delete");
b=getResult("Mean");
bx=getResult("XM");
by=getResult("YM");
run("Clear Results");
width=getWidth;
height=getHeight;

//bottom left square
makeRectangle(0,3*height/4,width/4,height/4)
;
roiManager("Add");
roiManager("Select", newArray(0,1));
roiManager("AND");
roiManager("add");
roiManager("Deselect");
roiManager("Select", 1);
roiManager("Delete");
roiManager("Select", 1);
roiManager("Measure");
roiManager("Select", 1);
roiManager("Delete");
c=getResult("Mean");
cx=getResult("XM");
cy=getResult("YM");
run("Clear Results");
width=getWidth;
height=getHeight;

//bottom right square
makeRectangle(3*width/4,3*height/4,width/4,h
eight/4);
roiManager("Add");
roiManager("Select", newArray(0,1));
roiManager("AND");
roiManager("add");
```

```
roiManager("Deselect");
roiManager("Select", 1);
roiManager("Delete");
roiManager("Select", 1);
roiManager("Measure");
roiManager("Select", 1);
roiManager("Delete");
d=getResult("Mean");
dx=getResult("XM");
dy=getResult("YM");
run("Clear Results");
roiManager("Select", 0);
roiManager("Delete");
roiManager("Deselect");

//make and apply gradient
run("Revert");
run("32-bit");
getVoxelSize(width1, height1,f,g);
width=getWidth; height=getHeight;
ax=((ax/width1)); //into pixels
ay=((ay/height1));
bx=((bx/width1));
mx=((mx/width1));
my=((my/height1));
cy=((cy/height1));

MeanABC=((a+b+c+m)/4)
az1=(((b+c+m)/3)/a); //y1
bz3=(((a+c+m)/3)/b); //y3 b
cz3=(((a+b+m)/3)/c); //y3 c
mz2=(((a+b+c)/3)/m);//y2

x1=ax
x2=mx
x3=bx
y1=ay
y2=my
y3=cy
xCOEFa=(((x1*(bz3-mz2))+(x2*(az1-
bz3))+(x3*(mz2-az1)))/((x1-x2)*(x1-x3)*(x2-
x3)));
yCOEFa=((y1*(cz3-mz2))+(y2*(az1-
cz3))+(y3*(mz2-az1)))/((y1-y2)*(y1-x3)*(y2-
y3));
xCOEFb=(((mz2-az1)/(x2-x1))-
(xCOEFa*(x1+x2)));
yCOEFb=(((mz2-az1)/(y2-y1))-
(yCOEFa*(y1+y2)));
xCOEFc=(az1-(xCOEFa*(x1^2))-(xCOEFb*x1));
yCOEFc=(az1-(yCOEFa*(y1^2))-(yCOEFb*y1));
run("Select None");
run("Macro...",
"code=v=(v*(((("+xCOEFa+"*x*x)+("+xCOEFb+"*x)
+"+xCOEFc+"+("+yCOEFa+"*y*y)+("+yCOEFb+"*y)+
"+yCOEFc+")/2))");
run("Remove Overlay");
```

B.1.3 Hoechst Local Area Contrast Normalization

```
run("Set Measurements...", "area mean
standard min centroid center median limit
display redirect=None decimal=3");
run("Clear Results");
width=getWidth;
height=getHeight;
squarew=(width/6);
squareh=(height/6);
```

```
run("16-bit");
run("8-bit");
run("Enhance Contrast...", "saturated=0.1");
r=0;

//for (d=0; d<4; d++){
for (x=0; x<6; x++){
for (y=0; y<6; y++){
```

```
    makeRectangle(x*width/6,y*height/6,squar
ew,squareh);

    // Push saturated down

    roiManager("Add");
    run("Clear Results");
    roiManager("select",0);setThreshold(5,
255);
    roiManager("Measure");mean=getResult("Me
an");
    stddev=getResult("StdDev");max=getResult
("Max");
    max1=(mean+1.7*stddev);

    roiManager("select", 0);
    run("Macro...",
"code=[if(v>"+max1+")v="+max1+"]");
    run("Clear Results");

    //descale everything below mean
    roiManager("select", 0);
    setThreshold(5, 255);
    roiManager("Measure");
    mean=getResult("Mean");
    stddev=getResult("StdDev");
    max=getResult("Max");
    cutoff=(mean);
    logoff=((log(cutoff))/cutoff);
    roiManager("select", 0);
    run("Macro...","code=[if(v<"+cutoff+")
      v=(exp(v*"+logoff+")/"+cutoff+")]");
    run("Clear Results");
```

```
    //log contrast
    run("Clear Results");
    roiManager("select", 0);
    roiManager("Measure");
    mean=getResult("Mean");
    stddev=getResult("StdDev");
    max=getResult("Max");
    roiManager("select", 0);
    run("Macro...",
"code=v=v*((log(v)/log("+max+")))");
    run("Clear Results");
    run("Select None");

    //scale everything from 0 to max to 0 to
255
    run("Clear Results");
    roiManager("select", 0);
    roiManager("Measure");
    mean=getResult("Mean");
    stddev=getResult("StdDev");
    max2=getResult("Max");
    scalar=255/max2;
    roiManager("select", 0);
    run("Macro...", "code=v=v*"+scalar);
    run("Clear Results");
    run("Select None");

    roiManager("select", 0);
    roiManager("Delete");
}
}
```

B.1.4 Maxima Point to ROI

```
run("Clear Results");
run("Revert");
run("Select None");
run("Subtract Background...", "rolling=50");
run("Gaussian Blur...", "sigma=1");
run("Find Maxima...", "noise=120 output=List
exclude");

for (i=0;i<nResults-1;i++){
    x=getResult("X",i);
    y=getResult("Y",i);
    makeOval(x-1, y-1, 2, 2);
    roiManager("Add");
}

array1 = newArray("0");;
for (i=1;i<roiManager("count");i++){
    array1 = Array.concat(array1,i);
    Array.print(array1);
}
roiManager("select", array1);
roiManager("Combine");
roiManager("Add");
roiManager("Delete");
run("Clear Results");


for (n=1;n<4;n++){
    roiManager("select", 0);
    run("Set...", "value=4095");
```

```
    run("Select None");
    run("Gaussian Blur...", "sigma=1");
}
run("Subtract Background...", "rolling=50");
setAutoThreshold("Moments dark");
run("Convert to Mask");
setOption("BlackBackground", true);
run("Make Binary");
run("Watershed");
run("Analyze Particles...", "
circularity=0.7-1.00 exclude include add");

roiManager("select", 0);
roiManager("Delete");
run("Revert");



//Move roi to centroid
count=roiManager("count")
getVoxelSize(width, height, depth, unit)
run("Set Measurements...", "centroid center
bounding display redirect=None decimal=3");
for (i=0;i<count;i++) {
    run("Clear Results");
    roiManager("select", i);
    roiManager("Measure");
    xb=getResult("Width")/width;
    yb=getResult("Height")/height;
    xm=getResult("XM")/width;
```

```
    ym=getResult("YM")/height;
    xc=(xm-(xb/2));
    yc=(ym-(yb/2));
    roiManager("select", i);
    Roi.move(xc,yc);
    roiManager("Update");
}
run("Set Measurements...", "area mean
standard min centroid center perimeter shape
integrated median skewness display
redirect=None decimal=3");
count1=roiManager("count")
array9 = newArray();;
for (i=0;i<count1;i++) {
          run("Clear Results");
          array9 = Array.concat(array9,i);
          roiManager("select", i);
          run("Fit Ellipse");
          roiManager("add");
}
roiManager("select", array9);
roiManager("Delete");
```

```
//filter
run("Revert");
array1 = newArray();;
run("Set Measurements...", "area mean
standard min centroid center perimeter shape
integrated median skewness display
redirect=None decimal=3");
for (i=0;i<roiManager("count");i++) {
          run("Clear Results");
          roiManager("select", i);
          roiManager("Measure");
          mean=getResult("Mean");
          if(mean<500){
              array1 =
Array.concat(array1,i);
          }
}
roiManager("select" array1)
roiManager("Delete")
```

B.1.5 Stack to Optimal Raw Image

```
dir = getDirectory("image");
run("Stack to Images");
for (z=1;z<4;z++){
selectWindow("c:1/3 z:"+z+"/3 - Series 1");
run("8-bit");
run("Duplicate...", "title=background.tif");
run("Gaussian Blur...", "sigma=100");
imageCalculator("Subtract create 32-bit", "c:1/3 z:"+z+"/3 - Series 1","background.tif");
selectWindow("c:1/3 z:"+z+"/3 - Series 1");close();
selectWindow("background.tif");close();
}

run("Images to Stack", "name=p21 title=c:2/3 use");
run("Images to Stack", "name=Hoechst title=c:1/3 use");
run("Images to Stack", "name=Dead title=c:3/3 use");
selectWindow("p21");
run("Scale...", "x=2 y=2 z=2 width=3476 height=3480 depth=6 interpolation=Bilinear
average process create");
run("Z Project...", "projection=[Max Intensity]");
selectWindow("Dead");
run("Scale...", "x=2 y=2 z=2 width=3476 height=3480 depth=6 interpolation=Bilinear
average process create");
run("Z Project...", "projection=[Max Intensity]");
selectWindow("Hoechst");
run("Scale...", "x=2 y=2 z=2 width=3476 height=3480 depth=6 interpolation=Bicubic average
process create");
run("Maximum 3D...", "x=1 y=1 z=3");//after interpolation, will find max vertically
run("Subtract Background...", "rolling=50 stack");
run("Z Project...", "projection=[Sum Slices]");

selectWindow("Hoechst-1");
close();
selectWindow("Hoechst");
close();
selectWindow("p21-1");
close();
selectWindow("p21");
close();
selectWindow("Dead-1");
close();
selectWindow("Dead");
close();

selectWindow("MAX_p21-1");
path=dir+"MAX_p21"
```

```
saveAs("Tiff",path);

selectWindow("MAX_Dead-1");
path=dir+"MAX_Dead"
saveAs("Tiff",path);

selectWindow("SUM_Hoechst-1");
path=dir+"SUM_Hoechst"
saveAs("Tiff",path);
```

B.1.6 Binary Threshold Drop

```
dir = getDirectory("image");

setBatchMode(true);
run("Stack to Images");
for (z=1;z<4;z++){
selectWindow("c:1/3 z:"+z+"/3 - Series 1");
run("8-bit");
run("Duplicate...", "title=background.tif");
run("Gaussian Blur...", "sigma=100");
imageCalculator("Subtract create 32-bit",
"c:1/3 z:"+z+"/3 - Series
1","background.tif");
selectWindow("c:1/3 z:"+z+"/3 - Series
1");close();
selectWindow("background.tif");close();
}

run("Images to Stack", "name=p21 title=c:2/3
use");
run("Images to Stack", "name=Hoechst
title=c:1/3 use");
run("Images to Stack", "name=Dead title=c:3/3
use");
selectWindow("Dead");
run("Scale...", "x=2 y=2 z=2 width=3476
height=3480 depth=6 interpolation=Bilinear
average process create");
run("Z Project...", "projection=[Max
Intensity]");
selectWindow("Hoechst");
run("Scale...", "x=2 y=2 z=2 width=3476
height=3480 depth=6 interpolation=Bicubic
average process create");
run("Maximum 3D...", "x=1 y=1 z=3");
run("Subtract Background...", "rolling=50
stack");
run("Z Project...", "projection=[Sum
Slices]");
selectWindow("p21");
run("Scale...", "x=2 y=2 z=1 width=3476
height=3480 depth=3 interpolation=Bilinear
average process create");


close("Hoechst-1");
close("Hoechst");
close("Dead-1");
close("Dead");
close("p21");
selectWindow("p21-1");
path=dir+"p21"
saveAs("Tiff",path);

selectWindow("MAX_Dead-1");
path=dir+"MAX_Dead"
saveAs("Tiff",path);

selectWindow("SUM_Hoechst-1");
path=dir+"SUM_Hoechst"
saveAs("Tiff",path);

//////// Start Maxima Contrast
minarea=80; //minimum area for nucleus

dir = getDirectory("image");
run("Set Measurements...", "area mean modal
min centroid perimeter limit shape integrated
median display redirect=None decimal=3");
run("Clear Results");
selectWindow("SUM_Hoechst.tif");
run("Revert");
run("Select None");

run("8-bit");run("Gaussian Blur...",
"sigma=5");
setThreshold(10, 255);
run("Measure");
cut=(getResult("Median"));
run("Min...", "value="+cut);
run("Subtract...", "value="+cut);
run("Kill Borders");
//run("Threshold...");
setThreshold(1, 255);
setOption("BlackBackground", true);
run("Convert to Mask");
run("Fill Holes");
minarea=80;
getVoxelSize(width, height, depth, unit);
min_pixel_area=minarea/width;//width=height
radius=(sqrt(min_pixel_area/3.14));

AreaStop=radius/3;
setAutoThreshold("Percentile dark");
run("Make Binary");
for (z=0;z<AreaStop;z++){
    run("Minimum...", "radius=3");run("Open");
}
print(AreaStop);


AreaStop=radius/3;
for (z=0;z<AreaStop;z++){
    run("Maximum...", "radius=3");run("Open");
}


sizeL=(80);
sizeH=(20000);
```

```
run("Analyze Particles...", "size="+sizeL+"-
"+sizeH+" circularity=0-1.00 exclude include
add");

close("SUM_Hoechst-killBorders");
selectWindow("SUM_Hoechst.tif");
run("Revert");
run("8-bit");

//filter
array3 = newArray();
run("Set Measurements...", "area mean
standard min centroid center perimeter
bounding fit shape integrated median skewness
display redirect=None decimal=3");
for (i=0;i<roiManager("count");i++) {
        print("iter"+i);
        run("Clear Results");
        roiManager("select", i);
        roiManager("Measure");
       max=getResult("Max");
       if(max<50){
           array3 = Array.concat(array3,i);
}
}

if(lengthOf(array3)>0){
    roiManager("select", array3);
    roiManager("Delete");
}

selectWindow("SUM_Hoechst.tif");
run("Revert");
run("8-bit");

run("Set Measurements...", "area mean
standard modal min center bounding median
display redirect=None decimal=3");
count=roiManager("count");
run("Enhance Contrast...", "saturated=0.0
normalize");
for (i=0;i<count;i++) {
    run("Clear Results");
    roiManager("select", i);
    run("Convex Hull");
    run("Enlarge...", "enlarge=2 ");
    roiManager("Update");
}


array2 = newArray();
for (i=0;i<roiManager("count");i++){
    array2 = Array.concat(array2,i);

}
roiManager("Select", array2)
roiManager("Combine");
roiManager("Add");
roiManager("Delete");
roiManager("Select", 0);
run("Clear Outside");
roiManager("Select", 0);
roiManager("Split");
roiManager("Delete");

count=roiManager("count");
for (i=0;i<count;i++) {
    roiManager("select", i);
    roiManager("Measure");
    cutoff=(getResult("Median"));
    logoff=((log(cutoff))/cutoff);
    run("Macro...", "code=[if(v<"+cutoff+")
v=exp(v*"+logoff+")]");
    run("Clear Results");
    roiManager("select", i);
    roiManager("Measure");
    max=getResult("Max");
    scalar=(255/max);
    roiManager("select", i);
    run("Multiply...", "value="+scalar);
}



array2 = newArray();
for (i=0;i<roiManager("count");i++){
    array2 = Array.concat(array2,i);

}
roiManager("Select", array2)
roiManager("Combine");
roiManager("Delete");


roiManager("Deselect");
run("Select None");
run("Hide Overlay");
run("Remove Overlay");



//fill in holes
selectWindow("SUM_Hoechst.tif");
run("Fill Holes (Binary/Gray)");
selectWindow("SUM_Hoechst-fillHoles");
run("Gaussian Blur...",
"sigma=1");run("Gaussian Blur...",
"sigma=1");run("Gaussian Blur...",
"sigma=1");
run("Unsharp Mask...", "radius=2 mask=0.90");
selectWindow("SUM_Hoechst-fillHoles");


run("8-bit");
run("Clear Results");
selectWindow("SUM_Hoechst-fillHoles");
setThreshold(1, 255);
run("Set Measurements...", "area mean
standard modal min median limit display
redirect=None decimal=3");
for (x=0;x<1;x++){
    run("Clear Results");
    selectWindow("SUM_Hoechst-fillHoles");
    run("Measure");
    mean1=getResult("Mean");
    med1=getResult("Median")/2;
    run("Min...", "value="+med1);
    run("Subtract...", "value="+med1);
}

run("Enhance Contrast...", "saturated=0
normalize");
selectWindow("SUM_Hoechst.tif");
dir=getDirectory("image");
selectWindow("SUM_Hoechst-fillHoles");
```

```
path=dir+"Hoechst_Enhanced.tiff";
saveAs("Tiff",path);



//Start reduced threshold ROI
selectWindow("Hoechst_Enhanced.tiff");
run("Gamma...", "value=1.14");
run("Median...", "radius=5");

run("Clear Results");
selectWindow("Hoechst_Enhanced.tiff");
setThreshold(1, 255);
run("Measure");
med=getResult("Median");
std=getResult("StdDev");


run("Set Measurements...", "area mean
standard modal min center bounding median
display redirect=None decimal=3");
for (y=0; y<3; y++){
z=3;
sizeL=80;
sizeU=1000;
if(y==2){
    z=med;
    sizeU=800;
}
Incr=(255-z)/5;
for (x=100; x<(255-z); x+=Incr){
    run("Select None");
    selectWindow("Hoechst_Enhanced.tiff");
    setThreshold(255-x, 255);
    run("Convert to Mask");
    run("Median...", "radius=3");
    upper=(1.00-(y*0.2));
    lower=(0.80-(y*0.2));

    run("Analyze Particles...",
"size="+sizeL+"-"+sizeU+"
circularity="+lower+"-"+upper+" exclude
include add");
    run("Revert");

}
}

//remove low mean rois since analyze
particles doesn't look at that
array4 = newArray();
run("Set Measurements...", "area mean
standard min centroid center perimeter
bounding fit shape integrated median skewness
display redirect=None decimal=3");
for (i=0;i<roiManager("count");i++){
        run("Clear Results");
        roiManager("select", i);
        run("Interpolate", "interval=2 smooth
adjust");
        roiManager("Update");

       roiManager("Measure");
       max=getResult("Max");
       r=getResult("Round");
       s=getResult("Solidity");
       a=getResult("Area");
       if((r<0.3 && s<0.95) || s<0.9){
        array4 = Array.concat(array4,i);
       }
}
if (lengthOf(array4)>0){
    roiManager("select", array4);
    roiManager("Delete");
}

//Start ROI grouping
selectWindow("Hoechst_Enhanced.tiff");roiMana
ger("Deselect");run("Select
None");run("Remove Overlay");
getVoxelSize(width, height, depth, unit);
run("Clear Results");
roiManager("Deselect");
run("Select None");run("Remove Overlay");
count=roiManager("count");
length=0;


run("Set Measurements...", "area mean
standard modal centroid shape integrated
display redirect=None decimal=3");
roiManager("Deselect");run("Select
None");run("Remove Overlay");
roiManager("Measure");
Table.rename("Results", "Data");
Table.set("Used",0,0,"Data");
Table.update;

//setup data table
for (j=0;j<count;j++){
    m=Table.get("Mean",j,"Data");
    a=Table.get("Area",j,"Data");
    c=Table.get("Circ.",j,"Data");
    s=Table.get("Solidity",j,"Data");
    r=Table.get("RawIntDen",j,"Data");
    f=Table.get("Round",j,"Data");
    std=Table.get("StdDev",j,"Data");
    d=(((r/a)*s*s));
    Table.set("Index num",j,j,"Data");
    Table.set("Rating",j,d,"Data");
}
Table.update;

array=newArray();
i=0;
g=1;
count1=count-1;
//for all ROIs
selectWindow("Hoechst_Enhanced.tiff");
while (i<count1-1){
    roiManager("Deselect");run("Select
None");run("Remove Overlay");
    //print(i);
    //skip rois that have been used
   while ((i!=count1) &&
(Table.get("Used",i,"Data")==1)){
    i=i+1;
   }
   array=newArray();
   Table.set("Used",i,1,"Data");
   max=0;
   maxroi=0;
   x=0;
   y=0;
   run("Clear Results");
   x=Table.get("X",i,"Data")/width;
   y=Table.get("Y",i,"Data")/height;

   //scan roi manager for other ROIs that
contain the center
   j=i;
   r=0;
```

```
   while (j<roiManager("count")){
    contain=3;
    Table.set("Index num",j,j,"Data");
    roiManager("Select", j);
    //roiManager("And");
    //run("Measure");
    //contain=getResult("Area");
    contain=Roi.contains(x, y);
    Table.set("Group",i,g,"Data");
    if (contain==1){
        array = Array.concat(array,j);
        Table.set("Used",j,1,"Data");
        Table.set("Group",j,g,"Data");
    }
    j=(j+1);
   }

   if (lengthOf(array)<=1){
    Table.set("Used",i,1,"Data");
    Table.set("Good ROI",i,2,"Data");

    Table.update;
   }

   if (lengthOf(array)>=2){

    run("Clear Results");run("Select None");
    roiManager("Select", array);
    roiManager("Measure");
    roiManager("Deselect");run("Select None");
    print(" array length "+lengthOf(array));

    //find max rating in the group
    for (j=0;j<lengthOf(array);j++){
    m=getResult("Mean",j);
    a=getResult("Area",j);
    c=getResult("Circ.",j);
    s=getResult("Solidity",j);
    r=getResult("RawIntDen",j);
    f=getResult("Round",j);
    std=getResult("StdDev",j);


//favor circularity over mean/area
    d=(((r/a)*s*s));
    Table.set("Index num",j,j,"Results");
    Table.set("Rating",j,d,"Results");
    }

    run("Summarize");
    last=(nResults-1);
    max=getResult("Rating", last);
    run("Clear Results");

    for (z=0;z<lengthOf(array);z++){
        maxroi=0;
        d=array[z];
        maxroi=Table.get("Rating",d,"Data");
   if (maxroi<max){
            Table.set("Bad ROI",d,2,"Data");
        }
        if (maxroi>=max) {
            Table.set("Good ROI",d,1,"Data");
        }
   }
   }
   Table.update;
   g=g+1;
   array=0;

}
```

```
//Delete ROIS tagged with "Bad ROIs"
array1 = newArray();
for (i=0;i<roiManager("count");i++){
   if (Table.get("Bad ROI",i,"Data")==2){
    array1 = Array.concat(array1,i);
   }
}
roiManager("Select", array1); //array for roi
under the max intden
roiManager("Delete");



//combine rois and split
array2 = newArray();
for (i=0;i<roiManager("count");i++){
   array2 = Array.concat(array2,i);

}
roiManager("Select", array2)
roiManager("Combine");
roiManager("Add");
roiManager("Delete");
roiManager("Select", 0);
roiManager("Split");
roiManager("Delete");



selectWindow("SUM_Hoechst.tif");
run("Revert");
run("8-bit");


//Final filter
run("Set Measurements...", "area mean
standard min centroid center perimeter
bounding fit shape integrated median skewness
display redirect=None decimal=3");
run("Clear
Results");roiManager("Deselect");run("Select
None");run("Remove Overlay");

array6 = newArray();
for (i=0;i<roiManager("count");i++){
   run("Clear Results");
   roiManager("Select", i);
   roiManager("Measure");
   mean=getResult("Mean");
   area=getResult("Area");
   s=getResult("Solidity");
   r=getResult("Round");
   if ((s<0.9 && mean<25) || area<50 || (r<0.4
&& mean<100) || mean<20){
    array6 = Array.concat(array6,i);
    //print(i);
   }
   area=100;
run("Clear
Results");roiManager("Deselect");run("Select
None");run("Remove Overlay");run("Clear
Results");
}

roiManager("Select", array6);
if (lengthOf(array6)>0){
roiManager("Delete");
```

```
}
//Filter End


//Cleanup make final adjustments
//selectWindow("Mask of
SUM_Hoechst.tif");close();
selectWindow("Hoechst_Enhanced.tiff");close()
;




roiManager("Deselect");
dir = getDirectory("image");
path=dir+"ROI_Set.zip";
roiManager("Save",path);


run("Set Measurements...", "area mean
standard min perimeter integrated median
display redirect=None decimal=3");
run("Clear
Results");roiManager("Deselect");run("Select
None");run("Remove Overlay");

selectWindow("SUM_Hoechst.tif");
run("Revert");
run("8-bit");
roiManager("Deselect");
roiManager("Measure");
String.copyResults();
pathh=dir+"Hoechst.txt";
saveAs("Results",pathh);
close("Results");



selectWindow("SUM_Hoechst.tif");
close();



selectWindow("p21.tif");
dir = getDirectory("image");
pathp=dir+"p21.txt";
run("8-bit");
run("Clear Results");run("Select None");
run("Set Measurements...", "mean standard min
integrated median display redirect=None
decimal=3");
roiManager("Deselect");
Table.create("p21 Data");
for (i=0;i<roiManager("count");i++){
   run("Clear Results");
   roiManager("Deselect");
   roiManager("select", i);
   roiManager("multi-measure measure_all");
   run("Summarize");
   last=(nResults-1);
   max=getResult("RawIntDen", last)-1;
   for (z=0;z<3;z++){
    slicemax=getResult("RawIntDen",z);
    if (slicemax>=max){
        Table.set("Slice",i,z+1,"p21 Data");
        Table.set("Label",i,
getResultString("Label",z),"p21 Data");
       Table.set("Mean",i,
getResult("Mean",z),"p21 Data");
       Table.set("StdDev",i,
getResult("StdDev",z),"p21 Data");
       Table.set("Min",i,
getResult("Min",z),"p21 Data");
       Table.set("Max",i,
getResult("Max",z),"p21 Data");
       Table.set("IntDen",i,
getResult("IntDen",z),"p21 Data");
       Table.set("Median",i,
getResult("Median",z),"p21 Data");
       Table.set("RawIntDen",i,
getResult("RawIntDen",z),"p21 Data");
    }
   }
}


run("Set Measurements...", "mean standard
integrated display redirect=None decimal=3");
for (i=0;i<roiManager("count");i++){
   run("Clear Results");
   roiManager("select", i);
   slice=Table.get("Slice",i,"p21 Data");
   Stack.setSlice(slice);
   run("Make Band...", "band=6");
   run("Measure");
   mean=getResult("Mean");
   std=getResult("StdDev");
   intd=getResult("IntDen");
   rintd=getResult("RawIntDen");
   Table.set("Band Mean",i,mean,"p21 Data");
   Table.set("Band StdDev",i,std,"p21 Data");
   Table.set("Band IntDen",i,intd,"p21 Data");
   Table.set("Band RawIntDen",i,rintd,"p21
Data");
}
close("Results");
roiManager("Deselect");
selectWindow("p21 Data");
Table.rename("p21 Data","Results");
Table.update;
String.copyResults
saveAs("Results",pathp);
close("Results");



selectWindow("p21.tif");close();
selectWindow("MAX_Dead.tif");
dir = getDirectory("image");
pathd=dir+"Dead.txt";
selectWindow("MAX_Dead.tif");
run("8-bit");
run("Clear Results");
run("Set Measurements...", "mean min display
redirect=None decimal=3");
roiManager("Deselect");
roiManager("Measure");
String.copyResults();
saveAs("Results",pathd);
close("Results");
selectWindow("MAX_Dead.tif");close();
close("Data");
close("Log");
close("ROI Manager");

setBatchMode(false);
```

B.1.7 p21 Variable Slice Measurement

```
dir = getDirectory("image");
rpath=dir+"ROI_Set.zip";
roiManager("Open", rpath)
start=getInfo("image.filename");



run("Scale...", "x=2 y=2 z=1 width=3476
height=3480 depth=3 interpolation=Bilinear
average process create");
run("8-bit");
getVoxelSize(width, height, depth, unit);
run("Stack to Images");

run("Images to Stack", "name=p21 title=c:2/3
use");
run("Images to Stack", "name=Hoechst
title=c:1/3 use");
run("Images to Stack", "name=Dead title=c:3/3
use");
close("Dead");
close(start);

selectWindow("p21");
path=dir+"p21";
saveAs("Tiff",path);
selectWindow("Hoechst");
path=dir+"Hoechst";
saveAs("Tiff",path);
selectWindow("Hoechst.tif");



run("Clear Results");run("Select None");
run("Set Measurements...", "mean standard min
integrated median display redirect=None
decimal=3");
Table.create("H Data");

for (i=0;i<roiManager("count");i++){
    selectWindow("Hoechst.tif");
    run("Clear Results");
    roiManager("Deselect");
    roiManager("select", i);
    roiManager("multi-measure measure_all");
    a1=getResult("Mean",0);
    a2=getResult("Mean",1);
    a3=getResult("Mean",2);
    run("Clear Results");
    enlarge=-2/width;
    roiManager("select", i);
    run("Enlarge...", "enlarge="+enlarge+"
pixel");
    roiManager("Update");
    roiManager("select", i);
    roiManager("multi-measure measure_all");
    //print(a1);
    b1=getResult("Mean",0);
    b2=getResult("Mean",1);
    b3=getResult("Mean",2);
    //print(b1);
    c1=(a1-b1);
    c2=(a2-b2);
    c3=(a3-b3);

Table.set("Sample",i,i,"H Data");
    if(c1>c2 && c1>c2){
        Table.set("Slice",i,1,"H Data");
    }
    if(c2>c3 && c2>c1){
        Table.set("Slice",i,2,"H Data");
    }
    if(c3>c1 && c3>c2){
        Table.set("Slice",i,3,"H Data");
    }
}
Table.update;

close("Hoechst.tif");




selectWindow("p21.tif");

pathp=dir+"p21_revised.txt";
enlarge=2/width;
Table.create("p21 Data");run("Set
Measurements...", "area mean standard min
integrated median stack display redirect=None
decimal=3");



for (i=0;i<roiManager("count");i++){
    run("Clear Results");
    roiManager("select", i);
    slice=Table.get("Slice",i,"H Data")-1;
    selectWindow("p21.tif");
    roiManager("multi-measure measure_all");
    //setSlice(Table.get("Slice",i,"H Data"));
    print("sample number: "+i);
    roiManager("select", i);
    roiManager("Measure");
    Table.set("Slice",i,getResult("Slice",
slice),"p21 Data");
    Table.set("Label",i,getResultString("Label
", slice),"p21 Data");
    Table.set("Mean",i,getResult("Mean",
slice),"p21 Data");
    Table.set("StdDev",i, getResult("StdDev",
slice),"p21 Data");
    Table.set("Min",i, getResult("Min",
slice),"p21 Data");
    Table.set("Max",i, getResult("Max",
slice),"p21 Data");
    Table.set("IntDen",i, getResult("IntDen",
slice),"p21 Data");
    Table.set("Median",i, getResult("Median",
slice),"p21 Data");
    Table.set("RawIntDen",i,getResult("RawIntD
en", slice),"p21 Data");
    run("Clear Results");

    roiManager("select", i);
    run("Enlarge...", "enlarge="+enlarge+"
pixel");
    roiManager("Update");
    roiManager("select", i);
    run("Make Band...", "band=6");
    roiManager("multi-measure measure_all");
    mean=getResult("Mean", slice);
    std=getResult("StdDev", slice);
    intd=getResult("IntDen", slice);
    rintd=getResult("RawIntDen", slice);
    Table.set("Band Mean",i,mean,"p21 Data");
    Table.set("Band StdDev",i,std,"p21 Data");
```

```
    Table.set("Band IntDen",i,intd,"p21
Data");
    Table.set("Band RawIntDen",i,rintd,"p21
Data");
    run("Clear Results");
}

Table.update;

close("Results");
roiManager("Deselect");
selectWindow("p21 Data");
```

```
//Table.rename("p21 Data","Results");
Table.save(pathp);
Table.update;
//String.copyResults;
//saveAs("Results",pathp);
close("Results");

close("p21_revised.txt");
close("H Data");
close("p21.tif");
close("Log");
close("ROI Manager");
```

B.1.8 fSM Donut ROI measure

```
//Hoechst/DAPI ROI merge
run("8-bit");
run("Subtract Background...", "rolling=50");
run("Minimum...", "radius=1");
run("Maximum...", "radius=1");
run("Gaussian Blur...", "sigma=1");
run("Bandpass Filter...", "filter_large=40
filter_small=4 suppress=None tolerance=5
autoscale saturate");
run("Subtract Background...", "rolling=50");
run("Enhance Contrast", "saturated=.35");
run("Subtract Background...", "rolling=50");
run("Remove Outliers...", "radius=5
threshold=10 which=Bright");
setOption("BlackBackgroud");
run("Make Binary");
run("Fill Holes");
run("Dilate");
run("Dilate");
run("Dilate");
run("Dilate");
run("Median...", "radius=3");
run("Close-");
run("Fill Holes");
run("Erode");
run("Erode");
run("Erode");
run("Erode");
run("Watershed");
run("Analyze Particles...", "size=10-Infinity
circularity=0.4-1.00 exclude include add");

//select and merge ROI

array1 = newArray("0");;
for (i=1;i<roiManager("count");i++){
        array1 = Array.concat(array1,i);
        Array.print(array1);
}
roiManager("select", array1);

roiManager("Combine");
roiManager("Add");
roiManager("Delete");
run("From ROI Manager");
roiManager("select", 0);
run("Make Inverse");
roiManager("Add");
roiManager("Delete");
```

```
//opens fSM channel
run("Open Next");

//fSM ROI
run("8-bit");
run("Maximum...", "radius=1");
run("Median...", "radius=3");run("Median...",
"radius=3");run("Median...", "radius=3");
run("Enhance Contrast...", "saturated=1");
run("Gaussian Blur...", "sigma=1");
run("IsoData Classifier",
"number_of_classes=7");
run("Median...", "radius=3");run("Median...",
"radius=3");run("Median...", "radius=3");
run("Make Binary");
run("Fill Holes");
run("Close-");
run("Median...", "radius=3");run("Median...",
"radius=3");run("Median...", "radius=3");
run("Erode");
run("Erode");
run("Erode");
run("Watershed");
run("Median...", "radius=3");run("Median...",
"radius=3");run("Median...", "radius=3");
run("Dilate");
run("Dilate");
run("Dilate");
run("Fill Holes");
run("Watershed");
run("Analyze Particles...", "size=100-
Infinity circularity=0.05-1.00 exclude
include add");
run("Revert");

//Select each ROI and 'add' to the inversed
combined DAPI channel
for (i=1;i<roiManager("count");i++){
    roiManager("Select", newArray(0,1));
    roiManager("AND");

    roiManager("add");
    roiManager("Deselect");
    roiManager("Select", 1);
    roiManager("Delete");
}
roiManager("Select", 0);
roiManager("Delete"); //deletes the combined
DAPI
```

```
//Measure doughnuts
roiManager("Deselect");
roiManager("Measure");
String.copyResults();
selectWindow("Results");
run("Close");
```

B.1.9 fSM Rotation Measure

```
run("Set Measurements...", "area mean standard min centroid perimeter display
redirect=None decimal=3");
dir = getDirectory("Choose a Directory");
imageTitle=getTitle();
for (d=0;d<roiManager("count");d++){
          run ("16-bit");
          roiManager("Select", d);
          ROIname=getInfo("roi.name");
          roiManager("Select", d);  //roiManager("Deselect");
          roiManager("Measure");
          run("Clear Outside");
          getVoxelSize(width, height, depth, unit);
          X1=getResult("X")/width;
          Y1=getResult("Y")/width;

          //Draw overlay line
          Length=200;
          theta=0;
          run("Clear Results");
          for (i=1;i<61;i++){

                    //run("Clear Results");
                    name= " "+theta+"_Degrees";
                    path=dir+imageTitle+"_Cell_"+d;
                    radians=theta*(PI/180);
                    X2=X1+(Length*cos(radians));
                    Y2=Y1+(Length*sin(radians));
                    makeLine(X1, Y1, X2, Y2,4);
                    roiManager("Add");
                    profile = getProfile();
                    for (n=0; n<profile.length; n++) {
                              setResult(name, n, profile[n]);
                    }
                    updateResults;
                    theta=theta+6;
}
          run("Revert");
          saveAs("Results",path+".csv");
}
array1 = newArray("0");;
for (i=1;i<roiManager("count");i++){
        array1 = Array.concat(array1,i);
        Array.print(array1);
}
roiManager("select", array1);
roiManager("Delete");
close();
selectWindow("Results");
run("Close");
```

B.2 Experiment Procedures

B.2.1 Pilot Poly-D-Lysine Qualification

Materials

Item	Use	Stock Solution	Working Solution
Poly-D-Lysine	Culture plate coating	200ug/ml	100ug/ml
Ethidium Homodimer-1	Dead stain	2mM	2uM
Hoechst 34580	Nuclear stain	99%	.03%
Hydrogen Peroxide	Cell Death Initiator	6%	6%, 3%, 1%
Poly-D-Lysine	Culture Plate Coating	200 ug/ml	100 ug/ml
Paraformaldehyde	Fixative	3.7%	3.7%
2x VWR 8 well Culture Plates			

Methods

Treatment Groups
Well 1 and 2: 6% Hydrogen Peroxide
Well 3 and 4: 3% Hydrogen Peroxide
Well 5 and 6: 1% Hydrogen Peroxide
Well 7 and 8: Control

Coating Preparation
- Poly-D-Lysine stock solution (200ug/ml): 25ml deionized H_2O sterilized and mixed with 5mg sterile PDL powder. Solution mixed in bottle PDL came in. All under sterile hood.
- Poly-D-Lysine working solution (100ug/ml): Dilute stock solution 1:1 with sterilized deionized H_2O

1. Apply 64ul working solution to each well for 5 minutes.
2. Dry for 1 hour.

Stain Preparation
Total solution required per stain: (16 wells) * (200ul/well) = 3.2ml solution
Ethidium Homodimer-1: (2uM working*3.2ml total)/2mM stock = 3.2ul stock into 3.2ml PBS
Hoechst:

Hydrogen Peroxide Preparation
Total per treatment: (4 wells) * (400ul/well) = 1.6ml total
6%: 1.6ml stock
3%: 0.8ml stock + 0.8ml PBS
1%: 0.533ml stock + 1.067ml PBS

Treatment Protocol

1. Remove culture media from culture plates
2. Add H_2O_2.....*30 seconds*
3. Wash 1x
4. Add EthD-1 .....*10 minutes*
5. Wash 3x
6. Add Paraformaldehyde..... *15 min*
7. Wash 3x
8. Ready for imaging

Confocal Imaging

One 20x image per well resulting in two images per treatment per culture plate.

Image Processing Technique

20x Cell Viability ImageJ macro used. Program creates a Region of Interest (ROI) in the Hoechst channel of the nucleus. The ROIs found are used to measure the relative expression of Ethidium Homodimer-1 found within the nucleus.

Data Analysis

Dead cell count quantified by EthD-1 internuclear expression with a threshold visually found and applied across all data sets. Threshold identified as max pixel value > 33 out of an 85 max scale.

B.2.2 Ethidium with Permeabilization Qualification

Materials

Item	Use	Stock Solution	Working Solution
Ethidium Homodimer-1	Dead stain	2mM	2uM
Hoechst	Nuclear stain	99%	.03%
Triton-x	Membrane Permeablization	1%	0.1%
Hydrogen Peroxide	Cell Death Initiator	6%	1%
Paraformaldehyde	Fixative	3.7%	3.7%
1x VWR 8 well Culture Plates			

Methods

Treatment Groups

Well 6, 7 & 8: Triton-x + Hoechst
Well 3, 4 & 5: Hoechst
Well 1, 2: Triton-x

Stain Preparation

(8 wells)*(200ul/well)*(1.1 pipette error)=1.76 ml total
Ethidium Homodimer-1: 1.76ul (2uM EthD-1) + 1.76ml(PBS)
Triton-x: 1.68ul+1.68ml(PBS)
Hoechst: 0.504ul+1.68ml(PBS)

Hydrogen Peroxide Preparation
(8 wells)*(400ul/well)=3.2ml
533ul(H_2O_2)+ 2.667ml(PBS)

Treatment Protocol
1. Remove Media
2. Wash 1x
3. Add H_2O_2 1% (1 min)
4. Wash 2x
5. Add EthD-1 (10 min)
6. Wash 2x
7. Add Paraformaldehyde (15 min)
8. Wash 3x
9. Add Triton-x (20 min)
10. Wash 2x
11. Add Hoechst (15 min)
12. Wash 3x

Confocal Imaging
Two 40x images in the middle of each well.

Image Analysis
Qualitative assesment.

B.2.3 Poly-D-Lysine Qualification 2

Materials

Item	Use	Stock Solution	Working Solution
Ethidium Homodimer-1	Dead stain	2mM	2uM
Hoechst	Nuclear stain	99%	0.03%
Triton-x	Membrane Permeablization	1%	0.1%
Paraformaldehyde	Fixative	3.7%	3.7%
4x VWR 8 well Culture Plates			

Methods

Treatment Groups
Plate 1: Control, no coating
Plate 2: PDL Conc: 100ug/ml, Incubation: 5 min
Plate 3: PDL Conc: 100ug/ml, Incubation: 30 min
Plate 4: PDL Conc: 200ug/ml, Incubation: 30 min

Treatment Protocol
1. Replace media
2. UV at 35mJ
3. Store 1 day in incubator
4. Wash 1x
5. Add EthD-1 (15 min)
6. Wash 2x

7. Add Paraformaldehyde (15 min)
8. Wash 3x
9. Add Hoechst (15 min)
10. Wash 3x

Confocal Imaging
Per well: 10x stitch, 3x3 matrix, z: -4 µm, 0 µm, +4 µm

B.2.4 Poly-D-Lysine Qualification 3

Materials

Item	Use	Stock Solution	Working Solution
Ethidium Homodimer-1	Dead stain	2mM	2uM
Hoechst	Nuclear stain	99%	.03%
Triton X-100	Membrane Permeablization	1%	0.1%
Rabbit anti-p21	p21 Primary	50 µg at 0.2 mg/ml	1:400
AlexaFluor 488 anti-rabbit	p21 Secondary	2 mg/mL	1:400
Blocking Solution	Reduce non-specific binding	10%	1%
Paraformaldehyde	Fixative	3.7%	3.7%
2x 1-well Culture Plates			

Methods

Treatment Groups
Plate 1: Control, no coating
Plate 2: PDL Conc: 100ug/ml, Incubation: 30 min

Stain Preparation
Total volume: 5.17ml
EthD-1: 5.17 ul+ 5.17 ml (PBS)
Hoechst: 1.551 ul+ 5.17 ml (PBS)
Blocking: 51.7 ul + 5.17 ml (PBS)
p21 Primary: 12.925 ul + 5.17 ml (PBS)
p21 Secondary: 12.925 ul + 5.27 ml (PBS)
Triton-x: 5.17 ul + 5.17 ml (PBS)

Treatment Protocol
Day 1
1. Remove culture Media from culture plates
2. Add EthD-1 - *10 minutes*
3. Remove EthD-1 (No washes)
4. Add Paraformaldehyde - *20 minutes*
5. Wash 3x
6. Add Triton-x - *20 minutes*
7. Wash 3x
8. Add blocking solution – *overnight*

Day 2

9. Remove Blocking Solution
10. Wash 2x
11. Add p21 primary – *9 hours*
12. Wash 2x
13. Add AF488 – *1 hour*
14. Wash 2x
15. Add Hoechst – *15 minutes*
16. Wash 3x

Ready for confocal imaging

Confocal Imaging
1-well plates split into 3 zones.
Per zone: 10x stitch, 3x3 matrix, z: -4 µm, 0 µm, +4 µm

B.2.5 p21 Expression of SM Treated KRT 1

Materials:

Item	Use	Stock Solution	Working Solution
Ethidium Homodimer-1	Dead stain	2mM	2uM
Hoechst	Nuclear stain	99%	.03%
Triton-x	Membrane Permeablization	1%	0.1%
Rabbit anti-p21	p21 Primary	50 µg at 0.2 mg/ml	1:400
AlexaFluor 488 anti-rabbit	p21 Secondary	2 mg/mL	1:400
Blocking Solution	Reduce non-specific binding	10%	1%
Paraformaldehyde	Fixative	3.7%	3.7%
8x 1-well Culture Plates			

Methods

Treatment Groups
2x plates for each: UV+SM+, UV-SM+, UV+SM-, UV-SM-
All plates: 100 ul/ml Poly-D-Lysine incubation for 30 min, dry for 1 hour.
UV: 35 mJ

Stain Preparation
Total Volume per stain: (8 Plates)*(11.75 wells/1-well plate)*(200ul/well)*(1.1)=20.68ml
EthD-1: 20.68ul+ 20.68ml (PBS)
p21 Primary: 51.7ul + 20.68mL (PBS)
p21 Secondary, AF488: 51.7ul + 20.68ml (PBS)
Hoechst: 6.204ul + 20.68ml (PBS)
Triton-x: 20.68ul + 20.68ml (PBS)
Blocking: 206.8ul + 20.68ml (PBS)

Treatment Protocol
Day 1
1. Remove culture Media from culture plates
2. Add EthD-1 - *15 minutes*
3. Remove ErthD-1 (No washes)
4. Add Paraformaldehyde - *25 minutes*
5. Wash 3x

6. Add Triton-x - *20 minutes*
7. Wash 3x
8. Add blocking solution – *overnight*

Day 2

9. Remove Blocking Solution
10. Wash 2x
11. Add p21 primary – *9 hours*
12. Wash 2x
13. Add AF488 – *1 hour*
14. Wash 2x
15. Add Hoechst – *20 minutes*
16. Wash 3x

Ready for confocal imaging

Confocal Imaging:
10x magnification, 3x3 stitch matrix, Z-stack; 3 images ±1 µm

Statistical methods
one-way ANOVA, data represented as mean Integrated-Density p21 expression, $\alpha=0.01$

B.2.6 p21 Expression of SM Treated KRT 2

Materials:

Item	Use	Stock Solution	Working Solution
Ethidium Homodimer-1	Dead stain	2mM	2uM
Hoechst	Nuclear stain	99%	.03%
Triton-x	Membrane Permeablization	1%	0.1%
Rabbit anti-p21	p21 Primary	50 µg at 0.2 mg/ml	1:400
AlexaFluor 488 anti-rabbit	p21 Secondary	2 mg/mL	1:400
Blocking Solution	Reduce non-specific binding	10%	1%
Paraformaldehyde	Fixative	3.7%	3.7%
8x 1-well Culture Plates			

Methods

Treatment Groups
2x plates for each: UV+SM+, UV-SM+, UV+SM-, UV-SM-
All plates: 100 ul/ml Poly-D-Lysine incubation for 30 min, dry for 1 hour.
UV: 35 mJ

Stain Preparation
Total Volume per stain: (8 Plates)*(11.75 wells/1-well plate)*(200ul/well)*(1.1)=20.68ml
EthD-1: 20.68ul(2mM EthD-1) + 20.68ml (PBS)
p21 Primary: 51.7ul + 20.68mL (PBS)
p21 Secondary, AF488: 51.7ul + 20.68ml (PBS)
Hoechst: 6.204ul + 20.68ml (PBS)

Triton-x: 20.68ul + 20.68ml (PBS)
Blocking: 206.8ul + 20.68ml (PBS)

Treatment Protocol

Day 1

1. Remove culture Media from culture plates
2. Add EthD-1 - *15 minutes*
3. Remove ErthD-1 (No washes)
4. Add Paraformaldehyde - *20 minutes*
5. Wash 3x
6. Add Triton-x - *20 minutes*
7. Wash 3x
8. Add blocking solution – *overnight*

Day 2

9. Remove Blocking Solution
10. Wash 2x
11. Add p21 primary – *9 hours*
12. Wash 2x
13. Add AF488 – *1 hour*
14. Wash 2x
15. Add Hoechst – *20 minutes*
16. Wash 3x

Ready for confocal imaging

Confocal Imaging:
40x magnification, 3x3 stitch matrix, Z-stack; 3 images ± 1um

B.2.7 p21 Expression of SM Treated KRT 3

Materials:

Item	Use	Stock Solution	Working Solution
Ethidium Homodimer-1	Dead stain	2mM	2uM
Triton-x	Membrane Permeablization	1%	0.1%
Rabbit anti-p21	p21 Primary	50 µg at 0.2 mg/ml	1:400
AlexaFluor 488 anti-rabbit	p21 Secondary	2 mg/mL	1:400
Blocking Solution	Reduce non-specific binding	10%	1%
Paraformaldehyde	Fixative	3.7%	3.7%
8x 1-well Culture Plates			

Methods

Treatment Groups
2x plates for each: UV+SM+, UV-SM+, UV+SM-, UV-SM-
All plates: 100 ul/ml Poly-D-Lysine incubation for 30 min, dry for 1 hour.
UV: 35 mJ

Stain Preparation
Total Volume per stain: (8 Plates)*(11.75 wells/1-well plate)*(200ul/well)*(1.1)=20.68ml
EthD-1: 20.68ul(2mM EthD-1) + 20.68ml (PBS)
p21 Primary: 51.7ul + 20.68mL (PBS)
p21 Secondary, AF488: 51.7ul + 20.68ml (PBS)
Triton-x: 20.68ul + 20.68ml (PBS)

Blocking: 206.8ul + 20.68ml (PBS)

Treatment Protocol

Day 1

1. Remove culture Media from culture plates
2. Add EthD-1 - *15 minutes*
3. Remove ErthD-1 (No washes)
4. Add Paraformaldehyde - *20 minutes*
5. Wash 3x
6. Add Triton-x - *20 minutes*
7. Wash 3x
8. Add blocking solution – *overnight*

Day 2

9. Remove Blocking Solution
10. Wash 3x
11. Add p21 primary – *9 hours*
12. Wash 3x
13. Add AF488 – *1 hour*
14. Ready for confocal imaging

Confocal Imaging:
100x magnification, 4 images per plate.

B.2.8 Fluorescent Sphingomyelin Distribution Time Study

Materials:

Item	Use	Stock Solution	Working Solution
Hoechst	Nuclear stain	99%	.03%
fSM	SM trafficking	1mM	5uM
Paraformaldehyde	Fixative	3.7%	3.7%
8x 8-well Culture Plates			

Methods

Treatment Groups
Eight 8-well plates fixed at t(n) hours
t(n) :

a. 0 hr
b. 1 hr
c. 1 hrb
d. 2 hrs
e. 4 hrs
f. 6 hrs
g. 9 hrs
h. 12 hrs

Treatment Protocol

1. Remove culture media
2. Add fSM/media solution – *1 hour*
3. Remove solution
4. Add culture media
5. Wait, t(n) hours
   a. Add PFA – *20 min*
   b. Remove & wash 3x
   c. Add Hoechst – *15 min*
   d. Remove Hoechst & wash 3x

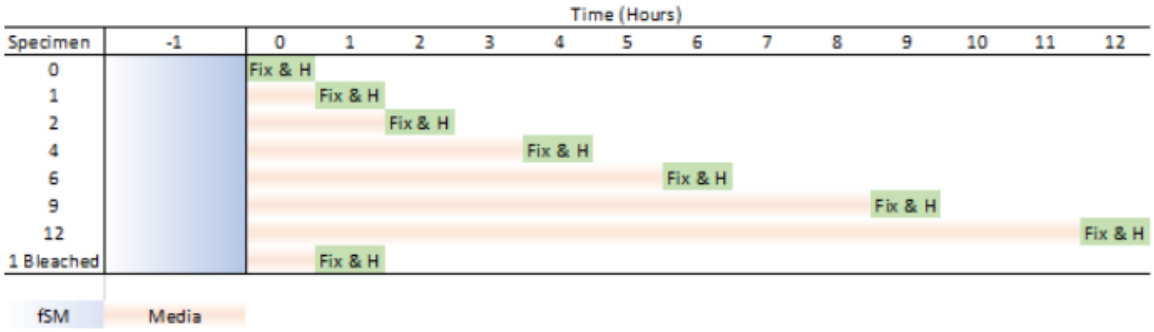

Confocal Imaging:
Three 60x magnification images per treatment. Three Z-stack 100x magnication images per treatment.

B.2.9 Fluorescent Sphingomyelin Live Cell Distribution Dynamics

Materials:

Item	Use	Stock Solution	Working Solution
fSM	SM trafficking	1mM	5uM
1x 1-well Culture Plate			

Methods

1. Set-up and initialize confocal microscope
2. Set-up and start heating the confocal incubator on the microcope's stage
3. Heat up a small insulated box for travel
    a. Foam box from reagent vender was used
    b. Heated by placing a leftover room-temperature icepack in a plastic bag in waterbath for 10min
4. Bring four liquid containers filled with PBS, fSM/media solution, cell culture media and nothing for waste
    a. Shield fSM from light
5. Bring pipetting materials needed
    a. 1ml pipette and tips, 0.2ml pipette will work too
6. Take cell culture plate with plated KRTs out of incubator and place in the heated box
    a. Make sure the plate won't fall, tip or lose any liquid during transportation
7. Carefully transport all materials from lab to confocal microcope
8. Move the incubator out of the way, place cell culture plate on the microscope and put incubator back in position
    a. Make sure placing the incubator back into position does not move the cell culture plate
    b. Keep lid on cell culture plate
9. Find cells of interest with epi-fluorescense
10. Make sure time lapse settings are ready

11. Quickly take off incubator, aspirate media, dispense fSM, make sure plate is not askew and place incubator back on
12. Immediately start imaging and adjust settings as needed
13. Leave fSM on for 1 hour while imaging
14. Quickly aspirate fSM and add culture media
15. Continue imaging